NEUROSCIENCE

Cellular neurochemical characterization and subcellular localization of Phospholipase C β1 in rat brain

Mario Montaña[1,3]*, Gontzal García del Caño[2]*, Maider López de Jesús[1,3], Imanol González-Burguera[1], Leire Echeazarra[1,3], Sergio Barrondo[1,3], Joan Sallés[1,3]

[1]Departamento de Farmacología, [2]Departamento de Neurociencias. Facultad de Farmacia (Vitoria-Gasteiz, Spain), Universidad del País Vasco (UPV//EHU). [3]Centro de Investigación Biomédica en Red de Salud Mental, CIBERSAM, Spain.

*Mario Montaña and Gontzal García del Caño contributed equally to this work.

Short title: PLCβ1 expression in different cell populations of rat brain

Number of text pages: 68

Number of figures: 20

Number of Tables: 5

Corresponding autor: Joan Sallés, Departamento de Farmacología, Facultad de Farmacia, Universidad del País Vasco (UPV/EHU), Paseo de la Universidad, 7, 01006-Vitoria-Gasteiz, Spain. Phone number: +34 945 01 3113. Fax number: +34 945 01 33 27. E-mail address: joan.salles@ehu.es

Abbreviations: Obtained from Paxinos and Watson (2007).

ABSTRACT

In this report, we describe a complete and detailed neuroanatomical distribution map of the phospholipase C beta1 (PLCβ1) isoform along the adult rat neuraxis, and define the phenotype of cells expressing PLCβ1, along with its subcellular localization in cortical neurons as assessed by double-immunofluorescence staining and confocal laser scanning. Immunohistochemical labelling revealed a considerable morphological heterogeneity among PLCβ1-positive cells in the cortex, even though there was a marked predominance of pyramidal morphologies. As an exception to the general non-matching distribution of GFAP and PLCβ1, a high degree of co-expression was observed in radial glia-like processes of the spinal cord white matter. In the somatosensory cortex, the proportion of GABAergic neurons co-stained with PLCβ1 was similar (around 2/3) in layers I, II-III, IV and VI, and considerably lower in layer V (around 2/5). Dobule immunofluorescence against PLCβ1 and nuclear speckles markers SC-35 and NeuN/Fox3 in isolated nuclei from the rat cortex, showed a high overlap of both markers with PLCβ1 within the nuclear matrix. In contrast, there was no apparent co-localization with markers of the nuclear envelope and lamina. Finally, we carried out Western blot experiments in cortical subcellular fractions to asses whether the subcellular expression pattern of PLCβ1 involved specifically one of the two splice variants of PLCβ1. Notably, PLCβ1a/1b ratios were statistically higher in the cytoplasm than in the nuclear and plasma membrane fractions. These results provide a deeper knowledge of the cellular distribution of the PLCβ1 isoform in different cell subtypes of the rat brain, and of its presence in the neuronal nuclear compartment.

Keywords: PLCβ1, SC-35, NeuN/Fox3, lamin B1, cortical intact nuclei, GABAergic neurons.

1. INTRODUCTION

The large family of phosphatidylinositol-4,5-bisphosphate (PIP_2)-specific phospholipase C isozymes (PLC) can be subdivided into six classes by sequence homology, PLCβ1-4, PLCγ1-2, PLCδ1-4, PLCε, PLCζ and PLCη1-2 (Suh et al. 2008). Although PIP_2-PLCs share many common features, the PLCβs are distinguished by their C-terminal region (Rebecchi and Pentyala 2000). This C-terminal region, consisting of approximately 450 amino acids, has determinants for regulation by heterotrimeric G-proteins (Wu et al. 1993; Kim et al. 1996). G-protein coupled receptors (GPCRs) stimulate PLCβ activity by activating Gq (Gαq subunits) and Gi (Gβγ subunits) proteins (Smrcka et al. 1993; Camps et al. 1992; Drin and Scarlata 2007). All PLCβ are strongly activated by GTP-bound Gαq in the following order: β1, β4>β3>β2 (Smrcka et al. 1993) and, additionally, PLCβ2 and PLCβ3 are activated by Gβγ subunits (Camps et al. 1992).

In the rodent brain, mRNA of each PLCβ family member displays distinct, largely reciprocal expression; PLCβ1 mRNA in the telencephalon, PLCβ2 in the white matter, PLCβ3 in the caudal cerebellum and PLCβ4 in the rostral cerebellum and brainstem (Ross et al. 1989; Tanaka and Kondo 1994; Watanabe et al. 1998a). By Northern blot, and PCR analysis of embryonic and adult rodent and human tissues, it has been detected the expression of PLCβ1 in all adult rat and human tissues tested, at varying relative levels (Caricasole et al. 2000; Peruzzi et al. 2002). Typically, higher signal intensities were observed in some CNS areas, such cerebral cortex, amygdala, caudate nucleus and hippocampus (Caricasole et al. 2000; Peruzzi et al. 2002). In the last five years, it has been published the most comprehensive study on the distribution of the PLCβ1 in the mouse brain, showing that it is highly expressed in the somatodendritic compartment of principal neurons of the telencephalon (Fukaya et al. 2008). Several fundamental properties are notable in cellular expression and subcellular localization of the PLCβ1 in

the rodent brain (Watanabe et al. 1998a; Nakamura et al. 2004; Nomura et al. 2007; Fukaya et al. 2008). First, single neurons express a single major PLCβ isoform. Second, PLCβ1 is present in association with the smooth endoplasmic reticulum or plasma membrane. Third, PLCβ1 is accumulated at the perisynaptic site of excitatory synapses, and thereby exhibits extensive overlap with mGluR1, mGluR5 and M1 receptors (Fukaya et al. 2008).

A prominent feature of the analysis of expression and functional activity of PLCβ1 (mRNA and protein) in human foetal and adult brain cortex is that it is highly expressed in adult but almost absent in foetal cortex (Caricasole et al. 2000; Peruzzi et al. 2002; Ruiz de Azúa et al. 2006). The difference of expression and functional activity that it is evident between prenatal and postnatal brain cortex could hint at a role of PLCβ1 during brain development. The implication of PLCβ1 signalling pathway, activated by metabotropic glutamate receptors (mGluRs), in activity-dependent development of the cerebral cortex has been demonstrated in PLCβ1 (-/-) knockout mice (Hannan et al. 1998; Hannan et al. 2001; Spires et al. 2005). Collectively, the PLCβ1 signalling pathways, activated via type mGluR-I, is implicated in cortical "barrel" formation since both PLCβ1 (-/-) and mGluR-5 (-/-) knockout mice fail to form cortical barrels in response to thalamocortical axon segregation (Hannan et al. 1998; Hannan et al. 2001). PLCβ4, another member of the PLCβ family, has also been shown to regulate synapse elimination in climbing fibres of the developing cerebellum (Kano et al. 1998). Interestingly, recent behavioural characterization of the PLCβ1 (-/-) knockout mice has demonstrated the presence of several schizophrenia-like endophenotypes (Koh et al., 2008; McOmish et al., 2008a,b). Furthermore, recent results showed that PLCβ1 transcript levels were decreased in the dorsolateral prefrontal cortex from subjects with schizophrenia, although the decrease in levels of PLCβ1 mRNA did not translate into a

change in levels of total PLCβ1 protein (Udawela et al., 2011). However, as previously discussed (Udawela et al., 2011), changes might be restricted to specific cellular compartments, making the decrease in PLCβ1 levels undetectable. In this sense, previous evidences showed that in non-neural cells PLCβ1-signalling is present in subcellular compartments such as the nucleus, where it could play a pivotal role in regulation of cell proliferation and differentiation (Cocco et al. 2009), and recent data show that phosphorylation of PLCβ1 by protein kinase C affects its localization its subcellular localization and its association with other proteins (Aisiku et al., 2010, 2011). Therefore, the above evidences aimed us to study PLCβ1-expression in the rat brain at cellular and subcellular levels. In the present study, we addressed this issue in adult rat brain sections and isolated intact nuclei by double immunofluorescence staining and confocal laser scanning.

In this report, we carried out an extensive and detailed neuronatomical analysis of PLCβ1 expression in the central nervous system of adult rats. We also describe the relationships of PLCβ1 positive cells to GABAergic neurons and GFAP-immunopositive radial glia-like processes of the spinal cord white matter. Moreover, we were able to collect information that provide histological support and characterize the presence of PLCβ1 in the nuclear compartment of rat brain cerebral cortex.

2. EXPERIMENTAL PROCEDURES

2.1. Animals

Male albine Sprague-Dawley rats, weighing 200-250 g at the time of arrival were kept in a controlled environment (12 h light-dark cycle, lights on at 08:00 h A.M., and 22 ± 2 °C room temperature) with food and water provided ad libitum, for at least seven days before experiments proceeded. All experimental procedures were carried out during the

morning (between 10:00 and 12:00 A.M.). Rats were carefully handled in accordance with the guidelines of the European Communities Council Directive of November 24, 1986 (86/609/EEC). Furthermore, this study included experiments carried out in fresh frozen cerebral tissue from wild-type and PLCβ1-knockout mice (10-13 weeks old, generated on a SV129/C57BL6 background strain from heterozygous pure strain parents), kindly donated by Professor H.-S. Shin (Kim et al. 1997; Shin et al., 2005).

2.2. Tissue preparation

Rats were anesthetized intraperitoneally with an overdose of choral hydrate (1g/kg, i.p.; Panreac Química S.A., Castellar del Vallés, Barcelona, Spain) and transcardially perfused with 0,37 % (w/v) sulphide solution at a constant flow of 30 ml/min (Heidolph Instruments GmbH & Co. KG, Pumpdrive PD 5106, Schwabach, Germany) for 4 minutes, followed by buffered 4% (w/v) p-formaldehyde (Sigma, St. Louis, MO, USA) for 4 minutes. After that, brains were removed and kept immersed in the same fixative medium during 4 hours. Next, brains were transferred to phosphate buffer 0,1 M, pH 7,4 (PB) containing 30% sucrose and kept at 4ºC and constant stirring until they felt. Tissue sections (40 μm thick) were obtained from frozen brains using a microtome (Leitz-Wetzlar 1310, Wetzlar, Germany) provided with a specific sensor to control temperature (5MP BFS-Physitemp Controller, Clifton, New Jersey, USA). Finally, sections were cryoprotected by incubations in increasing concentrations (5, 10 and 20% v/v) of dimethyl sulphoxide (Sigma, St. Louis, MO, USA) in PB. Thereafter, tissue sections were subjected to a permeabilization protocol consisting of three freeze-thawing cycles in isopentane at -80 °C and then stored frozen until use.

2.3. Immunohistochemistry and double immunofluorescence

Brain sections were incubated free-floating with the same amount of freshly prepared reaction solutions in all cases. Sections were treated for 20 min with 1% H_2O_2 in phosphate buffered saline 0,1 M, pH 7,4 (PBS) to inactivate endogenous peroxidase. Thereafter, they were incubated at room temperature for 1 h in blocking solution, consisting of 1% serum albumin bovine (BSA; Sigma, St. Louis, MO, USA) and 1 % normal serum from the species in which the secondary antibody was raised, diluted in PBS. Subsequently, tissue sections were incubated overnight at 4ºC in primary antibody (Table 2) diluted in blocking solution. Sections were then incubated for 1 h at room temperature in a specific biotinylated affinity purified secondary antibody (Vector Laboratories, Burlingame, CA, USA) diluted 1:200 in blocking solution. Sections were then processed by the avidin-biotin-peroxidase method using the Vectastain kit (Vector Laboratories) and reacted with 0.05% 3,3'-diaminobenzidine tetrahydrochloride and 0.01% H_2O_2 in 50 mM Tris-HCl, pH 7.6. Finally, the sections were mounted onto gelatin-coated slides, air-dried, dehydrated and coverslipped using DPX (Fluka, Buchs, Switzerland).

For immunofluorescence, sections were preincubated in blocking solution as above, followed by overnight incubation with the corresponding combination of primary antibodies (Table 2). Thereafter, sections were incubated for 1 h in an adequate combination (Table 3) of fluorescent-dye conjugated secondary antibodies diluted 1:400 in blocking solution. All secondary antibodies were purchased either from Invitrogen Molecular Probes (Invitrogen S.A., Spain) or from Jackson ImmunoResearch Laboratories, Inc. (West Grove, PA, USA). When available, secondary antibodies adsorbed against several species were used. Additionally, incubations in secondary antibodies were performed sequentially and the second secondary antibody was preincubated for 1 h at room temperature in blocking solution containing 0,01 µg/ml

purified IgGs and 1% serum corresponding to the host animal of the primary antibody recognized by the first secondary antibody. Finally, sections were extended and mounted with Mowiol reagent (Calbiochem, Bad Soden am Taunus, Germany) onto gelatin-coated slides.

Negative controls included, double immunolabelling against the same protein using primary antibodies obtained from different host species, neutralization of antibodies with an excess of antigen, or replacement of antibodies with the serum or IgGs corresponding to host species primary antibody in case antigen was not available. Furthermore, immunohistochemical analysis was conducted on wild-type and PLCβ1-knockout mice. To mimic transcardial fixation conditions used in rat, freshly frozen tissue blocks of approximately 2-3 mm thickness were incubated for 10 minutes in 0,37 % (w/v) sulphide solution at 4ºC under constant stirring and then in 4% paraformaldehyde at 4ºC. After 5 hours, tissue blocks were transferred to a 30% buffered sucrose cryoprotective solution. Thereafter, tissue was sectioned and treated as described above.

Immunofluorescence experiments to define the localization of PLCβ1 within subdomains of neuronal nuclei from rat cortex were carried out in intact nuclei obtained from rat brain homogenates (see below). Isolated nuclei seeded on gelatin-coated slides were immersed in 0,37 % (w/v) sulphide solution for 2 min followed by incubation in buffered 4% paraformaldehyde for 5 min, both at RT. Double immunofluorescence labeling was done as described above, except that all solutions contained 0,22% gelatin (w/v).

2.4. Microscope studies and imaging

Immunostained brain sections were examined with an Olympus BX50F optic microscope (Olympus, Tokyo, Japan) equipped with a high-resolution digital camera (Olympus and Soft Imaging Systems, Tokyo, Japan). Images were digitised using CellA software for image acquisition with automatic or manual exposure control (Olympus and Soft Imaging Systems, Tokyo, Japan).

Fluorescent images were captured sequentially on an Olympus Fluoview FV500 confocal microscope (Olympus, Tokyo, Japan) equipped with a diode laser line of 405 nm, an Argon laser line of 457, 488 and 514 nm, HeNe laser line of 543 nm and 633 nm. Alexa Fluor 488 was viewed using 505/525 nm BP filters and Alexa Fluor 568 using 560–600 nm BP filters. Images were viewed using a pinhole of 1 airy unit and objectives of 4X (0.16 numerical aperture -NA-, Plan Apochromat) 10X (0.40 numerical aperture -NA-, Plan Apochromat), 20X (0.70 NA, Plan Apochromat), 40X (0.85 NA, Plan Apochromat), or 60X (1.40 NA, Plan Apochromat). Viewing of Z-stacks and minor despeckling was performed on the Fluoview Image Browser software, version 5.0 (Olympus, Tokyo, Japan). Images were subsequently exported to TIFF format.

Boundaries of nuclei and areas of the central nervous system were determined on the basis of variations in the intensity of the immunohistochemical reaction, morphological features of immunostained structures, and Nissl staining distribution in neighbouring sections. Nomenclature is according to the Swanson Stereotaxic Atlas (1992). Contours of central neuronal nuclei, areas and layers were performed on micrographs with Macromedia Freehand 11 for Macintosh. These drawings were exported using an interchangeable EPS format and opened using Adobe Photoshop CS3 for Macintosh. Panoramic images of coronal and parasagittal sections were assembled from

micrographs obtained through the 4X objective using the photomerge feature of Adobe Photoshop CS3. All figures were compiled and labelled using Adobe Photoshop CS3.

2.5. Cell counts

To calculate the percentage of cortical GABAergic neurons that co-express PLCβ1, we acquired confocal laser images of 40 µm-thick brain sections doubly immunolabelled with a cocktail of antibodies specific for GABAergic populations and with anti-PLCβ1 R-233 antibody (Table 2), and visualized in the red and green channels respectively (see tables 2-3). A total of 8 sampling areas from the right and left cortices of 4 animals were acquired for analysis using a 20X objective. Images from each channel were assembled on Adobe Photoshop CS3, thus obtaining sampling areas consisting of 625 µm-wide columns that extended from the pial surface down to the white matter of the primary somatosensory cortex. The red and green channels from each sampling area were placed in two separate layers of Adobe Photoshop files. With the green channel hidden, each red pseudocoloured immunopositive neuron was labelled manually with a white dot. Neuronal somata (often with attached primary and sometimes secondary dendrites) that could be clearly differentiated from background staining were considered immunopositive. Dots and the images of immunostained GABAergic and PLCβ1-labelled cells were overlapped and GABAergic cells were classified as PLCβ1-immunonegative or PLCβ1-immunopossitive. Finally, double-labelled cells were subclassified as moderate-to-intensely stained or weakly stained depending on the PLCβ1-signal intensity. Two independent observers counted cells in each sampling area, and then common criteria for the two categories of staining intensity were established.

2.6. Tissue sampling and preparation of subcellular fractions

After sacrificing the animals by decapitation, the brains were immediately removed and cerebral cortices dissected out on ice and stored at -80ºC. The preparation of subcellular fractions from rat cerebral cortex, enriched in cytosolic (CYT) and plasma membrane (P2) proteins, was performed essentially as previously described for rat and human brain tissues (Thompson, 1973; Garro et al. 2001; Sallés et al. 2001). Prior to homogenization, frozen brain tissue samples were thawed in ice-cold hypotonic homogenization buffer: 20 mM Tris-HCl buffer, pH 7.0, 1 mM ethylene glycol-bis (β-aminoethyl ether, EGTA), and protease inhibitors (1 mM phenylmethylsulfonyl fluoride, PMSF, and 0.5 mM iodoacetamide). The samples were homogenized in 20 volumes of the same hypotonic buffer using a glass homogenizer with a Teflon pestle, and the homogenate was then centrifuged at 1100 x *g* for 10 min. The supernatant was kept and the pellet (containing unbroken cells, debris and nuclei) discarded. The supernatant was centrifuged at 40.000 x *g* for 10 min to obtain a supernatant (CYT fraction) and a pellet, which was washed twice by resuspension with fresh homogeneization buffer, followed by centrifugation at 40,000 x *g* for 10 min to obtain a final pellet (P2 fraction). Both fractions were aliquoted and stored until use.

To obtain highly purified intact nuclei, useful for both immunofluorescence and Western blot analyses, we used the procedure previously reported by Thompson et al., (1973) and Dent et al. (2010) with slight modifications. Cerebral cortices dissected from from 4 adult rats were placed in ice-cold 0.32 M sucrose containing 1 mM $MgCl_2$ and protease inhibitors. The cortices were then chopped finely and homogenized to give a 20% (w/v) homogenate in 2.0 M sucrose in 1 mM $MgCl_2$ containing protease inhibitors. The homogenate was then diluted with and equal volume of homogenizing medium, filtered through one layer of muslin and centrifuged at 4ºC for 60 min at 64,000 x g in a

SW40Ti rotor (331302; Beckman) at 4ºC for 30 min. The resulting pellet was washed with 0.32 M sucrose containing 1 mM $MgCl_2$ and protease inhibitors, and centrifuged for 5 min at 1,500 x *g* to obtain a final pellet containing highly purified intact nuclei (N fraction). Finally, nulei were resuspended in a volume of 10 ml 1 mM $MgCl_2$ (containing protease inhibitors) and counted under a light-phase microscope. Nuclei set aside for Western blot analysis were divided into alicuots of of 4 x 10^6 nuclei, pelleted by centrifgation at 1,500 x for 5 min *g*, and stored at -80ºC until use. Nuclei used for immunofluorescence analysis were suspended in Tris buffer (10 mM Tris-HCl, pH 7.2, 2 mM $MgCl_2$ and protease inhibitors) at a dilution of 2 x 10^6 nuclei/ml. Finally, 25 µl drops were laid on gelating-coated slides, allowed to dry at room temperature, and stored at -80ºC until use.

2.7. Immunodetection of PLCβ1 in subcellular fractions

Western blot studies were performed as previously reported for PLC isozymes in human brain with minor modifications (Garro et al. 2001; López de Jesús et al. 2006; Ruiz de Azúa et al. 2006). Briefly, samples of CYT, P2 and N fractions were boiled in Laemmli denaturation buffer (62.5 mM Tris-HCl, pH 6.8, 10% glycerol, 5% β-mercaptoethanol, 2% SDS, 0.01% bromophenol blue) plus 0.15 mM dithio-threitol (DTT). Denatured proteins were were run-yoked on the same electrophoresis SDS-polyacrylamide (SDS-PAGE) gradient gel (5-12%) using the Mini Protean II gel apparatus (Bio-Rad; Hercules, CA, USA). Proteins were transferred to polyvinylidene fluoride (PVDF) membranes (Amersham Biosciences) using the Mini TransBlot transfer unit (Bio-Rad; Hercules, CA, USA) at 90V constant voltage for 1 h at 4ºC. Blots were blocked in 5% non-fat dry milk/phosphate-buffered saline containing 0.5% BSA and 0.2% Tween for 1 h, and incubated with antibodies against PLCβ1 or against several proteins specific to

particular subcellular compartments: [i] β-tubulin as a cytosolic marker, Na^+/K^+ ATPase, [ii] NR1 subunit of the NMDA receptor, SNAP-25 and 58-K Golgi protein as markers of the membrane fraction, and [iii] nuclear pore complex as a nuclear marker (see table 2 for details). Blots were washed and incubated with specific horseradish peroxidase conjugated secondary antibodies diluted to 1:10000 in blocking buffer for 2 h at room temperature. Immunoreactive bands were incubated with the ECL system according to the manufacturer instructions (Amersham Bioscience; Buckingamshire, UK).

2.8. Data Analysis

PLCβ1a and β1b specific bands were acquired using an ImageQuant 350 imager (GE Healthcare, Madrid, Spain) and quantified by densitometry analysis using ImageJ image analysis software (ImageJ, NIH, Bethesda, MD, USA), and results were expressed as arbitrary units of integrated optical density (OD). Differences OD of immunoreactivity between splice variants PLCβ1a and PLCβ1b in each fraction and between fractions for each variant were analyzed by two-way analysis of variance (ANOVA) followed by Bonferroni post hoc test. Differences between ratios of PLCβ1a/PLCβ1b immunoreactivity were analyzed by one-way ANOVA followed by Bonferroni post hoc test. $P< 0.05$ was considered statistically significant.

3. RESULTS

3.1. Specificity of antibodies

Specificity of antibodies to PLCβ1 used in the present study was confirmed by double immunofluorescence in frozen sections of rat brain cortex (R-233, PLCβ1$_{36-87}$, G12 and D-8 antibodies), preabsorption with the immunizing peptide (PLCβ1$_{36-87}$, and G-12 antibodies), and Western blot analysis of crude membranes from rat brain (N-ter, R-233, PLCβ1$_{36-87}$, D-8 and G12 antibodies). Confocal laser scanning analysis revealed an almost identical distribution of the immunofluorescence signals provided by either the rabbit polyclonal R-233 or the mouse monoclonal D-8 antibodies, both recognizing an internal epitope shared by PLCβ1a and 1b splice variants (Figs. 1A-D). Of the two antibodies, R-233 apparently yielded the better signal-to-noise relationship, although the specificity could not be fully tested due to the unavailability of a commercial antigen for preabsorption assays. This prompted us to test the PLCβ1$_{36-87}$ antibody raised against a 52 amino acid peptide near the amino terminus of PLCβ1 (Figs. 1A, 1E-G), which has been tested for specificity in PLCβ1-knockout mice (Fukaya et al. 2008). By combining R-233 and PLCβ1$_{36-87}$ antibodies, we observed high overlap (Figs. 1E-G), although PLCβ1$_{36-87}$ yielded a non-overlapping punctuate and diffuse staining. Preabsorption of PLCβ1$_{36-87}$ with the corresponding immunizing peptide for two hours at a 5:1 ratio of peptide to antibody protein reduced greatly but not completely immunolabelling, suggesting that part of the signal obtained was non-specific (supporting Figs. S1A-B). We then performed double immunofluorescence experiments using the monoclonal D-8 antibody and the rabbit polyclonal G-12 antibody against an antigen consisting of the last 51 residues of the PLCβ1a splice variant (Fig 1A), which is commercially available. As shown in figures 1H-J, the distribution of immunolabelling obtained with D-8 and

G-12 antibodies was nearly identical, whereas staining was virtually undetectable using G-12 antibody preabsorbed at a 3:1 ratio of peptide to antibody protein (supporting Figs. S1C-D). This negative control proved the specificity of G-12 and, indirectly, of R-233 and D8 antibodies. Finally, conventional immunohistochemistry using the N-ter antibody at 1:50 dilution provided a weak signal with a distribution resembling that obtained with R-233, PLCβ1$_{36\text{-}87}$, D-8 and G-12 antibodies (supporting Fig. S2), although immunofluorescence signal was almost under detection threshold, making it useless for co-localization experiments. Results of Western blot analysis in homogenates of crude membranes from the rat cortex were also indicative of the specificity of antibodies. Thus, antibodies against sequences common to PLCβ1a and 1b isoforms (N-ter, R-233, PLCβ1$_{36\text{-}87}$, D-8) recognized two bands with apparent molecular masses consistent with previous reports (Lee et al., 1987; Lee et al., 1993; Fukaya et al., 2008), whereas G-12 antibody only detected the heaviest band, in agreement with its expected specificity for the PLCβ1a isoform (Figs. 1A, K). Finally, we confirmed that R-233 antibody yields no staining in PLC-β1-null mice (kindly donated by Professor Shin; as assesed by immunofluorescence in tissu sections and Western blot in crude homogenates (Fig. 2). All these evidences indicate that R-233 and D-8 antibodies (used for subsequent immunohistochemical and immunofluorescence experiments), and N-ter antibody (used for Western blot analysis) are highly specific for the peptides they were designed against.

3.2. General observations

The general distribution of PLCβ1-immunolabelling is illustrated in figure 3 and summarized in table 5. As shown in low magnification micrographs of parasagittal and

coronal sections of the rat brain immunostained using the rabbit anti-PLCβ1 R-233 antibody, there was a clear predominance of immunoreactivity in telencephalic regions over diencephalon, brainstem and cerebellum. Moderate and very intense immunostaining was observed in the olfactory bulb and olfactory tract (closed arrowheads in figure 3), respectively. Immunolabelling was present in all cortical layers, being intense to very intense in layer V throughout all cortical regions. A slightly weaker and more irregularly distributed signal was present layers II/III, whereas the rest of cortical layers were weak to moderately labelled (Figs. 3A1-4, B1-4). PLCβ1 was distributed densely in the pyramidal layer throughout all subregions of the Ammon's horn and in the dentate gyrus (Figs. 3A1-4, B3). Within the septum, the PLCβ1-staining was particularly strong in the dorsal part of the lateral septum (LSd; Fig. 3B2). Among the nuclei of the basal ganglia, the caudate-putamen exhibited highest levels of immunoreactivity (CP) (Figs. 3A1-4, B1-2), whereas PLCβ1 was weaklier detected in the globus pallidus (GP, Figs. 3A2-3). Notably, a discrete ventrolateral portion of the caudate-putamen, which displayed very strong immunostaining, stood out clearly against the surrounding tissue (open arrowheads in Figs. 3A1, B2). Caudally to the basal ganglia, intense immunostaining was found in the bed nucleus of stria terminalis (BST; Fig. 3A4). In general, PLCβ1 was undetectable or very weak in the thalamus, except in the reticular thalamic nucleus (RT, asterisks in Figs 3A2-4) and some nuclei located near the median parasagittal plane, where we could observe moderate immunolabelling (see bellow). With some exceptions that will be described later, hypothalamic nuclei were PLCβ1-negative or exhibited weak immunoreactivity. In most regions and nuclei of the brainstem, PLCβ1-signal was either undetectable or barely above the background. Notably, motor somatic neurons of the brainstem and

spinal cord were moderate to intensely labelled (XII and upward arrows in Fig. 3B5), and dense immunostaining was seen in lamina II of the dorsal horn (see bellow, Figs. 12E, G). The intensity of staining was distributed unevenly throughout the cerebellum, varying from weak in anteromedial regions (Fig. 3A4) to moderate or intense in posteromedial ones (Fig. 3A1). The layer distribution of PLCβ1-immunlabelling in the cerebellum will be described later in more detail.

Results from Western blot analysis of plasma membrane preparations (P2) obtained from selected brain regions were well correlated with the overall description of PLCβ1-immunostaing distribution. Thus, Western blot signals were significantly stronger in extracts obtained form neocortex, hippocampus and caudate-putamen than in those from cerebellum (Fig. 3C).

3.2.1. Telencephalon

Olfactory bulb and basal forebrain

At low-magnification, coronal sections through the main olfactory bulb (MOB) revealed moderate staining in most layers except at its most dorsal part, where a stronger immunostaining was systematically observed (Fig. 4A). At higher magnification, scattered cells of small size were clearly detected in the glomerular layer (MOBgl) within a background of diffuse immunolabelling. Very scarce PLCβ1-positive cells, which were hardly distinguishable from the background level, could be found in the external half of the outer plexiform layer (MOBopl). Weakly immunolabelled mitral cells formed an almost continuous row throughout the mitral layer (MOBml). The inner plexiform layer (MOBipl) was weakly and diffusely labelled, whereas abundant small-sized cells showing weak to moderate staining could be observed in the granule cell layer (Fig. 4B).

Immunostaining was prominent in neurons of layer II of the olfactory tubercle (OT), particularly in regions surrounding the islands of Calleja (isl), which could be easily delineated by the presence of an intense and diffuse signal (Figs. 4C-D). In these domains of layer II, very densely stained puncta apparently located within neuronal nuclei could be observed at high magnification (Fig. 4E). This pattern was also observed in neuronal populations of the cerebral cortex (see bellow). Apical dendrites form layer II neurons appeared weakly stained in layer I of the OT, but no positive cells could be observed either in layer I or in layer II (Fig 4D).

Isocortex

PLCβ1 immunostaining was present in all cortical regions, although with remarkable differences in intensity along the different layers and regions.

In the isocortex, layer V could be clearly distinguished from the rest due to the intense PLCβ1-signal present in pyramidal cells throughout all areas. Immunostaining formed a continuous row that was thicker rostrally than caudally (Figs. 3A-B, 5A-B), in line with the presence of a better developed layer V in rostrally located motor areas than in cortical regions devoted to sensory functions. Intermingled with cell somata of intensely stained layer V pyramidal neurons, immunopositive cells of different sizes and shapes, and displaying variable staining intensity could be observed, suggesting that not only principal neurons of isocortex but also other populations express PLCβ1 (Figs 5E-F). Immunoreactive neuropil around cell bodies of pyramidal neurons, which was composed at least in part of their basal dendrites, contributed to the overall intensity of PLCβ1-immunostaining in layer V. Labelling was also prominent in layers II-III of the isocortex, but its intensity was more irregular than in layer V, with highly

immunoreactive regions alternating with others displaying moderate staining (Figs. 3A-B, 5A-B). In highly immunoreactive regions of layers II-III, abundant pyramidal-like neurons, most of them lying deep in these layers, resulted intensely immunostained. Even though, strongly stained neurons of non-pyramidal shape could be also observed primarily lying above the deep row of strongly immunoreactive pyramidal-like neurons (Figs. 5A-D). In moderately immunoreactive regions of layers II-III, staining appeared almost homogeneously distributed. The signal was considerable weaker in neurons of layer IV compared to that seen in layers II-III and V, but numerous apical dendrites originating from layer V pyramids could be observed extending towards layer I, where they branched to form apical tufts. At this level, only occasional cells were immunolabelled (Figs. 4M, Q). We observed abundant PLCβ1-positive cells in layer VI of all isocortical regions. Immunostaining density appeared moderate in the cell bodies of most neurons, being more intense in neurons of pyramidal shape, most of them located deep in layer VI (Figs. 5C-D).

Transition cortex

PLCβ1-positive neurons were widely distributed throughout cortical layers II–VI of the prefrontal cortex, but with some differences between the various subdivisions of this region. The immunostaining pattern in the anterior cingulate cortex (AC) resembled that observed in the isocortex, except for the absence of layer IV, which is a constitutive feature of the prefrontal cortex. Layer V pyramids of the AC displayed the highest immunoreactivity but, at difference with isocortical pyramidal cells, staining of apical dendrites was weaker and only occasionally reached their most distal portions. PLCβ1was widely expressed in neurons of layers II-III of the AC with a similar pattern to that described for the moderately immunoreactive regions of layers II-III in the

isocortex. Immunostaining in layer VI of the AC was substantially similar to that observed in isocortical areas (Figs. 5I-J). Compared with the AC, staining intensity was considerably lower in layer V of the prelimbic cortex (PL) and labelling was almost absent from apical dendrites of pyramidal cells. In the rest of the layers, the immunolabelling pattern was basically the same in PL and AC (Figs. 5I, K). In the infralimbic cortex (IL), staining intensity was strong in cell bodies of layer V pyramids and trunks of their apical dendrites, but rarely extended beyond the limits between layers II-III and V. Compared with the AC and PL, immunostaining was considerably weaker in layers II-III and, to a lesser extent, in layer VI of the IL (Figs. 5I, L).

Again, in the perirhinal cortex, the highest PLCβ1-staining intensity was found in layer V pyramids, whose cell bodies appeared strongly immunostained. In this area, immunostaining was particularly conspicuous in apical dendrites of layer V pyramidal cells from their proximal trunks to their distal tufts in layer I. Dendrite morphology stood out clearly against the surrounding tissue of layers II-III, which showed considerably lower labelling than in isocortex (Figs. 5M-Q). The strong and high-contrast immunostaining in layer V pyramidal neuronal somata and dendrites allowed us to illustrate the detailed distribution of PLCβ1 in these compartments. Thus, at high magnification, densely immunostained puncta were seen in apparently nuclear locations of these cells (Fig. 5O). Diffuse labelling delineated the membrane of apical dendrites, which were decorated with small but highly immunoreactive spots situated at distances ranging approximately from 2 to 10 μm (Fig. 5P). The possibility that these particular patterns could reflect the concentration of neuronal PLCβ1 within known specialized cell subdomains, and that they could be generalized to isocortical areas, prompted us to

further analyze the subcellular localization of PLCβ1 in isocortex by confocal laser scanning (see bellow).

In the retrosplenial cortex (RSP), PLCβ1-immunostaining was present mainly in layer V, and to a lesser extent, in layer VI. In layers II-III there was a considerably weaker immunoreactivity, whereas only occasional neurons were seen in layer I. Regarding its distribution in the two subdivisions of RSP, immunolabelling was denser in the dorsal than in the ventral RSP (Fig. 5R).

Allocortex

The layer II of the piriform cortex (PIR) contained densely packed neuronal bodies that displayed moderate immunoreactivity. The density of PLCβ1-positive neuronal bodies decreased gradually with depth in layer III. Weak to moderately stained neurons were sparsely distributed throughout the endopiriform nucleus (EP). Only faint staining was observed in layer I (Fig. 5S).

In the entorhinal cortex, abundant neurons showing moderate immunolabelling were seen in the superficial half of layer II. Positive cells were much sparser in the deep half of layer II and in layer III. The density of immunopositive cells increased again in layer IV, where almost homogeneously distributed cells resulted moderately stained. A similar pattern could be observed in layers V and VI, although neurons showed slightly higher staining and tended to group more densely in layer V. Only occasional PLCβ1-positive cells could be found in layer I (Fig. 5T).

PLCβ1-immunostaining provided a detailed picture of the hippocampal cytoarchitecture. Thus, the various regions and layers of both the Ammon's horn and dentate gyrus (DG) resulted completely delineated by the immunohistochemical reaction. Low power

micrographs showed a continuous row of immunolabelling throughout the stratum pyramidale (sp) of the Ammon´s horn from CA1 to the most distal part of CA3 (Fig. 6A). Immunostaining was very strong in the CA1 and CA2 regions, decreasing gradually towards the distal end of CA3. Diffuse immunostaining was found within the strata oriens (so), radiatum (sr) and lacunosum-moleculare (slm). The limits of the various subregions of the Ammon's horn could be roughly defined by slight differences in the staining intensity at the level of the sr and slm (Fig. 6A). The cytoarchitectonic organization of the DG was also revealed by the intense immunostaining in the granular layer of DG (DGsg) compared to the molecular (DGmo) and, even more, to the polymorphic (DGpo) layers (Fig. 6A). At higher magnification, a strong immunohistochemical reaction was observed on perikarya of pyramidal cells of CA1 and CA2. Apical dendrites extending from these cells through the stratum radiatum (sr) towards the stratum lacunosum-moleculare (slm) could be distinguished against the background in both regions, but more conspicuously in CA2 than in CA1 (Fig. 6B-C). Notably, scattered putative GABAergic neurons of multipolar shape resulted moderate to very intensely immunostained in the so and sr along the Ammon's horn (Figs. 6B-D). Virtually all cell bodies of DG granule cells showed high expression of PLCβ1, and abundant but sparsely distributed cells of variable shape were weak to moderately immunostained in the DGpo (Fig. 6E).

Amygdala and extended amygdala

Moderately immunostained neurons were widely distributed throughout the amygdala, with no major apparent differences between its various subdivisions (Fig. 7A). In contrast, moderate to intensely immunostained neurons were found throughout the bed nucleus of the stria terminalis (BST) (Figs. 7B, 9A). Immunostaining was unevenly

distributed within this structure, such that densely packed clusters of intensely immunostained neurons were interspersed with more scattered cells that displayed weaker immunostaining (Figs. 7B-D). "Rosary-like" chains of moderate to intensely immunostained cells were found embedded within the stria terminalis (st) (Fig. 7E). These cells very probably correspond to previously described neurons of the supracapsular part of the BST (Alheid et al., 1998), a term that (for the rat) encompasses interrupted cell columns accompanying the stria terminalis as it traverses the dorsal part of the internal capsule (ic) (Alheid et al., 2004).

Septum

Extensive PLCβ1-immunostaining was observed throughout the lateral septum (LS), whereas it was barely distinguishable from background levels in the medial septum (MS) (Fig. 8A). Among the subdivisions of the LS, its dorsal part (LSd) displayed the strongest staining intensity. Immunohistochemical reaction localized intense immunoreactivity to perikarya and dendritic trunks of multipolar-shaped neurons of the (LSd). Weaker labelling in distal parts of dendrites formed a bushy network around cell bodies (Figs. 8A-B). We found a similarly high density of immunopositive cells in the ventral part of the LS (LSv) compared to the LSd, although staining was weaker and restricted to cell bodies in the former. In the intermediate part of the LS (LSi) the density of positive neurons was lower compared with either LSd or LSv. The overall PLCβ1-staining intensity was weaker in the LSi than in the LSd, although in the upper part of LSi many neurons and their proximal processes were as intensely stained as those of the LSd (Fig. 8A).

Basal nuclei

PLCβ1 was extensively expressed in the gray matter of the caudate-putamen, whereas striosomes where not immunolabelled. Some differences in the immunostaining intensity were observed throughout the caudate-putamen. Thus, it was slightly weaker rostrally (Fig. 3B1) and caudally (Fig. 9E) than at intermediate rostrocaudal levels (Figs. 3B2, 9A), where a ventrolaterally confined and oval-shaped core of particularly high immunoreactivity was invariably observed (Figs. 3A1, 3B2, 9A). As shown in figure 9A, corresponding to a coronal section at intermediate rostrocaudal levels of the caudate-putamen, PLCβ1-immunostaining decreased steadily from the dorsomedial aspect towards the ventrolateral one, and then rose drastically in the above mentioned highly immunoreactive core. Higher power micrographs showed that the regional differences resulted from different levels of immunostaining in cell bodies and neuropil (Figs. 9B-D, F). It is more than likely that the great majority of immunopositive cells correspond to medium-sized γ-aminobutyric acidergic (GABAergic) spiny cells (medium spiny neurons), because this phenotype accounts for more than 90% of striatal neurons (Graybiel et al. 1994; Tepper and Bolam 2004). In most neurons immunoreactivity was mainly restricted to the cell bodies (Figs. 9B-C, F), except in the highly immunoreactive ventrolateral core, where proximal parts of dendrites were also immunopositive (Fig. 9D). Diffuse staining of more distal dendritic branches is likely responsible for the higher neuropil labelling observed at this level compared with other parts of the caudate-putamen (Figs. 9 A, D).

Immunostaining was considerably weaker in the globus pallidus (GP) than in the caudate-putamen. At low magnification, the limits between caudate-putamen and GP and between the lateral and medial GP (GPl and GPm) could be easily defined on the basis of differences in intensity of staining (Fig. 9E). At high magnification, scattered neurons displaying moderate immunostaining on perikarya and proximal dendrites were

seen in both nuclei, which only differed in that the GPl showed a slightly denser diffuse neuropil staining compared with the GPm (Figs. 9G-H).

3.2.2. Diencephalon

PLCβ1 expression was weak or hardly detectable in the thalamus, in the greater part of its extent (Figs. 3A-B, 10A, 11A, Table 5), with most of the immunostaining being localized to the reticular nucleus (RT) and midline nuclei (Figs. 10-11). In the RT, we observed a large number of labelled cells of variable morphology that displayed moderate PLCβ1-immunoreactivity within their cell bodies and proximal dendrites (Fig. 10B). Abundant positive neurons were detected in midline nuclei throughout the rostrocaudal extent of the thalamus. Of the midline thalamic nuclei, parataenial (PT), reuniens (RE) and intermediodorsal (IMD) showed the highest immunoreactivity, and slightly weaker staining could be observed in the paraventricular (PVT) and perireuniens (PR) nuclei (Figs. 10A, 11A). In midline nuclei, immunoreactivity was largely confined to the cell bodies of small to medium-sized neurons. Most of them were moderately stained, although intense immunoreaction could be observed in individual cells (Figs. 10C-D, 11B). Weak labelling was also found in the intralaminar nuclei rhomboid (RH) (Fig. 11A) and parafascicular (PF). The immunolabelling was weak or undetectable in the rest of the thalamus. (see Table 5 for details).

As in the thalamus, labelling was weak or barely detectable in most parts of the hypothalamus (see Table 5). At low magnification, moderate staining was found in the medial preoptic nucleus (MPN) and in the lateral hypothalamic area (LHA). In the latter, the intensity of staining was more intense caudally than rostrally and, at high magnification, we could observe single neurons displaying high PLCβ1-immunoreactivity (Fig. 11C). Weaker labelling was detected in the paraventricular

nucleus (PVH), the anterior hypothalamic area (AHA), the medial part of the supramammillary nucleus (SUM) and the posterior hypothalamic nucleus (PHN) (Figs. 7B, 10A, 11A; Table 5). As an exception, putative histaminergic neurons of the tuberomammillary nucleus (TMN) were intensely immunolabelled (Inset in Fig. 11A).

3.2.3. Hindbrain

Cerebellum

PLCβ1-immunostaining was unevenly distributed throughout the cerebellum, being more intense laterocaudally than rostromedially (Fig. 3A). At caudal levels, moderate immunostaining was observed throughout all layers of the cerebellar cortex. At the level of the vermis and the paravermis, both the molecular layer (CBml) and the Purkinje cell layer (CBpl), showed a zebrin-like pattern, with diffuse staining bands alternating with others devoid of immunolabelling (open and closed stars in Fig. 12A). Within the positive modules, one could distinguish primary dendrites of Purkinje cells standing out faintly against the diffuse background. In the Purkinje cells layer, immunostaining was restricted to neuronal bodies located bellow the PLCβ1-positive bands of the molecular layer. Moderate labelling was observed in the granular layer (CBgl), where individual cell bodies of the granule cells were hardly distinguishable (Fig. 12A). In discrete regions of the flocular lobule immunostaining was conspicuous in all Purkinje cell bodies and their thicker dendrites (inset in Fig. 12A).

Brainstem

Apart from somatic and visceral motor nuclei, most regions of the brainstem were either very weakly stained or PLCβ1-immunonegative (Table 5). In the midbrain, weak

labelling was present in the nucleus of the optic tract (NOT), the external and dorsal cortices of the inferior colliculus (ECIC and DCIC), and the periaqueductal gray (PAG) (Figs. 12B-D, Table 5). Apparently, most of the cell bodies of brainstem motor neurons expressed PLCβ1 at moderate or high levels, showing a subtle rostrocaudal gradient, such that neurons were stained more intensely as were located in more caudal nuclei (Figs. 12C-D, 12F).

3.2.3. Spinal cord

All laminae of the spinal cord gray matter showed PLCβ1 expression, although with considerable variability in the intensity of staining (Fig. 12E, Table 5) Immunoreactivity was highest in lamina II, where densely labelled cell bodies were visible surrounded by a slightly less intense diffuse staining. A similar pattern was observed in lamina I, although cell bodies were much scarcer. The immunostaining was considerably lower in lamina III, where the majority of immunopositive cells were confined to its superficial third. Moderately stained neurons were sparsely distributed throughout laminae V-VIII and X, whereas motor neurons of the ventral horn (lamina X) were moderate to intensely immunolabelled. Only scattered positive cells were seen in lamina IV (Figs. 12E, G; Table 5). In the white matter, abundant immunopositive radial glia-like processes extended from the pial surface towards the gray matter. Immunoreactivity decreased steadily as they penetrated more deeply in the white matter. These structures were GFAP-positive as seen by double immunofluorescence analysis (see bellow).

3.3. Phenotype of PLCβ1-expressing cells

Double immunofluorescence with neuronal and astrocytic markers

The phenotype of PLCβ1-expressing cells was analyzed by double immunofluorescence staining of brain sections and confocal laser scanning. The first set of experiments conducted was aimed at exploring whether PLCβ1 was expressed exclusively in neurons. For this purpose, we performed double immunofluorescence labelling of PLCβ1 and the pan-neuronal marker NeuN. This later protein was detected in every cell soma identified by PLCβ1-staining throughout the gray matter. Figure 13 illustrates this in regions of the central nervous system highly expressing PLCβ1. In all encephalic regions analyzed by confocal microscopy, PLCβ1 immunoreactivity was predominantly found in cell somata, although weaker labelling was also observed in cell processes corresponding, at least in part, to dendrites of immunopositive neurons (Figs. 13A-F). In lamina II of the spinal dorsal horn, moderate to intense fluorescent signal was detected in puncta and processes surrounding the PLCβ1-positive cell bodies (Figs. 13 G-H).

To check the possibility that PLCβ1 could be expressed in astrocytic processes, we carried out combined PLCβ1 and GFAP immunofluorescence labelling experiments. In the gray matter of all areas analyzed, no matching between both markers was observed. As shown in figures 14A-I, strongly stained GFAP immunopositive cell processes were distributed in regions virtually devoid of PLCβ1 labelling. In contrast with the loose distribution of GFAP immunolabelling in the cerebral cortex and anterior horn of the spinal cord (Figs. 14A-C, G-H), astrocytes wrapped tightly around the cell bodies of the CA1 pyramids, resulting in a slight degree of GFAP-PLCβ1 overlap at the level of astrocyte-neuron junctions (Figs. 14D-F). As an exception to the general non-matching distribution of GFAP and PLCβ1, a high degree of co-expression was observed in radial glia-like processes of the spinal cord white matter (Figs. 14J-L), being particularly

evident in the portions closest to the pial surface. This pattern was not seen in the white matter bundles of brain.

Double immunofluorescence with markers of cortical GABAergic neurons

As described above, immunohistochemical labelling revealed a considerable morphological heterogeneity among PLCβ1-positive cells in the cortex, even though there was a marked predominance of pyramidal morphologies. These observations prompted us to examine whether GABAergic neurons also express PLCβ1. For this purpose we performed double immunofluorescence by combining the polyclonal anti-PLCβ1 R-233 antibody with a cocktail of monoclonal antibodies against calretinin, parvalbumin and somatostatin expressing neurons, which account for the majority of cortical GABAergic neurons (Kawaguchi and Kubota 1997; Tamamaki et al. 2003). To measure the percentage of GABAergic cells expressing PLCβ1, we chose the somatosensory cortex as representative of the neocortex.

Even though immunodetected GABAergic cells were seen through the depth of the cortex, they were more abundant in layers II-III, IV and VI than in layer V, whereas in layer I very few cells were immunopositive (Figs. 15A, 16). This distribution correlates fairly well with that described by Gonchar and Burkhalter (1997) in the rat primary visual cortex. Counts of the percentage of double immunolabelled neurons showed that 68,8 ± 2,16 % (S.E.M.) of the total GABAergic population was PLCβ1-immunopositive, with almost half of these neurons displaying moderate to high levels of immunofluorescence, as judged qualitatively. The proportion of GABAergic neurons co-stained with PLCβ1 was considerably higher in layers I, II-III, IV and VI (68,71± 11,71 %, 74,73±4,70 %, 61,99±4,82 % and 81,74±2,37 %, respectively), than in

layer V (41,76 ± 5,95 %) (Figs. 15-16), with statistically significant differences for comparisons between the percentage in layer V and that in layers I, II-III and IV.

Most co-immunolabelled neurons displayed moderate PLCβ1-immunofluorescence as compared with layer V pyramids, which are the cells showing the highest immunoreactivity as described above. Even though, among the doubly stained cells, some of them were showed intense PLCβ1-immunofluorescence, particularly in layers II-III.

3.4. Subcellular location of PLCβ1 in the cortex

Double immunofluorescence experiments

We conducted double immunofluorescence assays to analyze the subcellular localization of PLCβ1 in the isocortex. These experiments were aimed at confirming the presence of PLCβ1 in close vicinity to postsynaptic densities as previously observed by biochemical (Taguchi et al. 2007) and ultrastructural approaches (Fukaya et al. 2008), as well as to define the precise location of nuclear PLCβ1 in native nervous tissue.

Antibodies against PLCβ1 and the postsynaptic density protein PSD-95 were combined for immunofluorescence labelling and posterior confocal laser scanning analysis. In the cerebral cortex, substantial overlap was observed between PLCβ1 and PSD-95 on dendrites, where co-localization was evident in a considerable proportion of puncta (Figs. 17A-C), although not all PLCβ1 puncta were PSD-95-positive and viceversa.

To confirm the location of PLCβ1 in the nucleus, as suggested by immunohistochemical results, we combined PLCβ1-immunofluorescence with Hoechst's chromatin staining in tissue sections of the adult rat cortex. PLCβ1-positive dots were clearly distinguishable within the nuclear matrix as observed by confocal laser scanning analysis (Figs. 17. D-I).

In order to confirm and extend these results, we isolated intact nuclei form adult rat cortex to improve antibody penetration, and conducted different double labelling experiments. First, double-labelling assays using the polyclonal anti-PLCβ1 R-233 antibody and a monoclonal antibody to the postmitotic neuronal marker NeuN/Fox was combined with Hoechst staining, showing that only nuclei of neuronal origin were PLCβ1-positive (Figs. 18A-C). At high resolution, PLCβ1-signal displayed a punctate pattern composed of bright foci distributed throughout the nucleoplasm in nuclear subdomains poor in Hoechst's chromatin staining (Figs. 18 D-F), suggesting that PLCβ1 is a component of the nuclear matrix. The distribution of PLCβ1 within the nucleus was then analyzed in more detatil by double immunofluorescence experiments with the R-233 antibody combined with markers of the nuclear envelope and lamina, and of different components of the nuclear speckles, where PLCβ1 has been detected in various cell types (Avazeri et al. 2000; Tabellini et al. 2003; Martelli et al. 2005; Bavelloni et al. 2006; Miyara et al. 2008; Fiume et al. 2009). As shown in figures 18G-L, we observed no overlap with antibodies to nuclear pore complex or to lamin B1, indicating that PLCβ1 is internal to the nuclear envelope and lamina.

Double immunofluorescence against PLCβ1 and the nuclear matrix component NeuN/Fox3, recently shown to be a marker of the nuclear speckles in neurons (Dent et al., 2010), revelaed a similar distribution of both markers and a high overlap between PLCβ1- and NeuN/Fox-immunopositive puncta (Fig. 19A-C). Similar results were obtained when antibodies against PLCβ1 and the SC-35 (a nuclear speckles marker) were combined (Fig. 19D-F). PLCβ1 was also highly expressed PIP_2-rich regions of neuronal nuclei (Fig. 19G-I).

Western blot analysis of PLCβ1 in subcellular fractions

Immunohistochemical experiments showing enrichment of PLCβ1 in nuclear locations (see above), suggest its presence in neuronal nuclei. In view of the essential roles attributed to PLCβ1 in several cell lines (for review, Cocco et al. 2009), and of the lack of data about the nuclear localization of this protein in neurons, PLCβ1-expression was analyzed in nuclear (N), plasma membrane (P2) and cytosolic (CYT) fractions.

We first tested putative enrichment of N, P2 and CYT fractions. For that purpose, Western blot assays were carried out in every fraction of neocortical samples using antibodies raised against β-tubulin, Na^+/K^+ ATPase, NR1 subunit of the NMDA receptor, SNAP-25, 58-K Golgi protein and nuclear pore complex (NPCx). As expected, when PVDF membranes were incubated with the anti-NPCx antibody, a unique and strong immunoreactive band was only observed in samples of N fraction, while a band corresponding in size to the Na^+/K^+ ATPase, NR1 subunit of the NMDA receptor, SNAP-25, 58-K Golgi protein were specifically detected only in P2 fraction (Fig. 20A). We then measured the expression levels of the splice variants of PLCβ1, PLCβ1a and β1b in N, P2 and CYT fractions, using an antibody raised against a common N-terminal sequence of PLCβ1 (Fig. 1; Table 2). Immunoblot analysis revealed specific immunoreactivity for both spliced variants of PLCβ1 (1a and 1b) in every fraction (Fig. 20B). To fully investigate subcellular distribution of PLCβ1a and PLCβ1b, we measured the immunoreactivity of them using increasing amounts of total protein in N, P2 and CYT fractions. Analysis of the standard curves revealed a linear relationship between the amount of protein in each lane and the relative optical density of PLCβ1a and PLCβ1b in all fractions (Fig 20B). The analysis of the slopes revealed a higher immunoreactivity of PLCβ1a than of PLCβ1b in all subcellular fractions, although the

expression of PLCβ1a was significantly higher only in CYT fraction (Figs. 20C, Table 4). The comparative study between PLCβ1a/1b ratios was significantly higher in CYT than in N and P2 fractions (inset in Fig 20C, Table 4).

4. DISCUSSION

This work provides a distribution map of PLCβ1expression along the adult rat neuraxis in far greater detail than heretofore. Additionally, this study shows for the first time useful and until now unknown evidences about cellular expression and subcellular distribution of PLCβ1 in the rat brain that we can summarize as follows:

1) As expected, PLCβ1 was expressed exclusively in neurons of all encephalic regions analyzed. However, as an exception to the general non-matching distribution of GFAP (astrocyte marker) and PLCβ1, a high degree of co-expression was observed in radial glia-like processes of the spinal cord white matter (Figs. 14J-L), being particularly evident in the portions closest to the pial surface.

2) In somatosensory cortex, 68,8 ± 2,16 % of the total GABAergic population was PLCβ1-immunopositive, with almost half of these neurons displaying moderate to high levels of immunofluorescence, as judged qualitatively, More than 60% of GABAergic neurons were co-stained with PLCβ1 in layers I, II-III, IV and VI, whereas this percentage was substantially lower (41,76 ± 5,95 %) in layer V (Figs. 15-16). These results undoubtedly show that PLCβ1, far from being unique to principal cells of the cortex, is also widely expressed in GABAergic populations.

3) In PLCβ1-immunopositive intact nuclei of cerebral cortex, we observed a high overlap with the signals provided by the markers of the nuclear speckles NeuN/Fox3 and SC-35 (Figs. 19G-L). In contrast, we found no co-localization with markers of the

nuclear nuclear envelope and lamina.

4.1. Technical considerations

An important contribution of the present study lies in the spatial resolution achieved at the light and confocal microscopic levels thanks to key modifications of the established histological method for immunodetection. It has become clear that tissue fixation and processing can strongly influence the outcome of immunohistochemical experiments due to their strong impact on tissue antigenicity (Fritchy, 2008). Before performing the main experiments, we tried out different fixation protocols and antibody dilutions. Variables tested were washing buffers, composition of fixatives, duration of perfusion and post-fixation times, antigen retrieval, and concentration of primary antibodies. We found that a simple brief perfusion with 0.37% sulphide buffer before paraformaldehyde fixation notably improved sensitivity of the immunohistochemical and immunofluorescence labelling, allowing for a higher spatial resolution at the light and confocal microscope levels. This fixation procedure has been widely used to perform Timm staining (Sloviter, 1982; Tauck and Nadler, 1985; Davenport et al., 1990; Mitchell et al., 1993), and it has been described as a good method for improving immunoreactivity without compromising the immunostaining profile of different proteins (Mitchell et al., 1993). Shortening the duration of paraformaldehyde perfusion and post-fixation times was also critical. In our hands, immunostained structures were clearly distinguishable from background, allowing us to map the distribution of PLCβ1 in the rat brain. The high co-localization found in double immunofluorescence experiments using couples of antibodies either raised in different species or directed against different regions of PLCβ1 discards the possibility that our findings could be attributed to an artifactual effect of our methodological modifications. In addition,

neuroanatomical distribution of PLCβ1 protein described here (see discussion bellow) correlates well with that previously reported in the mouse brain using "in situ" hybridization (Ross et al. 1989; Watanabe et al. 1998a; Allen Mouse Brain Atlas, 2009). Taken together, our results argue against the possibility of an artifact due to our methodological modifications.

4.2. Correlation with previous immunohistochemical and in situ hybridization studies

The gross distribution of PLCβ1-immunohistochemical staining in the rat central nervous system described here is consistent with previous evidences in mice, showing a predominant expression of PLCβ1 protein (Fukaya et al. 2008) in cerebral cortex, caudate-putamen and hippocampus, along with lower levels in diencephalon, brainstem and cerebellum. In addition, we found strong immunoreactivity in functionally relevant telencephalic regions shown to express high mRNA levels, such as the olfactory tubercle, the lateral part of dorsal septum and the bed nucleus of stria terminalis (Watanabe et al. 1998a). Moreover, our results of PLCβ1 protein distribution are accurately correlated with previous mapping using in situ hybridization approach (compare our figures with those of the Allen Mouse Brain Atlas, 2009). This highly concordant distribution was also seen in regions of lower PLCβ1 expression, such as reticular and midline nuclei of thalamus or motor neurons of the brainstem and spinal cord. Also in good agreement with the images available in the Allen Mouse Brain Atlas (2009) is the intense immunoreactivity found in the lamina II of spinal cord. With regards to the cell morphologies, our results are roughly in line with those of Fukaya et al. (2008). Nevertheless, we detected PLCβ1 not only in the somatodendritic domain of principal cells of cerebral cortex and hippocampus but also in putative inhibitory

neurons, again agreeing with in situ hybridization (Watanabe et al. 1998a; Allen Mouse Brain Atlas, 2009), leading us to explore the possibility that cortical GABAergic neurons might express PLCβ1 (see discussion bellow).

The high anatomical resolution achieved in our immunohistochemical analysis allowed to observe a high overlap between PSD-95 and PLCβ1 signals in the cerebral cortex, thus confirming a well defined subcellular location for PLCβ1, which previously could be only demonstrated by Western blot analysis of subcellular fractions (Taguchi et al. 2007) or electron microscopy (Fukaya et al. 2008). A reasonable explanation of this is that our fixation method may have exposed epitopes localized to the postsynaptic densities. In this regards, several evidences indicate that postsynaptic density proteins are inaccessible to antibodies due to limited penetration (Fritschy et al. 1998; Watanabe et al. 1998b) and, in fact, Fukaya et al. (2008) could detect PLCβ1 at postsynaptic densities only by postembedding immunogold, whereas they were unable to demonstrate a clear postsynaptic membrane labelling in free floating sections. In agreement with evidence that PLCβ1 is mostly located at presynaptic sites (Fukaya et al. 2008) and with its apparent absence from the PSD-95 complex (Dosemeci et al. 2007), the intensity levels of PLCβ1 and PSD-95 signals were not correlated each to other, as expected for two proteins that do not interact despite their close proximity.

Collectively, the precise neuroanatomical data presented here provide neurobiologists with a framework for achieving a deeper understanding of PLCβ1 localization and functions in discrete regions of the central nervous system in both physiological and pathological conditions.

4.3. Spinal cord and glial PLCβ1

All laminae of the spinal cord gray matter showed PLCβ1 expression, intensity of staining varied considerably among them (Fig. 12B, Table 5). Immunoreactivity was highest in lamina II. Interestingly, CB1 cannabinoid receptor mRNA is expressed in intrinsic dorsal horn neurons (Mailleux and Vanderhaegen 1992; Agarwal et al. 2007) and, indeed, high levels of CB1 protein are present in laminae I and II (Farquhar-Smith et al. 2000). Given the anti-hyperalgesic effects of cannabinoids, our results add a new element into the established anatomical basis underlying the regulation of nociceptive transmission by endocannabinoids (PLCβ-dependent production) acting on CB1 cannabinoid receptors at spinal levels.

Our combined PLCβ1- and GFAP-immunofluorescence labelling experiments showed no matching between both markers throughout gray matter of the central nervous system. As shown in figures 14A-I, strongly stained GFAP immunopositive cell processes were distributed in regions virtually devoid of PLCβ1 labelling. As an exception to the general non-matching distribution of GFAP and PLCβ1, a high degree of co-expression was observed in radial glia-like processes of the spinal cord white matter (Figs. 14J-L), being particularly evident in the portions closest to the pial surface. At the moment, the role played by PLCβ1 signalling in the physiological functions of astrocytes seems negligible as compared with other members of the PLCβ family. In fact, a precise panel of glial PLC isoforms has been determined in two very useful cellular models for studying in vitro glial biology and pathology: astrocytes obtained from i) foetal primary cultures of rat brain and ii) an established glioma cell line, rat astrocytoma C6 cell line, and PLCβ1 isoform was exclusively expressed in C6 cells (Lo Vasco et al. 2007).

4.3. Distribution of PLCβ1 in GABAergic neurons of the somatosensory cortex

As described above, immunohistochemical labelling revealed a considerable morphological heterogeneity among PLCβ1-positive cells in the cortex, even though there was a marked predominance of pyramidal morphologies. The neuronal population of the neocortex is constituted by 70-80% of pyramidal neurons and the remaining 20-30% by local circuit neurons or interneurons (Kawaguchi and Kubota, 1997; Marín, 2012, see references therein). Local circuit interneurons have varied morphologies, that can be classified according to their anatomy, electrophysiology and expression of different calcium-binding proteins (calretinin, calbindin, and/or parvalbumin), and although typically GABAergic, they can also express a number of different neuropeptide co-transmitters, such as somatostatin, vasoactive intestinal peptide (VIP), neuropeptide Y, and cholecystokinin (CCK) (Cauli et al. 1997; Kawaguchi and Kubota 1997; De Felipe 2002; Bacci et al., 2003). The double immunofluorescence with anti-PLCβ1 and a cocktail of monoclonal antibodies against calretinin, parvalbumin and somatostatin expressing neurons, which account for the majority of cortical GABAergic neurons (Kawaguchi and Kubota, 1997) demonstrated that 68% of the total GABAergic population was PLCβ1-immunopositive. The proportion of GABAergic neurons co-stained with PLCβ1 was similar in layers I, II-III, IV, and VI, and significantly lower in layer V (41%) than in I, II-III, and VI. Our results demonstrating that that PLCβ1 is also widely expressed in GABAergic populations raise the question whether this marker (PLCβ1-positive) dissect the GABAergic interneurons population into two non-overlapping subsets, as demonstrated for the CB1 cannabinoid receptor (Bodor et al. 2005). The presence of PLCβ1 at interneuron-interneuron synapses adds a component of the cellular enzymatic cascade required for endocannabinoid synthesis, and suggests

that either layer can be able to produce and to release endocannabinoids. In this sense, although endocannabinoids and CB1 cannabinoid receptor activation play a role in regulating afferent inhibition onto pyramidal neurons, it is not clear whether they serve a similar function at interneuron-interneuron synapses. Therefore, these results may contribute to explain previous data showing that endocannabinoids and CB1 receptor activation in GABAergic interneurons play a role in regulating afferent inhibition onto GABAergic interneurons (Bacci et al. 2004; Beierlein and Regehr 2006; Ali 2007; Marinelli et al. 2008). In particular, in low-threshold-spiking (LTS) GABAergic neurons (CCK-positive) of the rat somatosensory cortical layer V, prolonged depolarization induces an autocrine hyperpolarisation mediated by somatodendritic CB1 cannabinoid receptors, due to the production of 2-AG by these interneurons (Bacci et al. 2004; Marinelli et al. 2008). Another study, suggests that depolarization-induced suppression of inhibition (DSI) may occur between GABAergic interneurons expressing CCK in the hippocampus (Ali 2007). In rat somatosensory cortex and hippocampus, CB1 immunoreactivity is mostly found on large cholecystokinin (CCK)-expressing interneurons (Katona et al. 1999; Tsou et al. 1999; Bodor et al. 2005). Both CB1 mRNA and immunoreactivity are rarely detected in interneurons positive for parvalbumin, calretinin, somatostatin, or VIP (Marsicano and Lutz 1999; Bodor et al. 2005). This is in contrast with a previous mapping report showing that VIP and calretinin co-localize with CCK in GABAergic interneurons in the frontal cortex (Kubota and Kawaguchi 1997). Furthermore, single-cell PCR analysis detects CB1 mRNA in more than half of the latter two types of interneurons (Hill et al. 2007). Moreover, neocortical interneurons expressing somatostatin or VIP also possess CB1 cannabinoid receptors in contradiction with the reported presence of CB1 cannabinoid receptors mainly on large CCK neurons (Hill et al. 2007). Therefore, although it is possible that there is a lack of

co-localization between PLCβ1 and CB1 cannabinoid receptors on GABAergic neurons, i.e. absence of PLCβ1 in large CCK-expressing interneurons, this specific point needs to be clarified in the future.

4.5. Nuclear localization of PLCβ1

Most of the research on signal transduction pathways based on PLCβ1 has been devoted to studying phenomena that take place at the plasma membrane. However, the work of several independent laboratories have consistently demonstrated that the phosphoinositide cycle (biosynthetic and hydrolytic machinery) is present in the cell nucleus, and may be important for various nuclear events such as mRNA export, DNA repair and gene transcription (Irvine 2003; Martelli et al. 2005). In fact, PLCβ1 was originally identified at the nuclear level (Martelli et al. 1992; Divecha et al. 1993), and now its role in the control of cell proliferation or cell cycle progression in several cellular models is well established (Cocco et al. 2009; Avazeri et al. 2003). The evidence obtained with confocal and electron microscope analysis indicates that enzymes required for the synthesis and hydrolysis of phosphoinositides are localized at the nuclear membrane and at ribonucleoprotein structures of the inner nuclear matrix involved in transcript processing within the interchromatin domains (Boronenkov et al. 1998; Osborne et al. 2001; Tabellini et al. 2003; Jones and Divecha 2004). With respect to PLCβ1, confocal and immune-electron microscopy and classical biochemical techniques provide evidence about its presence the nucleus of several cellular models. In rat liver, Swiss 3T3, MEL and PC-12 cells, PLCβ1 resides in the nuclear inner matrix and lamina, and this intranuclear partitioning is further stressed in *in situ* matrix preparations which demonstrate that PLCβ1 is a structural insoluble component of the

inner nuclear matrix and of the nucleolar remnant, while it is absent from the nuclear pore-lamina complex (Zini et al. 1993; Zini et al. 1994; Bertagnolo et al. 1995; Crljen et al. 2004; Fiume et al. 2009). Probably, PLCβ1 is preferentially located in subnuclear domains known as speckles, which are involved in splicing events and can be easily identified by specific markers, as the splicing factors (Bavelloni et al. 2006). Finally, it has been demonstrated that PLCβ1 and lamin B1 localize and physically interact in the nucleus of MEL cells (Fiume et al. 2009). With these evidences in mind, we sought to explore whether PLCβ1 is actually present in the nucleus of cells of neural origin. In our study, PLCβ1 and the nuclear speckles markers NeuN/Fox3 and SC-35 (Osborne et al. 2001; Tabellini et al. 2003; Dent et al., 2010) displayed an overlapping pattern, with the proteins being localized to chromatin-poor compartments (Figs. 19A-F). In contrast, no co-localization was found with nuclear pore complex and lamin B1. Clearly, the data reported here appear to shed new light on the presence of the PLCβ1 at the neuronal nuclear compartment.

As already shown in rodent and human tissues (Bahk et al. 1994; Caricasole et al. 2000; Peruzzi et al. 2002), PLCβ1 exists as two alternatively splice variants, the 150 kDa PLCβ1a (1216 aa) and the 140 kDa PLCβ1b (1141 aa), derived from alternative splicing at the 3' end of the gene (Caricasole et al. 2000; Peruzzi et al. 2002). The PLCβ1b variant replaces the 75 C-terminal residues of PLCβ1a with 32 residues unique to PLCβ1b (Bahk et al., 1994; Caricasole et al. 2000; Peruzzi et al. 2000). The importance of the PLCβ1 C-terminal domain may rely in two aspects. First of all, C-terminal region contains determinants for Gαq and phosphatidic acid stimulation, GAP activity, electrostatic dependent association with membrane lipids, nuclear localization, and phosphorylation/regulation by protein kinase Cα and MAP kinase (Bahk et al.

1994; Litosch 2000; Martelli et al. 2000; Xu et al. 2001a; 2001b). Although, a nuclear localization motif has been mapped to a cluster of lysine residues (between 1055 and 1072) which is common to both variants (Kim et al. 1996), PLCβ1a has in its unique C-terminal a typical nuclear export signal which may result in this variant being less concentrated in the nucleus (Bahk et al. 1994). Thus, although the two splice variants of PLCβ1 have identical Gαq-interacting domains and are comparably stimulated by Gαq, display a different subcellular localization; PLCβ1a being equally distributed in the plasma membrane, in the cytoplasm and in the nucleus, and the PLCβ1b almost completely nuclear, as demonstrated by Western blot and inmunofluorescence in several cell lines (C6Bu-1 glioma and MEL cells) and in rat liver tissue (Bahk et al. 1998; Faenza et al. 2000; Crljen et al. 2004; Fiume et al. 2005). In the last 5 years, by using cardiomyocytes it has been demonstrated the critical role of C-terminal region of PLCβ1b in targeting this splice variant to subcellular compartments as the sarcolemma (Grubb et al. 2008). Our immunoblot analysis using an antibody targeted against the common N-terminal of PLCβ1, was able to detect the presence of the two variants of PLCβ1 in different cell compartments (plasma membrane, cytosolic and nuclear fractions) obtained from cerebral cortex. However, PLCβ1a was clearly predominant in all the studied fractions.

Therefore, the deeper understanding of the neuroanatomical, cellular and subcellular location of PLCβ1 presented here may represent a starting point for considering additional research in order to characterize the distribution of its splice variants, and to shed light on the putative role of nuclear PLCβ1 pools in the regulation of cell cycle progression and differentiation in cells of neural origin.

5. ACKNOWLEDGMENTS

Authors thank to Professor H.-S. Shin (Center for Neural Science, Korea Institute of Science and Technology, Seoul, Korea) who has provided us the PLCβ1-KO mice. The authors wish to thank Ricardo Andrade (Servicio de Microscopía Analítica y de Alta Resolución en Biomedicina, SGIker: UPV/EHU, MICINN, GV/EJ, ESF) for skilful technical assistance with confocal microscopy experiments. We also thank Laura Ansotegi (Servicio General de Animalario del Campus de Álava, SGIker: UPV/EHU, MICINN, GV/EJ, ESF) for care of the animals, and Juan Pablo Villamor and Juan Manuel Rodríguez for their technical assistance.

6. GRANTS

This work was supported by grants the Basque Government (SAIOTEK SE-PE07UN21, SAIOTEK S-PE08UN29, GIC/IT-330-10 and BFI-07.277 to L.E.); University of the Basque Country (NUPV08/05 and 069/2005 to M.M.); and the Instituto de Salud Carlos III, Centro de Investigación Biomédica en Red de Salud Mental, CIBERSAM.

7. REFERENCES

Agarwal N, Pacher P, Tegeder I, Amaya F, Constantin CE, Brenner GJ, Rubino T, Michalski CW, Marsicano G, Monosy K, Mackie K, Marian C, Batkai S, Parolaro D, Fischer MJ, Reeh P, Kunos G, Kress M, Lutz B, Woolf CJ, Kuner R (2007) Cannabinoids mediate analgesia largely via peripheral type 1 cannabinoid receptors in nociceptors. Nat Neurosci 10:870-879.

Aisiku OR, Runnels LW, Scarlata S (2010) Identification of a novel binding partner of phospholipase C β1: Translin-associated factor X. PLos One 5: e15001

Aisiku OR, Dowal L, Scarlata S (2011) Protein kinase C phosphorylation of PLCβ1 regulates its cellular localization. Arch Biochem Biophys 509: 186-190.

Alheid GF, Beltramino CA, De Olmos JS, Forbes MS, Swanson DJ, Heimer L (1998) The neuronal organization of the supracapsular part of the stria terminalis in the rat: the dorsal component of the extended amygdala. Neuroscience 84:967-996.

Alheid GF, de Olmos J, Beltramino CA (2004) Amygdala and extended amygdala. In: Paxinos G, editor. The rat nervous system. San Diego: Academic Press. pp 495-578.

Ali AB (2007) Presynaptic Inhibition of GABAA receptor-mediated unitary IPSPs by cannabinoid receptors at synapses between CCK-positive interneurons in rat hippocampus. J Neurophysiol 98:861-869.

Allen Mouse Brain Atlas. 2009. Seattle (WA): Allen Institute for Brain Science. Available from: http://mouse.brain-map.org/welcome.do;jsessionid=2620F746C59ED847E897FC8621401A4F

Avazeri N, Courtot AM, Pesty A, Duquenne C, Lefevre B (2000) Cytoplasmic and nuclear phospholipase C-beta 1 relocation: role in resumption of meiosis in the mouse oocyte. Mol Biol Cell 11:4369-4380.

Avazeri N, Courtot AM, Pesty A, Lefevre B (2003) Meiosis resumption, calcium-sensitive period, and PLC-beta1 relocation into the nucleus in the mouse oocyte. Cell Signal 15:1003-1010.

Bacci A, Rudolph U, Huguenard JR, Prince DA (2003) Major differences in inhibitory synaptic transmission onto two neocortical interneuron subclasses. J Neurosci 23:9664-9674.

Bacci A, Huguenard JR, Prince DA (2004) Long-lasting self-inhibition of neocortical

interneurons mediated by endocannabinoids. Nature 431:312-316.

Bahk YY, Lee YH, Lee TG, Seo J, Ryu SH, Suh PG (1994) Two forms of phospholipase C-beta 1 generated by alternative splicing. J Biol Chem 269:8240-8245.

Bahk YY, Song H, Baek SH, Park BY, Kim H, Ryu SH, Suh PG (1998) Localization of two forms of phospholipase C-beta1, a and b, in C6Bu-1 cells. Biochim Biophys Acta 1389:76-80.

Bavelloni A, Faenza I, Cioffi G, Piazzi M, Parisi D, Matic I, Maraldi NM, Cocco L (2006) Proteomic-based analysis of nuclear signaling: PLC beta1 affects the expression of the splicing factor SRp20 in Friend erythroleukemia cells. Proteomics 6:5725-5734.

Beierlein M, Regehr WG (2006) Local interneurons regulate synaptic strength by retrograde release of endocannabinoids. J Neurosci 26:9935-9943.

Bertagnolo V, Mazzoni M, Ricci D, Carini C, Neri LM, Previati M, Capitani S (1995) Identification of PI-PLC beta 1, gamma 1, and delta 1 in rat liver: subcellular distribution and relationship to inositol lipid nuclear signalling. Cell Signal 7:669-678.

Bodor AL, Katona I, Nyiri G, Mackie K, Ledent C, Hajos N, Freund TF (2005) Endocannabinoid signaling in rat somatosensory cortex: Laminar differences and involvement of specific interneuron types. J Neurosci 25:6845-6856.

Boronenkov IV, Loijens JC, Umeda M, Anderson RA (1998) Phosphoinositide signaling pathways in nuclei are associated with nuclear speckles containing pre-mRNA processing factors. Mol Biol Cell 9:3547-3560.

Camps M, Hou C, Sidiropoulos D, Stock JB, Jakobs KH, Gierschik P (1992) Stimulation of phospholipase C by guanine-nucleotide-binding protein beta gamma subunits. Eur J Biochem 206:821-831.

Caricasole A, Sala C, Roncarati R, Formenti E, Terstappen GC (2000) Cloning and characterization of the human phosphoinositide-specific phospholipase C-beta 1 (PLC beta 1). Biochim Biophys Acta 1517:63-72.

Cauli B, Audinat E, Lambolez B, Angulo MC, Ropert N, Tsuzuki K, Hestrin S, Rossier J (1997) Molecular and physiological diversity of cortical nonpyramidal cells. J Neurosci 17:3894-3906.

Cocco L, Faenza I, Follo MY, Billi AM, Ramazzotti G, Papa V, Martelli AM, Manzoli L (2009) Nuclear inositides: PI-PLC signaling in cell growth, differentiation and pathology. Adv Enzyme Regul 49:2-10.

Crljen V, Visnjic D, Banfic H (2004) Presence of different phospholipase C isoforms in the nucleus and their activation during compensatory liver growth. FEBS Lett 571:35-42.

Davenport CJ, Brown WJ, Babb TL (1990) Sprouting of GABAergic and mossy fiber axons in dentate gyrus following intrahippocampal kainite in the rat. Exp Neurol 109: 180-190.

DeFelipe J (2002) Cortical interneurons: from Cajal to 2001. Prog Brain Res 136:215-238.

Dent MAR, Segura-Anaya E, Alva-Medina J, Aranda-Anzaldo A (2010) NeuN/Fox-3 is an intrinsic component of the neuronal nuclear matrix. FEBS Letters 584: 2767-2771.

Divecha N, Rhee SG, Letcher AJ, Irvine RF (1993) Phosphoinositide signalling

enzymes in rat liver nuclei: phosphoinositidase C isoform beta 1 is specifically, but not predominantly, located in the nucleus. Biochem J 289:617-620.

Dosemeci A, Makusky AJ, Jankowska-Stephens E, Yang X, Slotta DJ, Markey SP (2007) Composition of the synaptic PSD-95 complex. Mol Cell Proteomics 6:1749-1760.

Drin G, Scarlata S (2007) Stimulation of phospholipase C beta by membrane interactions, interdomain movement, and G protein binding--how many ways can you activate an enzyme?. Cell Signal 19:1383-1392.

Faenza I, Matteucci A, Manzoli L, Billi AM, Aluigi M, Peruzzi D, Vitale M, Castorina S, Suh PG, Cocco L (2000) A role for nuclear phospholipase C beta 1 in cell cycle control. J Biol Chem 275:30520-30524.

Farquhar-Smith WP, Egertova M, Bradbury EJ, McMahon SB, Rice AS, Elphick MR (2000) Cannabinoid CB1 receptor expression in rat spinal cord. Mol Cell Neurosci 15:510-521.

Fiume R, Faenza I, Matteucci A, Astolfi A, Vitale M, Martelli AM, Cocco L (2005) Nuclear phospholipase C beta1 affects CD24 expression in murine erythroleukemia cells. J Biol Chem 280:24221-24226.

Fiume R, Ramazzotti G, Teti G, Chiarini F, Faenza I, Mazzotti G, Billi AM, Cocco L (2009) Involvement of nuclear PLC beta1 in lamin B1 phosphorylation and G2/M cell cycle progression. FASEB J 23:957-966.

Fritschy JM, Weinmann O, Wenzel A, Benke D (1998) Synapse-specific localization of NMDA and GABA(A) receptor subunits revealed by antigen-retrieval immunohistochemistry. J Comp Neurol 390:194-210.

Fukaya M, Uchigashima M, Nomura S, Hasegawa Y, Kikuchi H, Watanabe M (2008) Predominant expression of phospholipase C beta1 in telencephalic principal neurons and cerebellar interneurons, and its close association with related signaling molecules in somatodendritic neuronal elements. Eur J Neurosci 28:1744-1759.

Garro MA, López de Jesus M, Ruiz de Azúa I, Callado LF, Meana JJ, Sallés J (2001) Regulation of phospholipase C beta activity by muscarinic acetylcholine and 5-HT2 receptors in crude and synaptosomal membranes from human cerebral cortex. Neuropharmacology 40:686-695.

Gonchar Y, Burkhalter A (1997) Three distinct families of GABAergic neurons in rat visual cortex. Cereb Cortex 7:347-358.

Graybiel AM, Aosaki T, Flaherty AW, Kimura M (1994) The basal ganglia and adaptive motor control. Science 265:1826-1831.

Grubb DR, Vasilevski O, Huynh H, Woodcock EA (2008) The extreme C-terminal region of phospholipase C beta1 determines subcellular localization and function; the "b" splice variant mediates alpha1-adrenergic receptor responses in cardiomyocytes. FASEB J 22:2768-2774.

Hannan AJ, Kind PC, Blakemore C (1998) Phospholipase C-beta1 expression correlates with neuronal differentiation and synaptic plasticity in rat somatosensory cortex. Neuropharmacology 37:593-605.

Hannan AJ, Blakemore C, Katsnelson A, Vitalis T, Huber KM, Bear M, Roder J, Kim D, Shin HS, Kind PC (2001) PLC-beta1, activated via mGluRs, mediates activity-dependent differentiation in cerebral cortex. Nat Neurosci 4:282-288.

Hill EL, Gallopin T, Ferezou I, Cauli B, Rossier J, Schweitzer P, Lambolez B (2007)

Functional CB1 receptors are broadly expressed in neocortical GABAergic and glutamatergic neurons. J Neurophysiol 97:2580-2589.

Irvine RF (2003) Nuclear lipid signalling. Nat Rev Mol Cell Biol 4:349-360.

Jones DR, Divecha N (2004) Linking lipids to chromatin. Curr Opin Genet Dev 14:196-202.

Kano M, Hashimoto K, Watanabe M, Kurihara H, Offermanns S, Jiang H, Wu Y, Jun K, Shin HS, Inoue Y, Simon MI, Wu D (1998) Phospholipase C beta4 is specifically involved in climbing fiber synapse elimination in the developing cerebellum. Proc Natl Acad Sci USA 95:15724-15729.

Katona I, Sperlagh B, Sik A, Kafalvi A, Vizi ES, Mackie K, Freund TF (1999) Presynaptically located CB1 cannabinoid receptors regulate GABA release from axon terminals of specific hippocampal interneurons. J Neurosci 19:4544-4558.

Kawaguchi Y, Kubota Y (1997) GABAergic cell subtypes and their synaptic connections in rat frontal cortex. Cereb Cortex 7:476-486.

Kim CG, Park D, Rhee SG (1996) The role of carboxyl-terminal basic amino acids in Gqalpha-dependent activation, particulate association, and nuclear localization of phospholipase C-beta1. J Biol Chem 271:21187-21192.

Kim D, Jun KS, Lee SB, Kang NG, Min DS, Kim YH, Ryu SH, Suh PG, Shin HS (1997) Phospholipase C isozymes selectively couple to specific neurotransmitter receptors. Nature 389:290-293.

Koh H-Y, Kim D, Lee J, Lee S, Shin H-S (2008) Deficits in social behavior and sensorimotor gating in mice lacking phospholipase Cβ1. Genes, Brain and Behavior 7: 120-128.

Kubota Y, Kawaguchi Y (1997) Two distinct subgroups of cholecystokinin-immunoreactive cortical interneurons. Brain Res 752:175-183.

Lee CW, Park DJ, Lee KH, Kim CG, Rhee SG (1993) Purification, Molecular-Cloning, and Sequencing of Phospholipase-C-beta4. J Biol Chem 268:21318-21327.

Lee KY, Ryu SH, Suh PG, Choi WC, Rhee SG (1987) Phospholipase-C Associated with Particulate Fractions of Bovine Brain. Proc Nat Acad Sci USA 84:5540-5544.

Litosch I (2000) Regulation of phospholipase C-beta1 activity by phosphatidic acid. Biochemistry 39:7736-7743.

Lo Vasco VR, Fabrizi C, Artico M, Cocco L, Billi AM, Fumagalli L, Manzoli FA (2007) Expression of phosphoinositide-specific phospholipase C isoenzymes in cultured astrocytes. J Cell Biochem 100:952-959.

López de Jesus M, Zalduegui A, Ruiz de Azúa I, Callado LF, Meana JJ, Sallés J (2006) Levels of G-protein alpha q/11 subunits and of phospholipase C-beta(1-4), -gamma, and -delta1 isoforms in postmortem human brain caudate and cortical membranes: potential functional implications. Neurochem Int 49:72-79.

Mailleux P, Vanderhaeghen JJ (1992) Distribution of neuronal cannabinoid receptor in the adult rat brain: a comparative receptor binding radioautography and in situ hybridization histochemistry. Neuroscience 48:655-668.

Marín O (2012) Interneuron dysfunction in psychiatric disorders. Nat Rev Neurosci 13:107-120.

Marinelli S, Pacioni S, Bisogno T, Di M, V, Prince DA, Huguenard JR, Bacci A (2008) The endocannabinoid 2-arachidonoylglycerol is responsible for the slow self-inhibition in neocortical interneurons. J Neurosci 28:13532-13541.

Marsicano G, Lutz B (1999) Expression of the cannabinoid receptor CB1 in distinct neuronal subpopulations in the adult mouse forebrain. Eur J Neurosci 11:4213-4225.

Martelli AM, Gilmour RS, Bertagnolo V, Neri LM, Manzoli L, Cocco L (1992) Nuclear localization and signalling activity of phosphoinositidase C beta in Swiss 3T3 cells. Nature 358:242-245.

Martelli AM, Billi AM, Manzoli L, Faenza I, Aluigi M, Falconi M, De PA, Gilmour RS, Cocco L (2000) Insulin selectively stimulates nuclear phosphoinositide-specific phospholipase C beta1 activity through a mitogen-activated protein (MAP) kinase-dependent serine phosphorylation. FEBS Lett 486:230-236.

Martelli AM, Fiume R, Faenza I, Tabellini G, Evangelista C, Bortul R, Follo MY, Fala F, Cocco L (2005) Nuclear phosphoinositide specific phospholipase C-beta 1: a central intermediary in nuclear lipid-dependent signal transduction. Histol Histopathol 20:1251-1260.

McOmish CE, Burrows E, Howard M, Scarr E, Kim D, Shin HS, Dean B, van den Buuse M, Hannan AJ (2008a) Phospholipase C beta1 knockout mice exhibit endophenotypes modelling schizophrenia which are rescued by environmental enrichment and clozapine administration. Mol Psycchiatry 13: 661-672.

McOmish CE, Burrows E, Howard M, Hannan AJ (2008b) PLCbeta1 knockout mice as a model of disrupted cortical development and plasticity: Behavioural endophenotypes and dysregulation of RGS4 gene expression. Hippocampus 18: 824-834.

Mitchell J, Best N, Sundstrom LE, Wheal HV (1993) The use of sodium sulphide-fixed brain tissue for immunocytochemical staining of activated microglia and reactive

astrocytes. Histochemistry 99: 91-94.

Miyara F, Pesty A, Migne C, Djediat C, Huang XB, Dumont-Hassan M, Debey P, Lefevre B (2008) Spontaneous calcium oscillations and nuclear PLC-beta1 in human GV oocytes. Mol Reprod Dev 75:392-402.

Nakamura M, Sato K, Fukaya M, Araishi K, Aiba A, Kano M, Watanabe M (2004) Signaling complex formation of phospholipase C beta4 with metabotropic glutamate receptor type 1alpha and 1,4,5-trisphosphate receptor at the perisynapse and endoplasmic reticulum in the mouse brain. Eur J Neurosci 20:2929-2944.

Nomura S, Fukaya M, Tsujioka T, Wu DQ, Watanabe M (2007) Phospholipase C beta 3 is distributed in both somatodendritic and axonal compartments and localized around perisynapse and smooth endoplasmic reticulum in mouse Purkinje cell subsets. Eur J Neuros 25:659-672.

Osborne SL, Thomas CL, Gschmeissner S, Schiavo G (2001) Nuclear PtdIns(4,5)P2 assembles in a mitotically regulated particle involved in pre-mRNA splicing. J Cell Sci 114:2501-2511.

Peruzzi D, Calabrese G, Faenza I, Manzoli L, Matteucci A, Gianfrancesco F, Billi AM, Stuppia L, Palka G, Cocco L (2000) Identification and chromosomal localisation by fluorescence in situ hybridisation of human gene of phosphoinositide-specific phospholipase C beta1. Biochim Biophys Acta 1484:175-182.

Peruzzi D, Aluigi M, Manzoli L, Billi AM, Di Giorgio FP, Morleo M, Martelli AM, Cocco L (2002) Molecular characterization of the human PLC beta1 gene. Biochim Biophys Acta 1584:46-54.

Rebecchi MJ, Pentyala SN (2000) Structure, function, and control of phosphoinositide-

specific phospholipase C. Physiol Rev 80:1291-1335.

Ross CA, MacCumber MW, Glatt CE, Snyder SH (1989) Brain phospholipase C isozymes: differential mRNA localizations by in situ hybridization. Proc Natl Acad Sci USA 86:2923-2927.

Ruiz de Azúa I, del Olmo E, Pazos A, Sallés J (2006) Transmembrane signaling through phospholipase C-beta in the developing human prefrontal cortex. J Neurosci Res 84:13-26.

Sallés J, López de Jesus M, Goni O, Fernandez-Teruel A, Driscoll P, Tobena A, Escorihuela RM (2001) Transmembrane signaling through phospholipase C in cortical and hippocampal membranes of psychogenetically selected rat lines. Psychopharmacology 154:115-125.

Shin J, Kim D, Bianchi R, Wong RKS, Shin HS (2005) Genetic dissection of theta rhythm heterogeneity in mice. Proc Natl Acad Acad Sci USA 102: 18165-18170.

Sloviter RS (1982) A simplified Timm stain procedure compatible with formaldehyde fixation and routine paraffin embedding of rat brain. Brain Res Bull 8: 771-774.

Smrcka AV, Sternweis PC (1993) Regulation of purified subtypes of phosphatidylinositol-specific phospholipase C beta by G protein alpha and beta gamma subunits. J Biol Chem 268:9667-9674.

Spires TL, Molnar Z, Kind PC, Cordery PM, Upton AL, Blakemore C, Hannan AJ (2005) Activity-dependent regulation of synapse and dendritic spine morphology in developing barrel cortex requires phospholipase C-beta1 signalling. Cereb Cortex 15:385-393.

Suh PG, Park JI, Manzoli L, Cocco L, Peak JC, Katan M, Fukami K, Kataoka T, Yun S,

Ryu SH (2008) Multiple roles of phosphoinositide-specific phospholipase C isozymes. BMB Rep 41:415-434.

Swanson LW (1992) Brain maps: structure of the rat brain. Amsterdam: Elsevier.

Tabellini G, Bortul R, Santi S, Riccio M, Baldini G, Cappellini A, Billi AM, Berezney R, Ruggeri A, Cocco L, Martelli AM (2003) Diacylglycerol kinase-theta is localized in the speckle domains of the nucleus. Exp Cell Res 287:143-154.

Taguchi K, Kumanogoh H, Nakamura S, Maekawa S (2007) Localization of phospholipase C beta1 on the detergent-resistant membrane microdomain prepared from the synaptic plasma membrane fraction of rat brain. J Neurosci Res 85:1364-1371.

Tamamaki N, Yanagawa Y, Tomioka R, Miyazaki J, Obata K, Kaneko T (2003) Green fluorescent protein expression and colocalization with calretinin, parvalbumin, and somatostatin in the GAD67-GFP knock-in mouse. J Comp Neurol 467:60-79.

Tanaka O, Kondo H (1994) Localization of mRNAs for three novel members (beta3, beta4 and gamma2) of phospholipase C family in mature rat brain. Neurosci Lett 182:17-20.

Tauck DL, Nadler JV (1985) Evicence of functional mossy fober sprouting in hippocampal formation of kainic acid-treated rats. J Neurosci 5: 1016-1022.

Tepper JM, Bolam JP (2004) Functional diversity and specificity of neostriatal interneurons. Curr Opin Neurobiol 14:685-692.

Thompson RJ (1973) Studies on RNA synthesis in two populations of nuclei from the mammalian cerebral cortex. J Neurochem 21: 19-40.

Tsou K, Mackie K, Sanudo-Pena MC, Walker JM (1999) Cannabinoid CB1 receptors

are localized primarily on cholecystokinin-containing GABAergic interneurons in the rat hippocampal formation. Neuroscience 93:969-975.

Udawela M, Scarr E, Hannan AJ, Thomas EA, Dean B (2011) Phospholipase Cβ1 expression in the dorsolateral prefrontal cortex from patients with schizophrenia at different stages of illness. Aust NZ J Psychiatry 45: 140-147.

Watanabe M, Nakamura M, Sato K, Kano M, Simon MI, Inoue Y (1998a) Patterns of expression for the mRNA corresponding to the four isoforms of phospholipase C beta in mouse brain. Eur J Neurosci 10:2016-2025.

Watanabe M, Fukaya M, Sakimura K, Manabe T, Mishina M, Inoue Y (1998b) Selective scarcity of NMDA receptor channel subunits in the stratum lucidum (mossy fibre-recipient layer) of the mouse hippocampal CA3 subfield. Eur J Neurosci 10:478-487.

Wu D, Jiang H, Katz A, Simon MI (1993) Identification of critical regions on phospholipase C-beta 1 required for activation by G-proteins. J Biol Chem 268:3704-3709.

Xu A, Suh PG, Marmy-Conus N, Pearson RB, Seok OY, Cocco L, Gilmour RS (2001a) Phosphorylation of nuclear phospholipase C beta1 by extracellular signal-regulated kinase mediates the mitogenic action of insulin-like growth factor I. Mol Cell Biol 21:2981-2990.

Xu A, Wang Y, Xu LY, Gilmour RS (2001b) Protein kinase C alpha -mediated negative feedback regulation is responsible for the termination of insulin-like growth factor I-induced activation of nuclear phospholipase C beta1 in Swiss 3T3 cells. J Biol Chem 276:14980-14986.

Zini N, Martelli AM, Cocco L, Manzoli FA, Maraldi NM (1993) Phosphoinositidase C isoforms are specifically localized in the nuclear matrix and cytoskeleton of Swiss 3T3 cells. Exp Cell Res 208:257-269.

Zini N, Mazzoni M, Neri LM, Bavelloni A, Marmiroli S, Capitani S, Maraldi NM (1994) Immunocytochemical detection of the specific association of different PIC isoforms with cytoskeletal and nuclear matrix compartments in PC12 cells. Eur J Cell Biol 65:206-213.

Captions to figures

Figure 1. Specificity of PLCβ1 antibodies. A. Schematic representation of the sequences of the rat PLCβ1a and PLCβ1b splice variants. Both isoforms share most of their primary structure and differ only in a short region of their C-terminal ends (coloured boxes). Numbers refer to the position of the corresponding amino acid residues in the sequences. Shaded boxes represent the regions recognized by antibodies N-ter, PLCβ136-87, R-233, D-8 and G-12. B-J. Confocal scanning fluorescent photomicrographs of layer V pyramidal cells of the rat cortex. Distribution of immunofluorescence signals using either the rabbit polyclonal R-233 or the mouse monoclonal D-8 antibodies was almost identical (B-D). Double immunofluorescence experiments with PLCβ136-87 and R-233 antibodies yielded similar results, although the overlap was not as complete as that seen by combining R-233 and D-8, mostly due to the presence of a punctate and diffuse staining with PLCβ136-87 antibody (E-G). Again, a high degree of co-localization could be observed by double immunofluorescence using D-8 and the rabbit polyclonal G-12 antibody, which recognizes a short C-terminal sequence unique to the PLCβ1a splice isoform (H-J). K. Immunoblot analysis of homogenates prepared form crude membranes of the rat cortex.

Antibodies to amino acid sequences shared by both splice variants (PLCβ136-87, R-233, D-8 N-ter), specifically recognize two bands with the apparent molecular weights of PLCβ1a and PLCβ1b, whereas G-12 antibody detected only the upper band corresponding to the PLCβ1a isoform. Scale bar = 50 μm.

Figure 2. Specificity of the rabbit polyclonal R-233 antibody. **A-H.** PLCβ1-immunofluorescence in histological sections of the adult brain from the wild-type (A-D) and PLCβ1-KO (E-H) mice. Low power micrographs of coronal sections at the level of the caudate-putamen and septum (A, E). Higher magnification views of the cortical layer V (B, F), dorsal part of the lateral septum (C, G) and caudate-putamen (D, H). Scale bars = 1 mm in E (applies to A, E); 100 μm in H (applies to B-D, F-H). **I.** (A) Frequency histogram of immunofluorescence intensity ranging from 0 to 4095 in the cerebral cortex of the wild-type and PLCβ1-KO mice. Measurements were made on images of the cerebral cortex acquired by confocal laser scanning using a 4X objective and under identical settings for the control and null mice. Each histogram was obtained from data of six frames of 0,23 mm^2. Quantification revealed a drastic decrease in the immunofluorescence intensity in the PLCβ1-KO (575,21 ± 192,31) with respect to the wild-type (1037,42 ± 128,82). **J.** Immunoblot with brain extracts from adult C57BL (lanes 1-3), wild-type (lanes 4-6) and PLCβ1-KO (lanes 7-9) mice using the rabbit polyclonal R-233 antibody. 5 μg (lanes 1, 4, 7), 10 μg (lanes 2, 5, 8) or 20 μg (lanes 3, 6, 9) of total protein was loaded per lane.

Figure 3. Gross neuroanatomical distribution of PLCβ1-immunohistochemical labeling in the adult rat central nervous system. **A-B.** Parasagittal (A) and coronal (B) sections from the rat brain immunostained using the R-233 antibody. Intense immunoreactivity

could be observed in telencephalic regions, being much weaker in the diencephalon, brainstem and cerebellum. Note the intense staining in the cortical layer V and, to a lower extent, in layer II/III. Immunoreactivity was particularly strong in basal forebrain areas (closed arrowheads). Also the hippocampal formation (Hipp), the bed nucleus of the stria terminalis (BST) and the dorsal part of the lateral septum (LSd) displayed an intense immunostaining. Prominent PLCβ1-immunostaining was found in the caudate-putamen (CP), where an oval-shaped core within its ventrolateral aspect stood out by an even higher immunoreactivity (open arrowheads). In the thalamus (Th), moderate PLCβ1-immunostaining could be observed in the reticular nucleus (asterisks). Labeling was very weak throughout the brainstem and spinal cord (SpC), except in motoneuronal pools of the brainstem (e.g. the motor nucleus of the XII cranial nerve) and spinal cord (arrows in A5). In the cerebellum, moderate PLCβ1-staining could be observed in its posterolateral portion, whereas it was barely detected in the rest of the cerebellum. The approximate distance from the midsagittal plane and bregma is indicated on the right of (A) ore bellow (B) each section. Scale bars = 2 mm (bar in A4 applies to A1-A4; bar in A5 applies to A5; bar in B5 applies to B1-B5). **C.** Representative image of western blot analysis (upper) of plasma membrane preparations (8 µg/lane) from selected regions of the rat brain, and bar graph (lower) showing the optical density of the PLCβ1a and PLCβ1b immunoblot signals relative to the PLCβ1a+1b density in the cortex. The data correspond to mean values from four independent experiments. Error bars indicate S.E.M. One-way analysis of variance followed by Tukey´s test demonstrated that immunoreactivity was significantly lower ($p < 0,001$) in the cerebellum compared to the other regions analyzed. No differences were found for the rest of comparisons.

Figure 4. Distribution of PLCβ1-immunoreactivity in the olfactory bulb and basal forebrain. **A.** Low magnification micrograph of a coronal section of the olfactory bulb showing the laminar distribution of PLCβ1-immunostaining. Note the higher staining intensity in the dorsal and, to a lesser extent, ventral aspects. **B.** Higher magnification of framed area in A. **C.** Low power micrograph showing the distribution of PLCβ1 in the basal forebrain in a coronal brain section. **D.** Higher magnification micrograph of framed area in C to illustrate the prominent immunostaining in layer II of the olfactory tubercle (OT) and the diffuse labeling pattern in the islands of Calleja. **E.** High power micrograph of framed area in D. Note the presence of immunostained puncta apparently located within neuronal nuclei (arrows). This pattern was also observed in neuronal populations of the cerebral cortex (see bellow). Scale bars = 300 μm in A, C; 100 μm in B, D; 20 μm in E.

Figure 5. PLCβ1-immunohistochemical staining pattern in the rat cortex. **A-B.** Low magnification micrographs of the primary somatosensory (A) and primary motor (B) isocortical areas showing the distribution of immunostaining. PLCβ was particularly prominent in layer V and, to a lesser extent, deep part of layer II/III, although immunopositive cells were widely distributed throughout the depth of isocortex. **C-H.** Higher magnification images of layers I-II/III (C-D), V (E-F) and VI (G-H) taken at the level of the primary somatosensory (C, E, G) and primary motor (D, F, H) cortices. **I-L.** Low power (I) and higher magnification (J-L) micrographs showing the distribution of PLCβ1 in the prefrontal cortex. Note the differences in the staining intensity between the different regions of the prefrontal cortex. Immunolabeling density was higher in the anterior cingulate cortex (AC) (J) than in the prelimbic (PL) (K) and infralimbic (IL) (L) areas. **M-Q.** Compared to other cortical areas, PLCβ1-staining in the perirhinal cortex

was characterized by an even stronger immunoreactivity in layer V pyramids, whose apical dendrites could be followed from their proximal trunks to their distal tufts in layer I (M-Q). Immunopositive dots located in apparently nuclear locations are particularly prominent in layer V pyramids of the perirhinal cortex (O). Apical dendrites of these neurons were decorated with highly immunoreactive puncta (P). **R-T.** PLCβ1-immunoreactivity in the retrosplenial, piriform and entorhinal cortices. Scale bars = 200 µm in B, M, R and T (bar in B applies to A-B); 100 µm in L and S (bar in L applies to J-L); 50 µm in H (bar in H applies to C-H); 300 µm in I; 15 µm in O; 20 µm in P and Q (bar in Q applies to N and Q).

Figure 6. PLCβ1-immunohistochemical staining in the hippocampal formation. **A.** Panoramic view of the hippocampal formation. Immunostaining could be observed throughout the stratum pyramidale the Ammon's horn (sp). decreasing gradually towards the distal end of CA3. The granular layer (sg) of dentate gyrus was also clearly immunopositive. **B-E.** Higher magnification of framed areas in A. Immunolabeling could be observed in cell somata of pyramidal cells throughout the Ammon's horn (B-D), as well as in dendritic trunks of CA1 and CA2 pyramids (B-C). The strata oriens (so) and radiatum (sr) contained a few scattered cells that were moderate to strongly immunopositive (arrowheads in B-D). Virtually all granule cells of the dentate gyrus resulted intensely stained, whereas numerous neurons appeared moderate to intensely immunolabeled in the polymorph layer (po) (E). Scale bars = 400 µm in A; 100 µm in E (applies to B-E).

Figure 7. Distribution of PLCβ1 in the amygdala and extended amygdala. **A.** Panoramic view of amygdaloid nuclei. Immunostaining was moderate and evenly distributed throughout the nuclei of the amygdaloid complex. **B.** Low magnification micrograph of

a coronal brain section at the level of the bed nucleus of the stria terminalis (BST), where abundant neurons appeared intensely immunostained. **C-E.** Higher magnification micrographs of areas framed in B. Abundant immunostained cellular perikarya (C), some of them forming densely packed clusters (D) are observed in the BST. Also, note the presence of "Rosary-like" chains of immunostained cells embedded within the stria terminalis (st) (E). Scale bars = 500 µm in A-B; 100 µm in E (applies to C-E).

Figure 8. PLCβ1 expression in the septal nuclei. **A.** Low magnification micrograph of the left rat septum showing the distribution of PLCβ1-immunostaining. Strongly stained neurons were observed throughout the lateral septum. Immunostaining intensity and cell density was highest in the dorsal part of the lateral septum (LSd). B. Higher magnification micrograph of the LSd. Both perikarya and dendrites of multipolar-shaped neurons resulted strongly immunostained. Scale bars = 300 µm in A; 100 µm in B.

Figure 9. Distribution of PLCβ1-immunostaining in the basal ganglia. **A-H.** Low power micrographs (A, E) show the PLCβ1-immunostaining distribution in coronal sections of the rat brain at middle (A, approximate bregma level -0,2 mm) and caudal (E), approximate bregma level -1,3 mm) levels of the rostrocaudal axis of the basal ganglia. Higher power micrographs in C-F and F-H correspond to areas framed in A and E, respectively. PLCβ1 is widely expressed throughout the caudate-putamen (CP), but with some differences in labeling intensity. Immunostaining was stronger at middle (A-D) than at caudal (E-F) levels. At middle levels, PLCβ1-immunostaining decreased steadily from the dorsomedial aspect (B) towards the ventrolateral one (C), and then rose drastically in a ventrolaterally confined oval-shaped core of very strong

immunoreactivity (D). Moderate PLCβ1-staining was found in the perikarya and dendrites of neurons scattered throughout the lateral (G) and medial (H) segments of the globus pallidus (GPl, GPm). Scale bars = 400 μm in E (applies to A and E); 100 μm in H (applies to B-D and F-H).

Figure 10. PLCβ1-expression in the rostral diencephalon. **A.** Low magnification micrograph to illustrate the distribution of PLCβ1-immunostaining in the rostral thalamus and hypothalamus. Labeling was mostly restricted to the reticular thalamic nucleus (RT) and to midline thalamic nuclei such as the parataenial (PT), paraventricular (PVT) and reuniens (RE). Hypothalamic nuclei resulted weakly labeled. **B-C.** High magnification micrographs of areas framed in A to illustrate the presence of immunopositive neurons displaying variable levels of staining density and morphologies in the RT (B), PT and PVT (C), and RE (D). Scale bars = 500 μm in A; 50 μm in D (applies to B-D).

Figure 11. PLCβ1-expression in the caudal diencephalon. **A.** Low magnification micrograph to illustrate the distribution of PLCβ1-immunostaining in the caudal thalamus and hypothalamus. Immunolabeling was distributed mainly in the midline nuclei, being highest in the paraventricular (PVT) and intermediodorsal (IMD) followed by reuninens (RE) and perireuniens (PR). At this rostrocaudal level, staining was scarce or barely detected above background in the rest of thalamic nuclei. Most hypothalamic regions were weakly labeled, except the lateral hypothalamic area (LHA), where numerous neurons were moderate to intensely stained, and the tuberomammillary nucleus (lower left inset taken from a more caudal section). Putative histaminergic neurons of this nucleus expressed high levels of PLCβ1. **B-C.** High magnification

micrographs of areas framed in A to illustrate the presence of immunopositive neurons displaying variable levels of staining density and morphologies in the IMD (B) and LHA (C). Scale bars = 500 µm in A; 100 µm in lower left inset; 50 µm in C (applies to B-C).

Figure 12. Distribution of PLCβ1-immunolabeling in the hindbrain and spinal cord. **A.** Micrograph of the cerebellar vermis from a coronal section. Moderate immunostaining was observed throughout all layers of the cerebellar cortex, where cell bodies of Purkinje cells were clearly distinguishable. Note the zebrin-like pattern with alternating stained (closed stars) and unstained (open stars) bands in the molecular layer (ml). Cells of the granular layer (gl) were also moderately labeled, although individual cells were difficult to distinguish. Immunostaining in Purkinje cell bodies and their thicker dendrites was stronger in discrete regions of the flocular lobule (lower right inset). **B.** Low magnification micrograph of a coronal section of the mesencephalon at the level of the inferior colliculus. Weak PLCβ1-immunostaining was found in neurons of the external (ECIC) and dorsal (DCIC) cortices of the inferior colliculus. A higher magnification micrograph of the ECIC is shown in the lower right inset. **C.** Coronal section of the mesencephalon at the level of the periaqueductal gray (PAG) and the nucleus of the III cranial nerve (III). Cells in the dorsal and dorsolateral parts of PAG were weakly labeled, whereas motor neurons of III were moderately PLCβ1-immunostained. **D, F.** Low (D) and high (F) magnification micrographs of a coronal section of the medulla oblongata immunostained for PLCβ1. Immunostaining was mostly confined to motor nuclei such as the hypoglossal nucleus (XII), including the lateral accessory (laXII), and the dorsal nucleus of the vagus nerve (DMX). **E, G-H.** Panoramic view (E) and high magnification (G-H) micrographs of the cervical spinal

cord. In the dorsal horn, immunostaining was highest in lamina II, followed by lamina I and lamina III (E, G). Abundant densely immunopositive cell bodies, hardly distinguishable form the surrounding diffuse staining, were seen in lamina II. PLCβ1 immunostained cells were scarcer in the rest of laminae. In the ventral horn, motor neurons of lamina IX stood out clearly against the surrounding tissue (H). More weakly stained cells were found in laminae VII-VIII (E, H). Scale bars = 100 μm in A (25 μm for the inset); 500 μm in B (100 μm for the inset), D and E; 100 μm in F and H; 50 μm in G; 100.

Figure 13. Double immunofluorescence labeling in different regions of the rat central nervous system using the anti-PLCβ1 rabbit polyclonal R-233 antibody (green) and a mouse monoclonal antibody recognizing the pan-neuronal marker NeuN (red). **A-C.** Layer V pyramidal neurons of the somatosensory cortex. **D-F**. Micrograph at the level of the CA1-CA2 transition zone of the Ammon's horn. **G-I.** Laminae I and II of the dorsal horn of the cervical spinal cord. Every cell soma identified by PLCβ1-staining was NeuN immunopositive (arrowheads). A-F and H-I are maximum intensity projections of three and six consecutive 0.5 μm-thick optical sections, respectively. Scale bars = 50 μm in C (applies to A-C) and F (applies to D-F); 25 μm in I (applies to G-I).

Figure 14. Double inmunofluorescence labeling in representative regions of the rat CNS using the anti-PLCβ1 rabbit polyclonal R-233 antibody (green) and a mouse monoclonal antibody recognizing the astrocyte maker GFAP (red). **A-C.** Layer V of the somatosensory cortex. **D-F**. CA1 region of the Ammon's horn. **G-I.** High magnification micrograph of spinal motor neurons at the level of the cervical spinal cord. **J-L.** Micrograph of the white matter of the spinal cord. No matching between PLCβ1 and

GFAP was observed throughout the white matter (A-I), except in radial glia-like processes of the spinal cord white matter (J-L). A-C and D-L are maximum intensity projections of three and two consecutive 0.5 µm-thick optical sections, respectively. Scale bars = 50 µm in C (applies to A-C) and F (applies to D-F); 25 µm in I (applies to G-I); 100 µm in L (applies to J-L).

Figure 15. Double inmunofluorescence labeling of the rat somatosensory cortex using cocktail of monoclonal antibodies against calretinin-, parvalbumin- and somatostatin-positive GABAergic populations (red) and the anti-PLCβ1 rabbit polyclonal R-233 antibody (green). **A-B.** Example of the 20x confocal maximum projection images used to estimate the percentage of GABAergic neurons that express PLCβ1. **C-R.** Higher magnification micrographs of areas framed in A-B to illustrate the presence of double (closed arrowheads) and single (open arrowheads) PLCβ1-immunolabeled cells in layers II-III (C-H), IV (I-K), V (L-O), VI (P-Q). Most GABAergic neurons were PLCβ1-immunopositive in all layers except layer V. All images are maximum intensity projections of 20 consecutive 0.5 µm-thick optical sections. Scale bars: 100 µm in B (applies to A-B), 50 µm in R (applies to C-R).

Figure 16. Bar graph showing the percentage of PLCβ1-immunoposite neurons from the GABAergic population immunodetected using a cocktail of monoclonal antibodies against calretinin, parvalbumin and somatostatin in the primary somatosensory cortex. Up to 60% of the total population of GABAergic neurons were PLCβ1-immunopositive, either in the entire depth of the cortex or in each layer except layer V, where this percentage was less than 50% and almost half of the doubly labeled neurons showed weak PLCβ1-immunostaining as estimated qualitatively. Black and gray areas

correspond to moderate-to-intensely or weakly stained for PLCβ1 as judged by two experienced observers. Only the values corresponding to the total percentage of doubly labeled cells was used for statistical analysis. One-way ANOVA followed by Tukey's test revealed statistical differences between layer V and the rest, *: $P<0.001$, **: $P<0.01$, ***: $P<0.05$, n = 8. Error bars indicate S.E.M. The upper right inset shows the percentage of GABAergic neurons (of the total immunodetected population) located in each layer of the primary somatosensory cortex.

Figure 17. **A-C.** Double inmunofluorescence labeling in rat cerebral cortex using a rabbit polyclonal antibody recognizing the postsynaptic density protein PSD-95 (green) and anti-PLCβ1 mouse monoclonal D8 antibody (red). **A-C, insets.** Higher magnification and orthogonal views of PSD-95 and PLCβ1-immunopositive puncta. A large amount of PSD-95 puncta was found to co-localize with PLCβ1-immunolabeling in apical dendrites of cortical pyramids, although not all PLCβ1 puncta were PSD-95-positive and viceversa and there was not a clear correlation between the intensity levels of both signals. **D-F.** Low magnification micrograph of immunofluorecence labeling in rat cortical pyramidal cells using the rabbit polyclonal R-233 antibody (green) combined with chromatin staining using the Hoechst's dye (red). Note the presence of intensly labeled rounded spots in neuronal nuclei. **G-I.** Higher magnification and orthogonal views of one of the PLCβ1-positive neurons shown in D-F. Immunoreactive spots were localized in the nuclear matrix. A-C are maximum intensity projections of 32 0.25 µm-thick optical sections. D-I images are maximum intensity projections of 14 0.25 µm-thick optical sections. Scale bars = 25 µm in C (applies to A-C); 5 µm in inset in C (applies to insets in A-C); 10 µm in F (applies to D-F); 5 µm in in I (applies to G-I).

Figure 18. PLC®1-immunofluorescence combined with NeuN (A-C), chromatin (D-F), nuclear pore complex (G-I) and lamin B1 (J-L) staining in intact nuclei isolated from the adult rat brain cortex. **A-C.** Double PLC®1- (A) and NeuN-immunofluorescence (B) labeling combined with Hoechst staining (C). Every NeuN-immunopositive nucleus exhibited strong PLC®1-immunoreactivity (filled arrowheads), whereas no PLC®1 staining was observed in nuclei devoid of NeuN (empty arrowheads). **D-F.** High magnification views of PLC®1-immunollabeled isolated nuclei (D) counterstained with Hoescht's dye (E). No overlapping was observed between PLC®1-immunofluorescent spots and patches of intense Hoechst staining (F). **G-I.** Double PLC®1- (G) and nuclear pore complex-immunofluorescence (H) showing that PLC®1 localizes internal to the nuclear envelope (I). **J-L.** Double PLC®1- (G) and lamin B1-immunofluorescence (H) showing that PLC®1 localizes internal to the nuclear lamina (I). Scale bars = 20 µm in C (applies to A-C); 5 µm in I (applies to D-I).

Figure 19. Combined immunofluorescence of PLC®1 and nuclear matrix markers in neuronal nuclei isolated from the adult rat brain cortex. **A-C.** Double PLC®1- (A) and NeuN-immunofluorescence (B). Both immunostainings exhibited similar distribution in the nucleoplasm (C). Numerous PLC®1-immunopositive puncta co-localized with or were in close apposition to NeuN-positive puncta. **D-F.** Double PLC®1- (D) and SC-35 immunofluorescence (E). PLC®1-immunlolabelling partially overlapped with SC-35-speckles. **G-I.** Double PLC®1- (G) and PIP_2-immunofluorescence (H). Note that the bulk of PIP_2-signal was confined to speckle-like structures, with only faint staining at the nuclear membrane. Domains exhibiting the most intense PLC®1- and PIP_2-stainings overlapped or were closely apposed to each other (H).

Figure 20. **A.** Western blot analysis of cytosolic (CYT), crude membranes (P2) and "isolated nuclei" (N) fractions with antibodies against PLCβ1 and subcellular fraction-specific antigens. For each marker, equal amounts of total protein (10 µg) were loaded on the same gel, **B.** Western blot analysis of PLCβ1a and PLCβ1b in the CYT, P2 and N fractions. Increasing amounts of proteins were loaded (2.5, 5, 10 and15 µg of from the CYT and P2 fractions, and 10, 15, 20 and 25 µg from the N fraction). **C.** Bar graph depicts the integrated optical density (in arbitrary units) of PLCβ1a- and PLCβ1b-immunoreactivity for every fraction. Two-way ANOVA revealed significant diferences between splice variants and subcellular fractions ($P<0.0001$ both; $P<0.005$ for splice variant-subcellular fraction interaction; Table 4 for details of the post hoc Bonferroni's test). PLCβ1a/PLCβ1b ratios of immunoreactivity revealed significantly higher values in CYT than in P2 and N fractions (inset; **: $P<0.01$, ***: $P<0.001$). All values shown in the bars are the mean ± SEM of four independent experiments.

Table 1

TABLE 1. Abbreviations

AC	anterior cingulated cortex	**IMD**	intermediodorsal thalamic nucleus
ACB	nucleus accumbens	**IMM**	intermediomedial cell column
aco	anterior commissure	**int**	internal capsule
act	anterior commissure (temporal limb)	**IOma**	inferior olivary complex (medial accessory olive)
AD	anterodorsal thalamic nucleus	**isl**	islands of Calleja
AHA	anterior hypothalamic area	**LA**	lateral amygdala
AHN	anterior hypothalamic nucleus	**LD**	lateral nucleus of amygdala
AI	agranular insular cortex	**LH**	lateral dorsal thalamic nucleus
alv	alveus	**LHA**	lateral habenular nucleus
AM	anteromedial thalamic nucleus	**ll**	lateral hypothalamic are
AQ	cerebral aqueduct	**lot**	lateral lemniscus
ARH	arcuate nucleus	**LP**	lateral olfactory tract
AV	anteroventral nucleus of thalamus	**LPO**	lateral posterior thalamic nucleus
BLAa	basolateral nucleus of amygdala (anterior part)	**LRNp**	lateral preoptic area
BLAp	basolateral nucleus of amygdala (posterior part)	**LSd**	lateral reticular nucleus (parvicellular part)
BMAa	basomedial nucleus of amygdala (anterior part)	**LSi**	lateral septal nucleus (intermediate part)
BMAp	basomedial nucleus of amygdala (posterior part)	**LSv**	lateral septal nucleus (ventral part)
BST	bed nucleus of stria terminalis	**LTD**	laterodorsal tegmental nucleus
CA1	field CA1 of the Ammmon's horn	**MA**	magnocellular preoptic nucleus
CA2	field CA2 of the Ammmon's horn	**MD**	mediodorsal thalamic nucleus
CA3	field CA3 of the Ammmon's horn	**MDRNd**	medullary reticular nucleus (dorsal part)
CBgl	granule cell layer of cerebellum	**MDRNv**	medullary reticular nucleus (ventral part)
CBml	molecular layer of cerebellum	**MEApd**	medial nucleus of amygdala (posterodorsal part)
CBpl	Purkinje cell layer of cerebellum	**MEApv**	medial nucleus of amygdala (posteroventral part)
Cc	corpus callosum	**MEV**	mesencephalic nucleus of trigeminal nerve
CEA	central nucleus of amygdala	**MH**	medial habenular nucleus
CEAc	central nucleus of amygdala (capsular part)	**ml**	medial lemniscus
CEAl	central nucleus of amygdala (lateral part)	**mlf**	medial longitudinal fasciculus
CEAm	central nucleus of amygdala (medial part)	**mo**	molecular layer of dentate gyrus
CeCv	central cervical nucleus	**MOB**	main olfactory bulb
cing	cingulum bundle	**MOBgl**	glomerular layer of MOB
CL	central lateral thalamic nucleus	**MOBopl**	outer plexiform layer of MOB
CLA	claustrum	**MOBml**	mitral layer of MOB
CM	central medial thalamic nucleus	**MOBipl**	inner plexiform layer
CNIC	**c**entral cortex of inferior colliculus	**MOb**	medulla oblongata
cic	commissure of inferior colliculus	**MOs**	motor secondary cortex
Cpd	cerebral peduncle	**MPN**	medial preoptic nucleus
CU	cuneate nucleus	**MPO**	medial preoptic area
cu	cuneate fasciculus	**MS**	medial septal nucleus
cuf	cuneate fascicle	**mtt**	mammillothalamic tract
CUN	cuneiform nucleus	**NLL**	nucleus of the lateral lemniscus
DCIC	dorsal cortex of inferior colliculus	**NTS**	nucleus of the solitary tract
dcs	dorsal corticospinal tract	**OB**	olfactory bulb
df	dorsal fornix	**opt**	optic tract
DGlb	lateral blade of dentate gyrus	**OT**	olfactory tubercule
DGmb	medial blade of dentate gyrus	**PAG**	periaqueductal gray
DGpo	polymorph layer of dentate gyrus	**PB**	parabrachial nucleus
DGsg	granule cell layer of dentate gyrus	**PCN**	paracentral thalamic nucleus
dhc	dorsal hippocampal commissure	**PH**	posterior hypothalamic nucleus
dl	dorsolateral fasciculus	**PIR**	piriform cortex
DMHa	dorsomedial hypothalamic nucleus (anterior portion)	**PL**	prelimbic cortex
DMHp	dorsomedial hypothalamic nucleus (posterior portion)	**PO**	posterior thalamic complex
DMX	dorsal motor nucleus of vagus nerve	**PR**	perireuniens nucleus
DR	dorsal raphe nucleus	**PRNr**	pontine reticular nucleus (rostral part)
ec	external capsule	**PT**	paratenial thalamic nucleus
ECIC	external cortex of inferior colliculus	**PVH**	paraventricular nucleus of hypothalamus
em	external medullary lamina of thalamus	**PVT**	paraventricular thalamic nucleus
EPd	endopiriform nucleus (dorsal part)	**py**	pyramidal tract
EPv	endopiriform nucleus (ventral part)	**RE**	reuniens nucleus
fi	fimbria	**RH**	rhomboid thalamic nucleus
fx	fornix	**RO**	raphe nucleus obscurus
GP	globus pallidus	**RSPd**	dorsal retrosplenial cortex
GPl	globus pallidus (lateral segment)	**RSPv**	ventral retrosplenial cortex
GPm	globus pallidus (medial segment)	**RT**	reticular nucleus of thalamus
GR	gracile nucleus	**rust**	rubrospinal tract
gr	gracile fasciculus	**SCH**	suprachiacmatic nucleus
IA	intercalated nuclei of amygdala	**scp**	superior cerebellar peduncle
IAD	interanterodorsal thalamic nucleus	**sct**	spinocerebellar tract
IAM	interanteromedial thalamic nucleus	**sctv**	ventral spinocerebellar tract
IC	inferior colliculus	**SI**	substantia innominata
IG	indusium griseum	**slm**	stratum lacunosum-moleculare
IL	infralimbic cortex		

TABLE 1 (continuation). Abbreviations

slu	stratum lucidum	**V3**	third ventricle
sm,	stria medullaris	**VAL**	ventral anterior-lateral complex
SMT	submedial thalamic nucleus	**VHMc**	ventromedial hypothalamic nucleus (central part)
so	stratum oriens	**VHMdm**	ventromedial hypothalamic nucleus (dorsomedial part)
sp	stratum pyramidale	**VHMvl**	ventromedial hypothalamic nucleus (ventrolateral part)
sptV	spinal tract of trigeminal nerve	**VL**	lateral ventricle
SPVC	spinal nucleus of trigeminal nerve (caudal part)	**VM**	ventral medial thalamic nucleus
sr	stratum radiatum	**VPL**	ventral posteromedial thalamic nucleus
st	stria terminalis	**VPM**	ventral posterolateral thalamic nucleus
S**TN**	subthalamic nucleus	**ZI**	zona incerta
sup	supraoptic commissure	**III**	oculomotor nucleus
ts	solitary tract	**XII**	hypoglossal nucleus
tsp	tectospinal pathway	**laXII**	lateral accessory hypoglossal nucleus

Table 2

TABLE 2. Primary antibodies used

Antibody name	Dilution (IH / IF)	Dilution (WB)	Clonality	Species	Immunizing antigen	Source, Catalog No.
PLCβ1 (D-8)	1:250	1:1000	Monoclonal	Mouse IgG_{2b}	Synthetic peptide corresponding to amino acids 831-1063 mapping within an internal region of rat PLCβ1 common to 1a and 1b splice variants	Santa Cruz Biotechnology, D-8: sc-5291
PLCβ1 (R-233)	1:500	1:2000	Polyclonal	Rabbit IgG	Synthetic peptide corresponding to amino acids 831-1063 mapping within an internal region of rat PLCβ1 common to 1a and 1b splice variants	Santa Cruz Biotechnology, R-233: sc-9050
PLCβ1a (G-12)	1:500	1:5000	Polyclonal	Rabbit IgG	Synthetic peptide corresponding to a unique C-terminal region of PLCβ1a splice variant	Santa Cruz Biotechnology, G-12: sc-205
PLCβ1 (N-ter)	1:50	1:2000	Monoclonal	Mouse IgG_1	Synthetic peptide corresponding to amino acids 4-159 of the rat PLCβ1 common to 1a and 1b splice variant	BD Transduction Laboratories, 610924
PLCβ1 (36-87)	1:200	1:2000	Polyclonal	Affinity purified goat serum	Synthetic peptide corresponding to amino acids 36-87 of the mouse PLCβ1 common to 1a and 1b splice variants	Frontier Institute Co. Ltd, PLCb1-Go-Af1000-1
Nuclear pore complex	1:2500	1:2000	Monoclonal	Mouse IgG_1	Nuclear pore complex mixture	Abcam, ab24609
Calretinin	1:10000		Monoclonal	Culture supernatant from mouse hybridoma	Recombinant human calretinin-22k	Swant, 6B3
GFAP	1:1500		Monoclonal	Mouse IgG_1	Synthetic peptide corresponding to a sequence of GFAP from pig spinal cord	Sigma, G3893 clone G-A-5
Lamin B1	1:100		Monoclonal	Mouse IgG_1	Synthetic peptide generated against purified cell nuclei from human epithelioid carcinoma	Santa Cruz Biotechnology, 8D1: sc-56144
NeuN	1:1000		Monoclonal	Mouse IgG_1	Purified cell nuclei from mouse brain	Chemicon, MAB377 clone A60
Parvalbumin	1:6000		Monoclonal	Lyophilized mouse ascites	Parvalbumin purified from carp muscles	Swant, PV 235
PIP_2	1:100		Monoclonal	Protein A purified mouse IgM	Liposomes (prepared from lipid A, phosphatidylcholine and cholesterol) containing synthetic di-palmitoyl PtdIns(4,5)P_2	Santa Cruz Biotechnology, 8D1: sc-56144
PSD-95	1:200		Monoclonal	Rabbit IgG	KLH-coupled synthetic peptide corresponding to residues surrounding Gly99 of human PSD-95	Cell Signalling, D27E11
SC-35	1:500		Monoclonal	Mouse IgG	Synthetic peptide sequence corresponding to a splicing factor SC-35	Abcam, ab11826
Somatostatin	1:50		Monoclonal	Rat IgG_{2b}	Synthetic peptide corresponding to amino acids 1-14 of bovine somatostatin	Chemicon, MAB354
β -tubulin III		1:3000	Polyclonal	Affinity purified chicken serum	Synthetic peptides conjugated to KLH corresponding to different regions shared by human and rat beta III tubulin gene product	Abcam, ab41489
58-K Golgi protein		1:1500	Polyclonal	Affinity purified rabbit serum	Synthetic peptide conjugated to KLH derived from within residues 200-300 of Human 58K Golgi protein	Abcam, ab5820
Na^+/K^+ ATPase		1:4000	Monoclonal	Mouse IgG_1	Synthetic peptide corresponding to a sequence between amino acids 496-506 of α1 subunit protein Na^+/K^+ ATPase from lamb kidney	Sigma, A277 clone M8-P1-A3
NR1 subunit of the NMDA receptor		1:1500	Polyclonal	Affinity purified rabbit serum	Synthetic non-phosphopeptide derived from human NMDAR1 around the phosphorylation site of serine 897 (R-S-S-K-D)	Abcam, ab52177
SNAP-25		1:4000	Monoclonal	Mouse IgG_1	Tissue / cell preparation: this antibody was raised against a crude synaptic preparation from the post mortem human brain	Abcam, ab24732

Table 3

TABLE 3. Combinations of antibodies for double immunofluorescence experiments

Primary antibodies		**Secondary antibodies**	
		First secondary	*Second secondary*
PLCβ1 (R-233)	PLC-β1 (D-8)	Alexa Fluor 488 goat anti-rabbit IgG; Invitrogen Cat. A-11034	Alexa Fluor 568 goat anti-mouse IgG; Invitrogen Cat. A-11031
	Nuclear Pore Complex		
	NeuN		
	GFAP		
	SC-35		
	Lamin B1		
	PIP_2		Alexa Fluor 568 goat anti-mouse IgM; Invitrogen Cat. A-21043
	Cocktail calretinin, parvalbumin, somatostatin		Alexa Fluor 568 goat anti-mouse IgG; Invitrogen Cat. A-11031 Alexa Fluor 568 goat anti-rat IgG; Invitrogen Cat. A-11077
	PLC-β1 (36-87)	DyLight 549 donkey anti-rabbit F(ab')2 fragment; Jackson ImmunoResearch Cat. 711-506-152	Alexa Fluor 488 donkey anti-goat IgG; Invitrogen Cat. A-11055
PLCβ1 (D-8)	PSD-95	Alexa Fluor 568 goat anti-mouse IgG; Invitrogen Cat. A-11031	Alexa Fluor 488 goat anti-rabbit IgG; Invitrogen Cat. A-11034

Table 4

TABLE 4. Results the Bonferroni post hoc test.

	PLCβ1a	PL Cβ1b
CYT *vs*. P2	n.s.	*
CYT *vs*. N	***	n.s.
P2 *vs*. N	***	**

	PLCβ1a *vs*. PLCβ1b
CYT	***
P2	n.s.
N	n.s.

*, $p < 0.05$; **, $p < 0.01$; ***, $p < 0.001$; n.s., no significant difference.

Table 5

TABLE 5. Relative intensities of PLCβ1-immunoreactivity in the adult rat brain

Region	Intensity
Telencephalon	
Olfactory and basal forebrain areas	
Main olfactory bulb	
Glomerular layer	++
Outer plexiform layer	+/-
Mitral layer	+
Inner plexiform layer	+/-
Granular layer	++
Anterior olfactory nucleus	++
Olfactory tubercle	
Layer I	+/-
Layer II	+++
Areas neighbouring Islands of Calleja	++++
Layer III	+/-
Islands of Calleja	+++
Cerebral cortex	
Isocortex	
Layer I	+/-
Layers II-III	+++
Layer IV	++
Layer V	++++
Layer VI	++
Anterior cingulate cortex	
Layer I	+/-
Layers II-III	+
Layer V	++++
Layer VI	++
Prelimbic cortex	
Layer I	-
Layers II-III	+/-
Layer V	++
Layer VI	+
Infralimbic cortex	
Layer I	-
Layers II-III	+/-
Layer V	+++
Layer VI	+
Perirhinal cortex	
Layer I	+/-
Layer II-III	++
Layer IV	++++
Layer VI	++
Enthorinal cortex	
Layer I	-
Layer II	++
Layer III	+
Layer IV	++
Layer V	++
Layer VI	+
Dorsal retrosplenial cortex	
Layer I	+/-
Layer II-III	+
Layer IV	+++
Layer VI	++
Ventral retrosplenial cortex	
Layer I	+/-
Layer II-III	+
Layer IV	++
Layer VI	+
Piriform cortex	
Layer I	-
Layer II	++
Layer III	+
Hippocampal formation	
CA1 region	
Stratum oriens	++
Pyramidal cell layer	++++
Stratum radiatum	++
Stratum lacunosum-moleculare	+
Hippocampal formation (continuation)	
CA2 region	
Stratum oriens	++
Pyramidal cell layer	++++
Stratum radiatum	++
CA3 region (proximal)	
Stratum oriens	++
Pyramidal cell layer	+++
Stratum lucidum	+
Stratum radiatum	+
CA3 region (distal)	
Stratum oriens	+/-
Pyramidal cell layer	++
Stratum radiatum	+
Hiliar region	+
Dentate gyrus	
Molecular layer	+
Granular layer	+++
Polymorphic layer	++
Subiculum	++++
Postsubiculum	+++
Amygdala and extended amygdala	
Amygdaloid complex	++
Bed nucleus of the stria terminalis	+++
Septum	
Medial septal nucleus	+/-
Lateral septal nucleus	
Dorsal part	++++
Intermediate part	++
Ventral part	++
Basal ganglia	
Caudate-Putamen	++++
Globus pallidus	++
Nucleus accumbens	+
Substantia innominata	+
Diencephalon	
Epithalamus	
Medial habenular nucleus	-
Lateral habenular nucleus	+/-
Thalamus	
Midline group	
Paraventricular nucleus	+
Parataenial nucleus	++
Nucleus reuniens	++
Anterior group	
Anteromedial nucleus	+/-
Anterodorsal nucleus	+/-
Anteroventral nucleus	-
Interanteromedial nucleus	+/-
Interanterodorsal nucleus	+/-
Lateral dorsal nucleus	+/- Medial group
Mediodorsal nucleus	+/-
Intermediodorsal nucleus	++
Submedial nucleus	+/-
Perireuniens nucleus	+
Lateral group	
Lateral posterior nucleus	+/-
Posterior complex	+/-
Ventral group	
Ventral anterior-lateral complex	+/-
Ventral medial nucleus	+/-
Ventral posterior complex	+/-
Geniculate group	
Medial geniculate complex	
Dorsal part	+/-
Ventral part	-
Medial part	+

TABLE 4 (continuation). Relative intensities of PLCβ1-immunoreactivity in the adult rat brain

Region	Intensity		Region	Intensity
Thalamus (continuation)			*Midbrain*	
Lateral geniculate complex			Pretectal region	
Dorsal part	-		Nucleus of the optic tract	+
Ventral part – lateral zone	+/-		Anterior pretectal nucleus	+/-
Ventral part – medial zone	-		Posterior pretectal nucleus	+/-
Intralaminar nuclei			Substantia nigra	
Rhomboid nucleus	+		Compact part	+/-
Central medial nucleus	+/-		Reticular part	+/-
Paracentral nucleus	+/-		Ventral tegmental area	+/-
Central lateral nucleus	+/-		Superior colliculus	
Parafascicular nucleus	+	Other nuclei	Zonal and superficial gray layers	-
Peripeduncular nucleus	+		Optic, and intermediate and deep layers	+/-
Reticular nucleus	++		Inferior colliculus	
Zona incerta & fields of Forel	+/-		External cortex	+
Subthalamic nucleus	+/-		Dorsal nucleus	+
Hypothalamus			Central nucleus	+/-
Periventricular zone			Periaqueductal gray	+
Suprachiasmatic preoptic nucleus	-		Mesencephalic Nucleus of the trigeminal	+/-
Anteroventral periventricular nucleus	-		Red nucleus	+/-
Paraventricular nucleus	+		Cuneiform nucleus	+/-
Arcuate nucleus	-		Laterodorsal tegmental nucleus	+/-
Posterior periventricular nucleus	-		Parabrachial nucleus	+/-
Medial zone			*Pons*	
Medial preoptic area	+/-		Locus coeruleus	+/-
Medial preoptic nucleus	++		Lemniscal nuclei	+/-
Anterodorsal preoptic nucleus	+/-		Pontine gray	-
Anteroventral preoptic nucleus	-		Pontine reticular formation	+/-
Suprachiasmatic nucleus	+/-		Vestibular nuclei	-
Anterior hypothalamic area	+		*Medulla Oblongata*	
Anterior hypothalamic nucleus	+		Gracile and cuneate nuclei	+/-
Tuberal area of hypothalamus			Cochlear Nuclei	-
Ventromedial hypothalamic nucleus	+/-		Nucleus dorsal ambiguous	++
Dorsomedial hypothalamic nucleus	+/-		Inferior olive	-
Ventral premammillary nucleus	+/-		Nucleus of the solitary tract	-
Mammillary body			Dorsal motor vagal nucleus	++
Tuberomammillary nucleus	+++		*Nuclei covering various brainstem levels*	
Supramammillary nucleus			Sensory trigeminal nuclei	+/-
Lateral part	+/-		Brainstem reticular formation	+/-
Medial part	+		Somatic motor nuclei	+++
Dorsal premammillary nucleus	+/-		Raphe nuclei	+/-
Medial mammillary nucleus	-		**Spinal cord**	
Lateral mammillary nucleus	+/-		Lamina I	+++
Posterior hypothalamic nucleus	+		Lamina II	++++
Lateral zone			Lamina III	++
Lateral preoptic area	-		Lamina IV	+
Lateral hypothalamic area	++		Laminae V-VIII, X	++
Posterior nucleus	+/-		Lamina IX	+++
Hindbrain			Radial glia-like processes of white matter	++
Cerebellum				
Cortex				
Molecular layer	++			
Purkinje cell layer	++			
Granule cell layer	++			
Deep cerebellar nuclei	+/-			

Note: Identification of brain and spinal cord regions was made according to the stereotaxic atlas of Swanson (1992). PLCβ1 immunostaining intensity was scored qualitatively. The symbols represent the relative levels of immunoreactivity: ++++, very intense immunoreactivity; +++, intense immunoreactivity; ++, moderate immunoreactivity; +, weak immunoreactivity; +/-, immunoreactivity intensity barely above background levels; -, background level of labeling.

Figure 1

Click here to download high resolution image

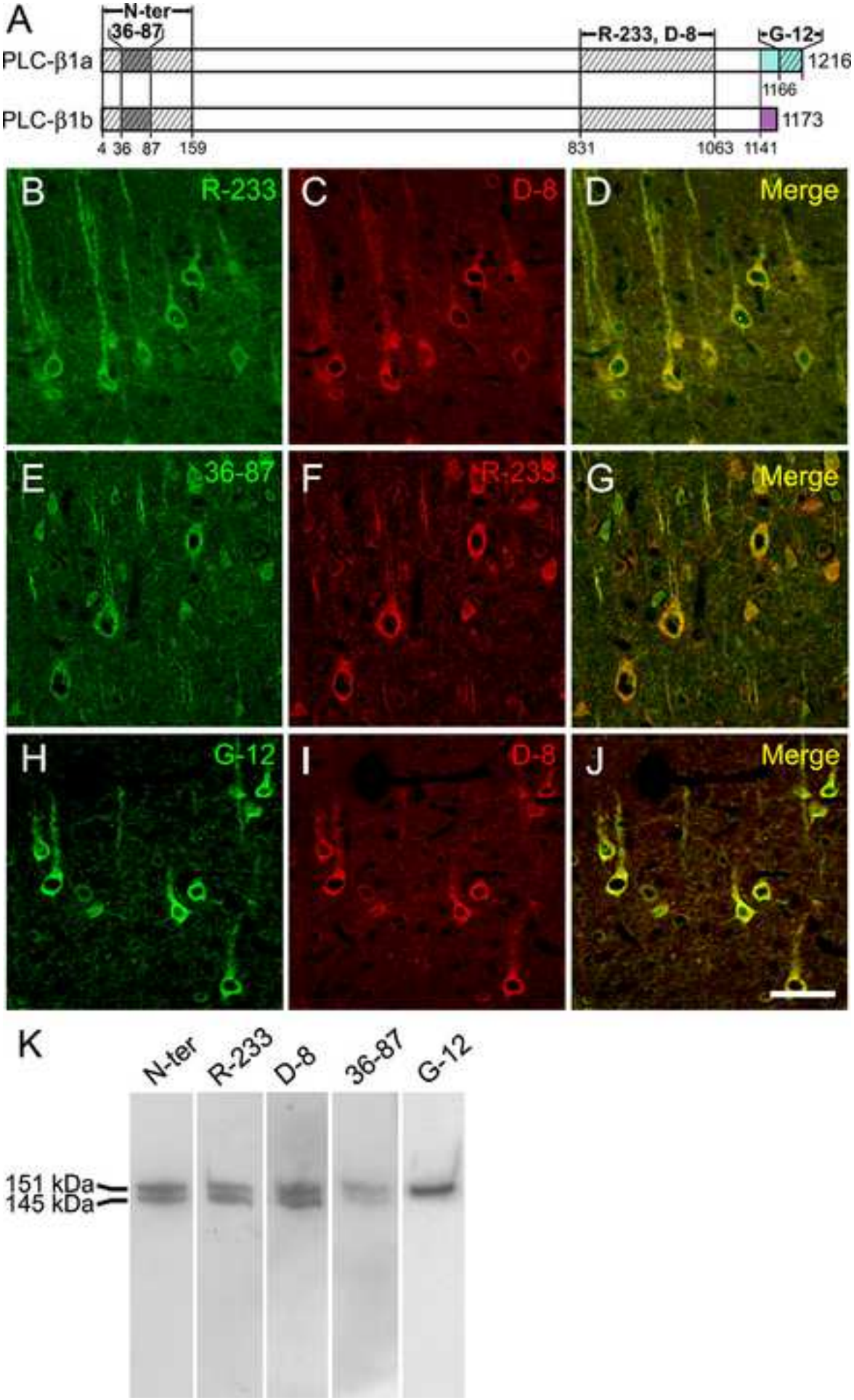

Figure 2

Click here to download high resolution image

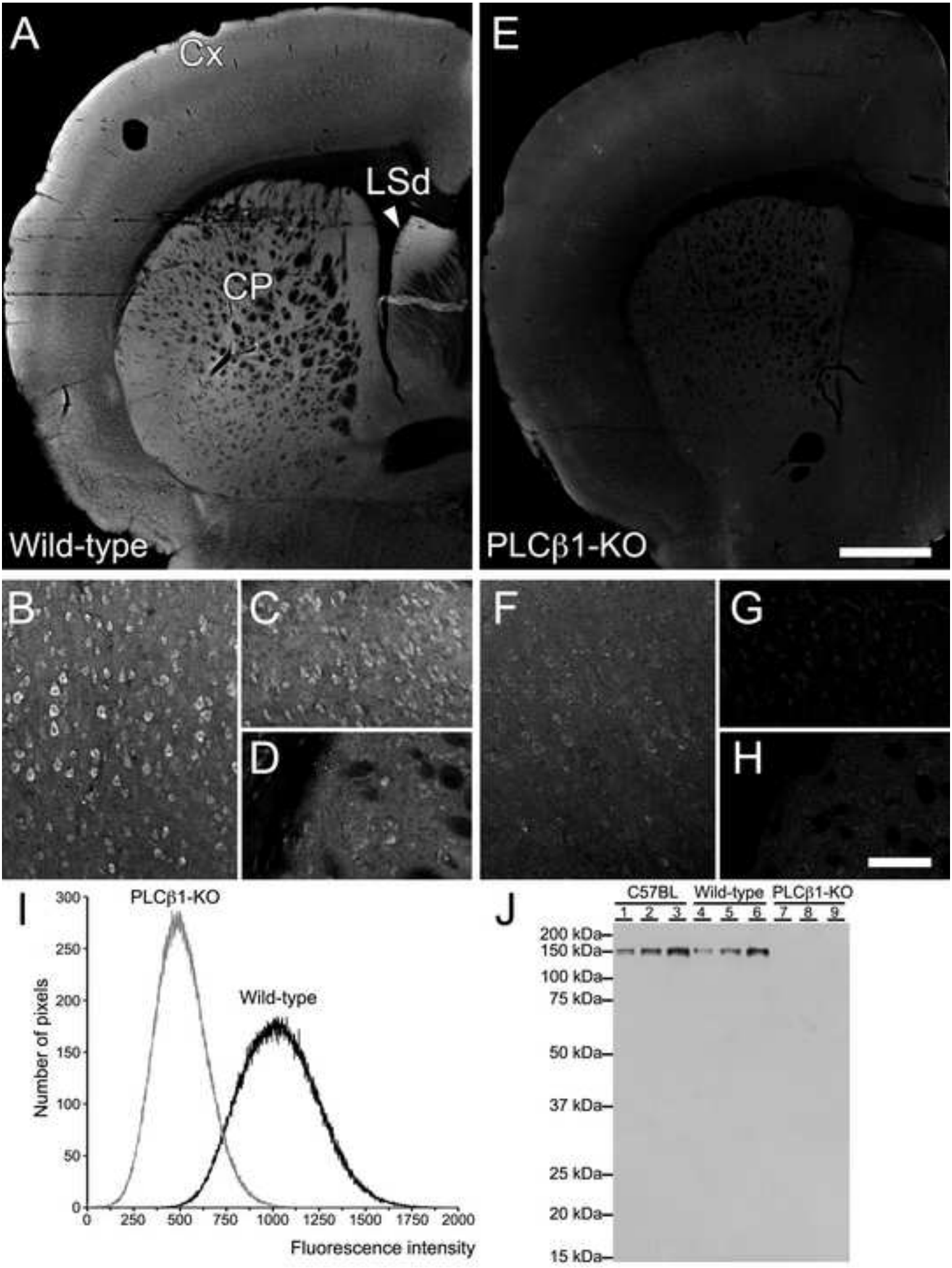

Figure 3

Click here to download high resolution image

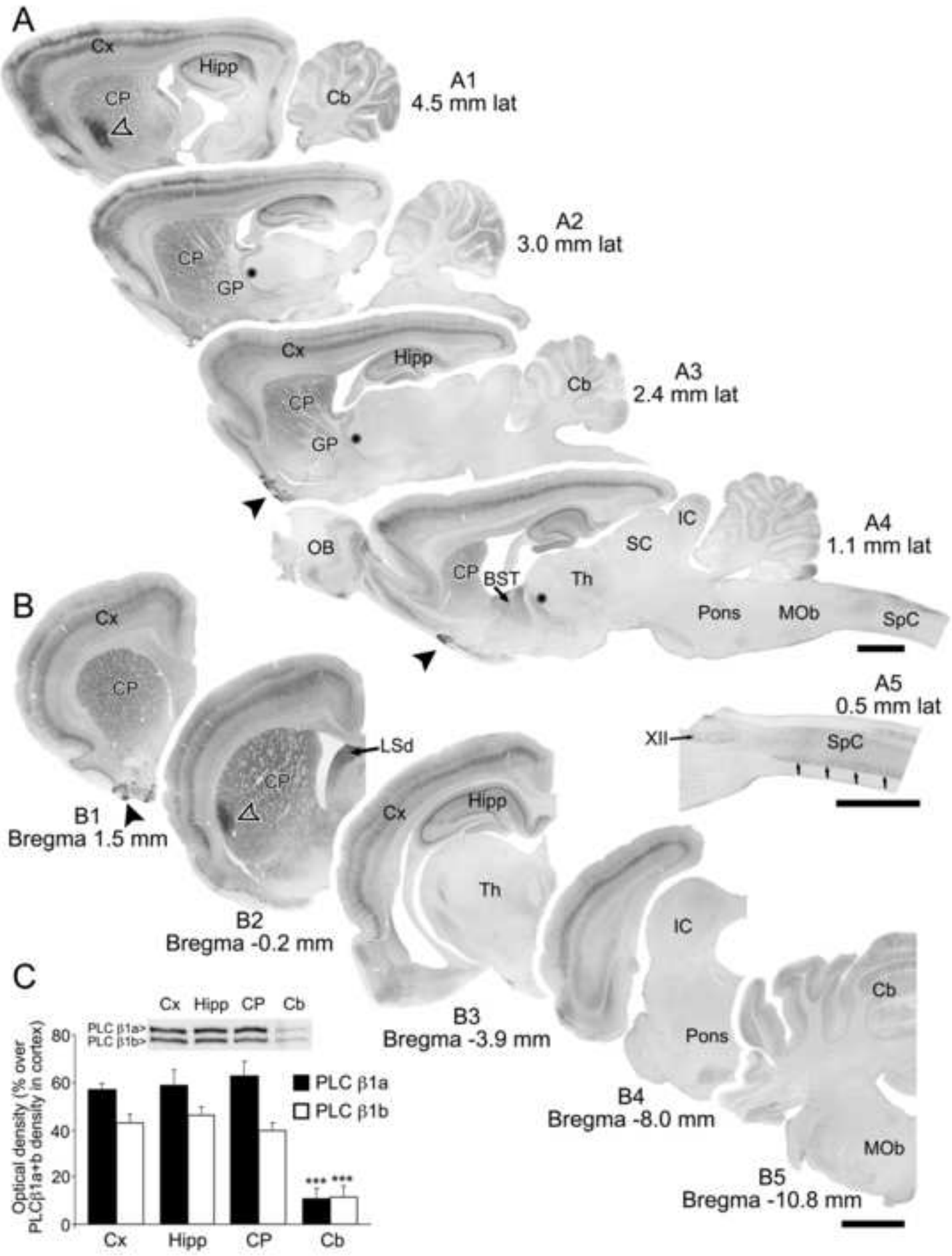

Figure 4

Click here to download high resolution image

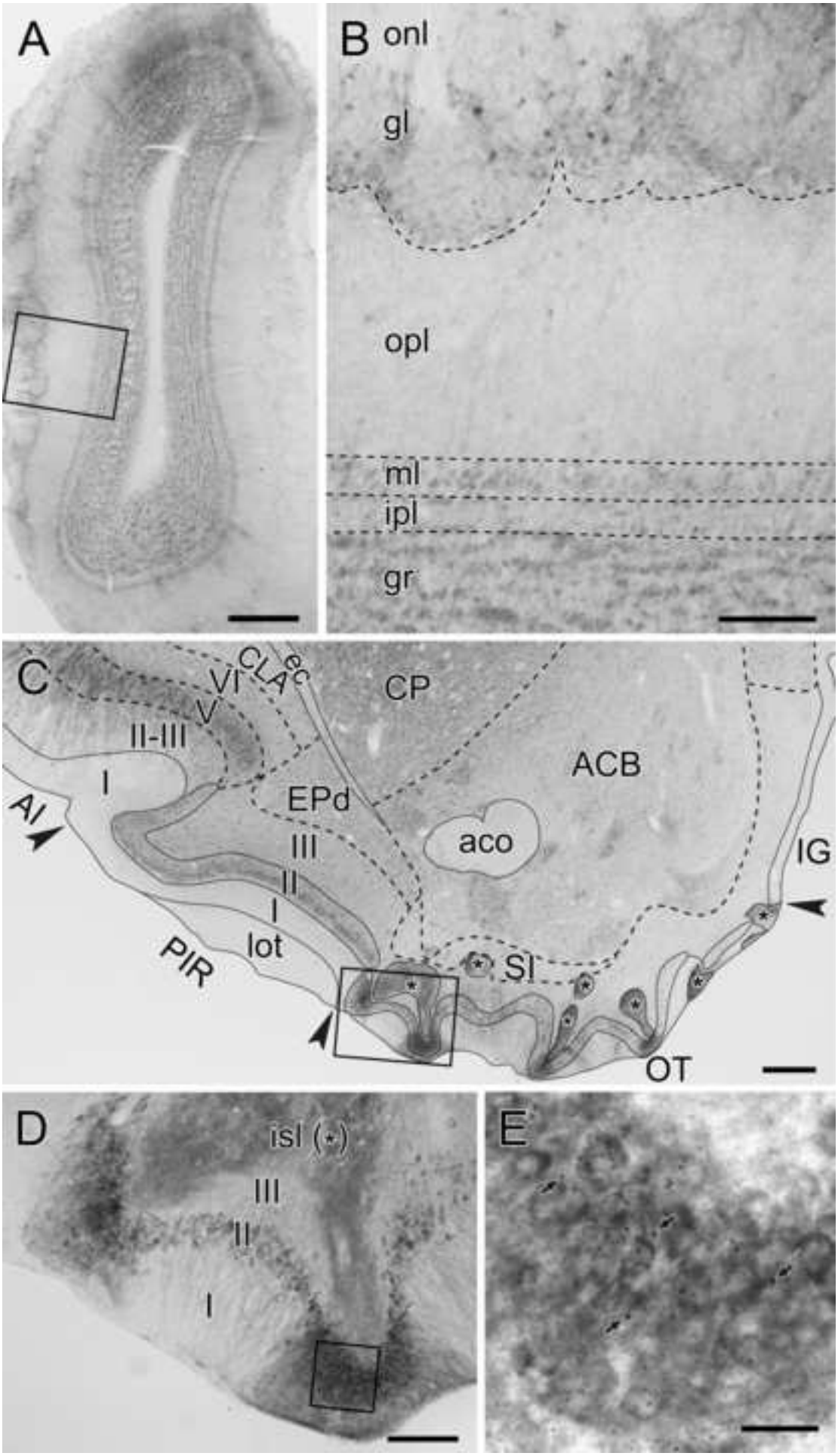

Figure 5

Click here to download high resolution image

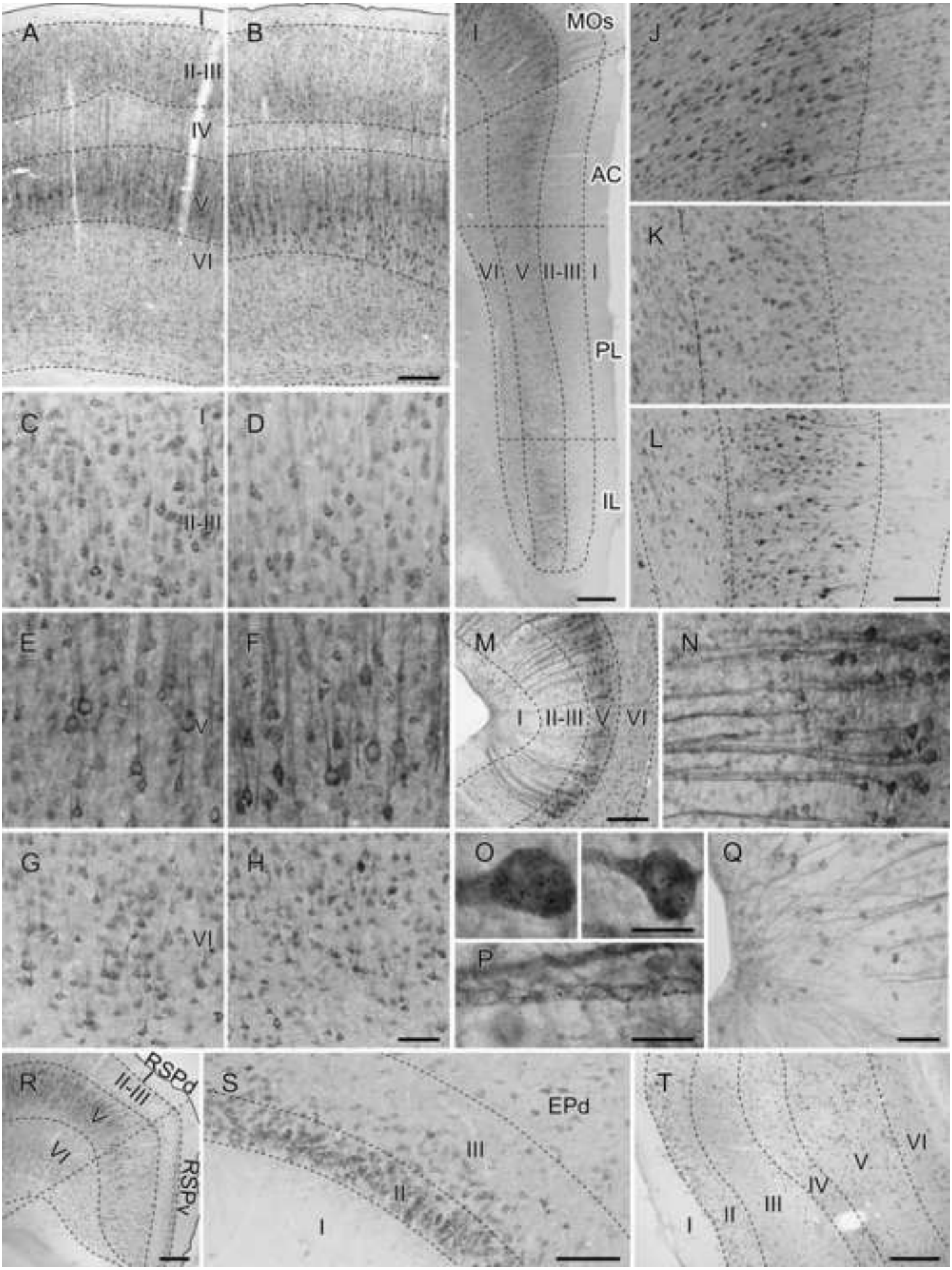

Figure 6

Click here to download high resolution image

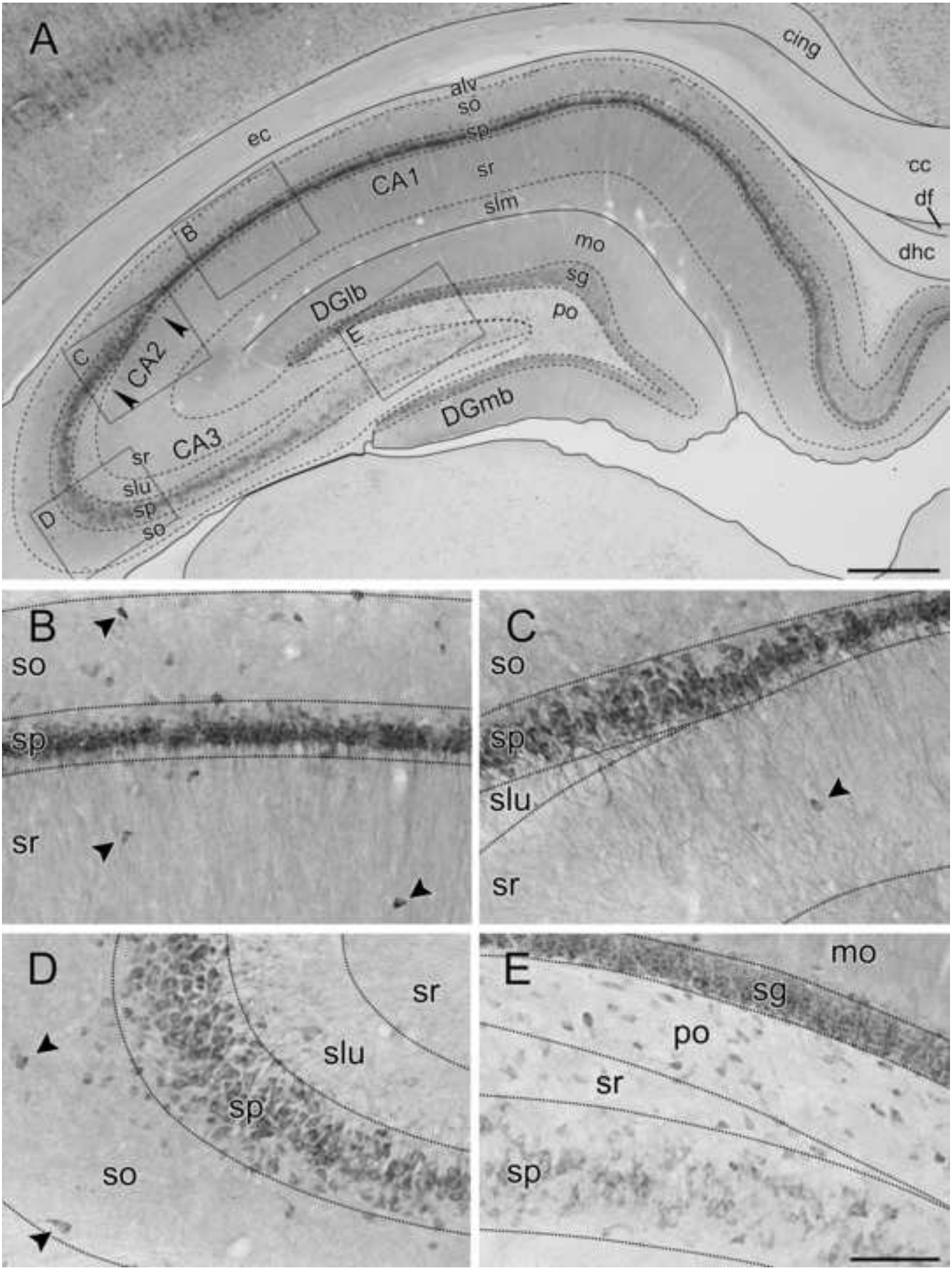

Figure 7

Click here to download high resolution image

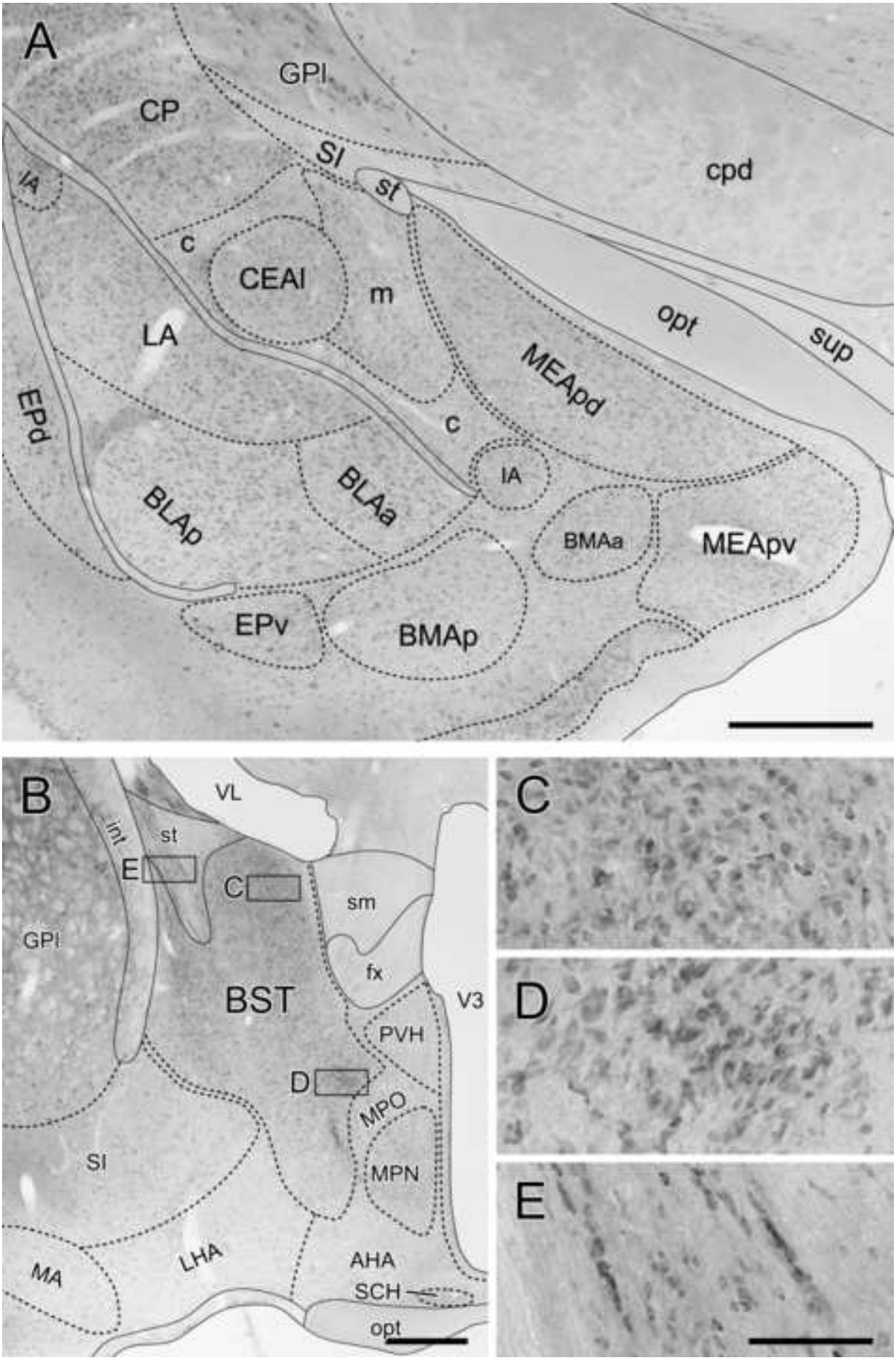

Figure 8

Click here to download high resolution image

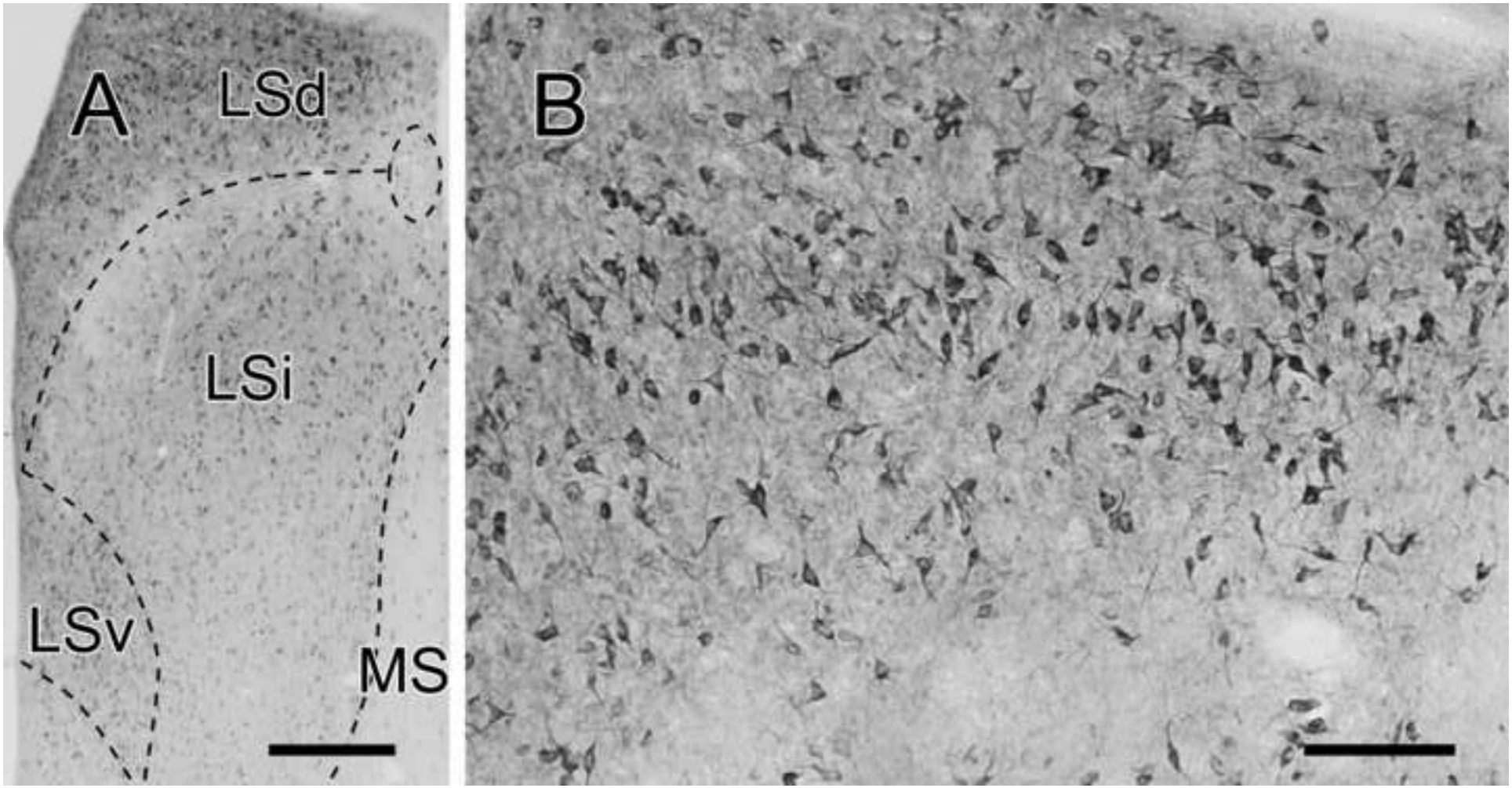

Figure 9

Click here to download high resolution image

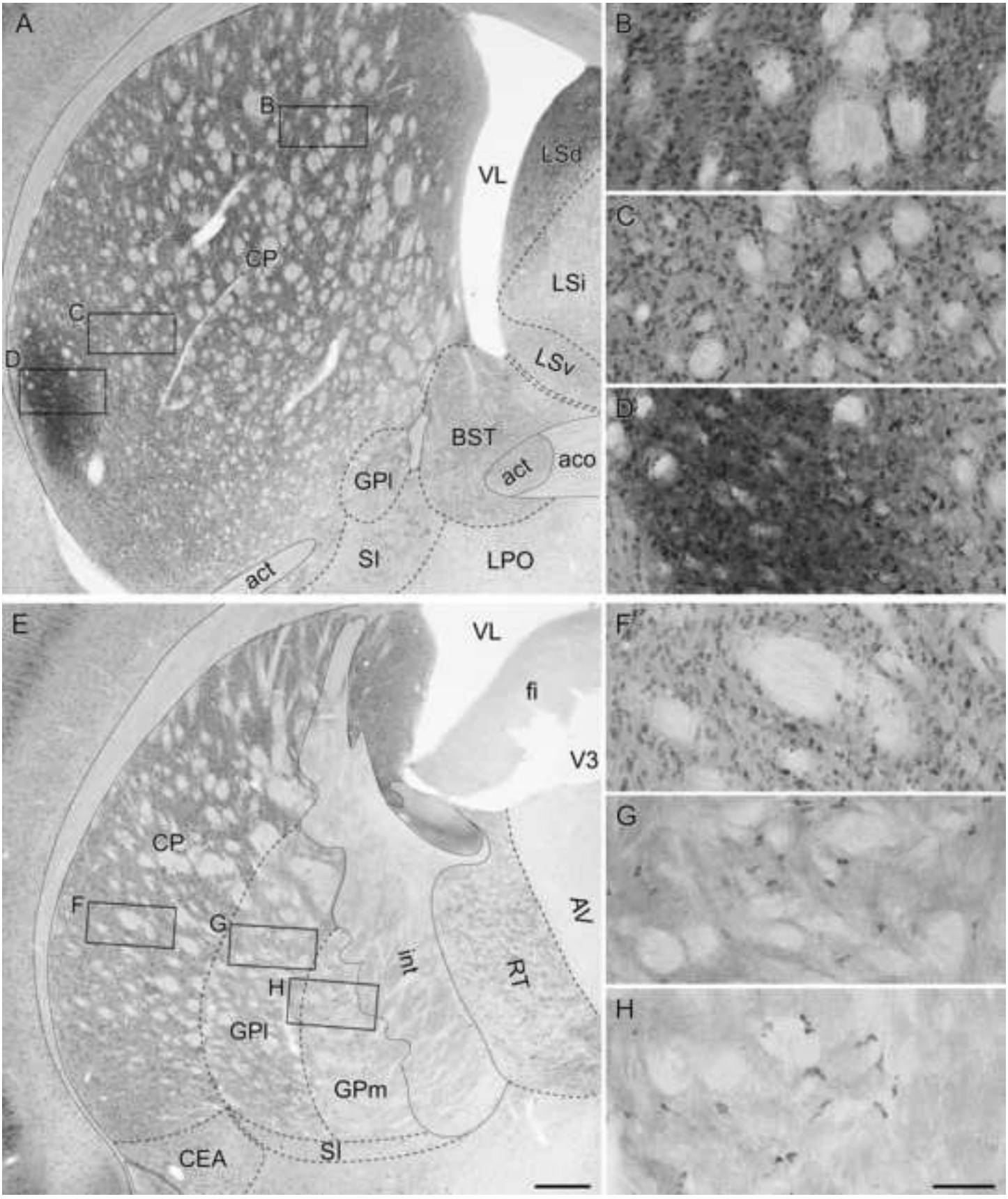

Figure 10

Click here to download high resolution image

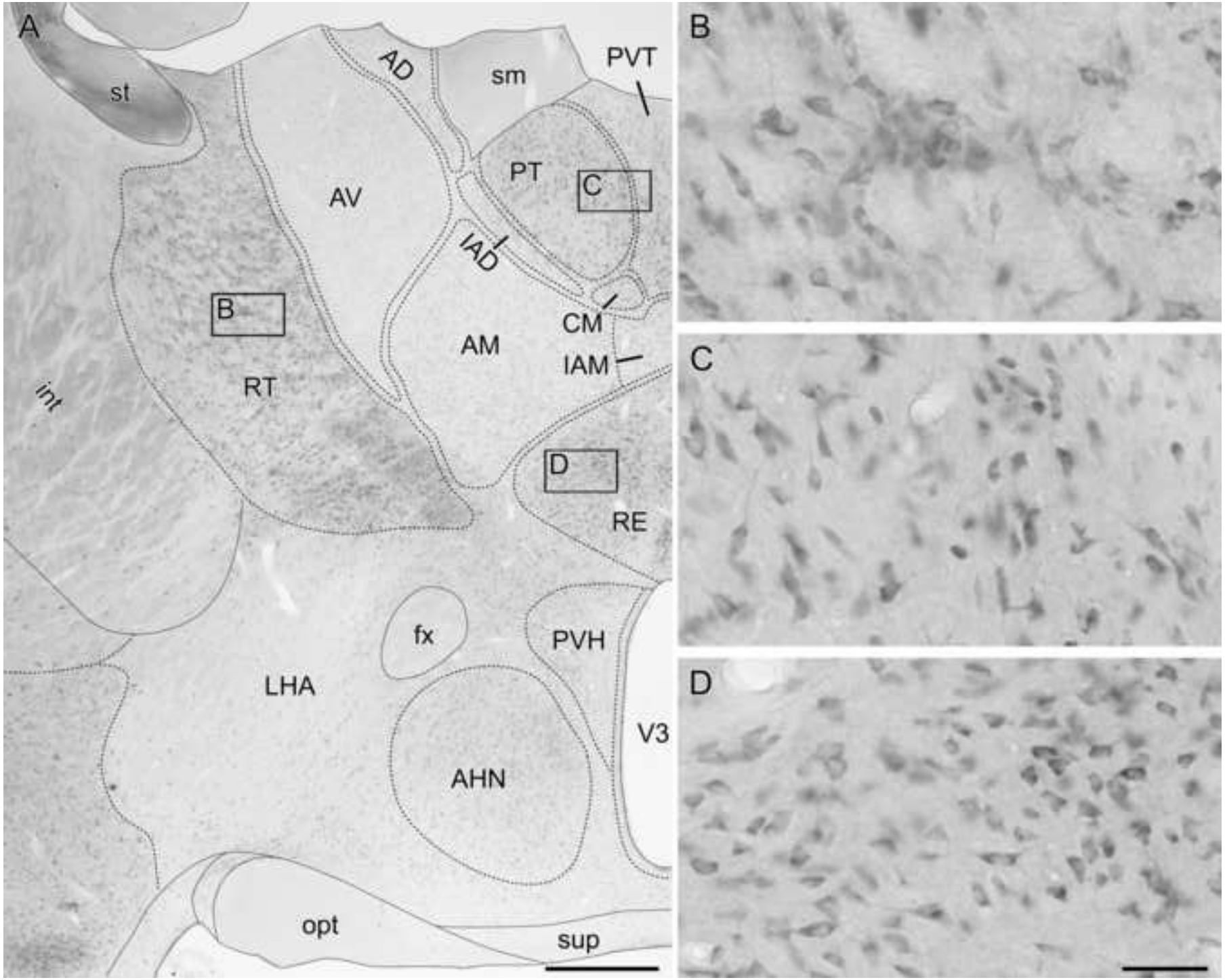

Figure 11

Click here to download high resolution image

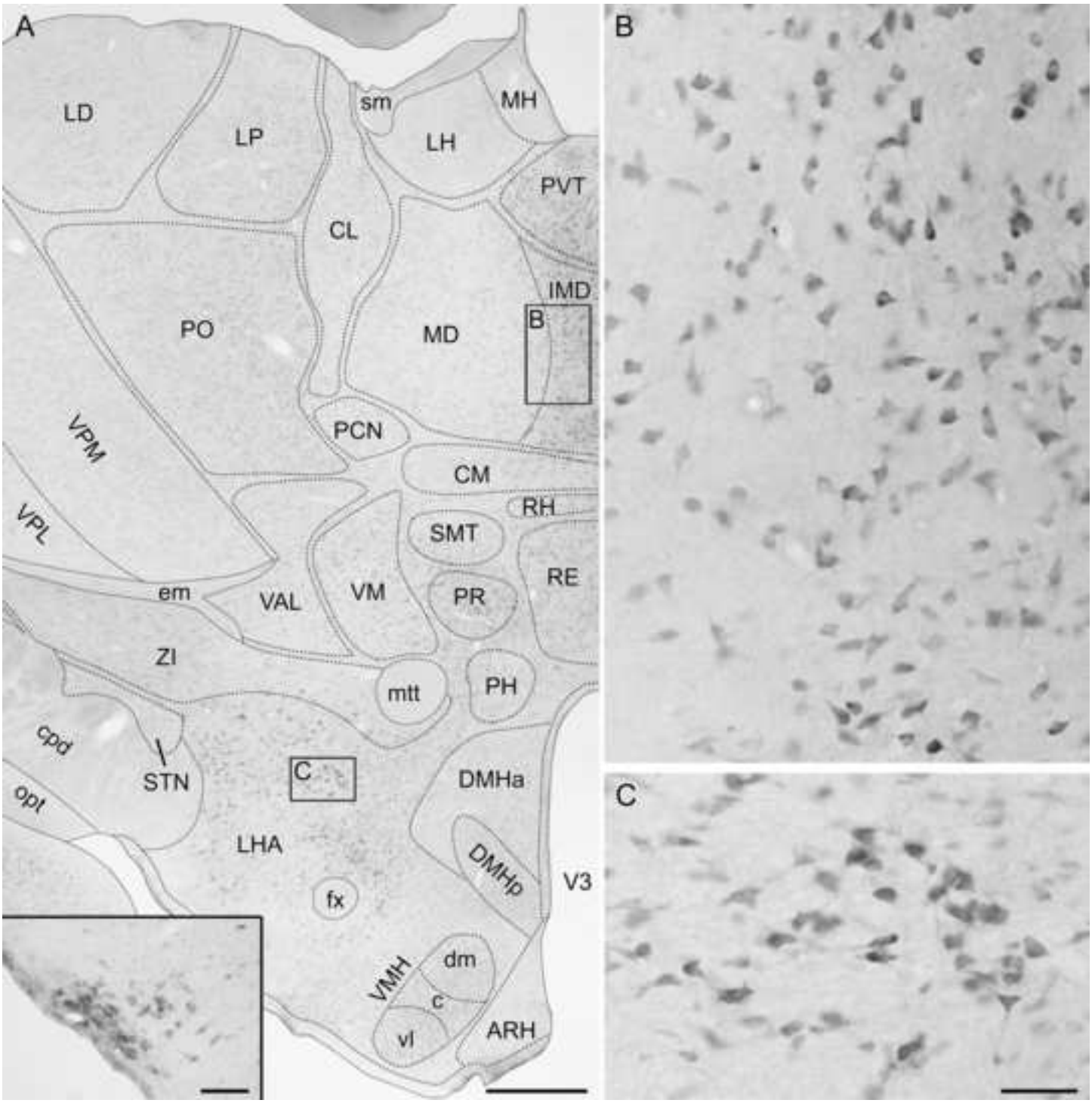

Figure 12

Click here to download high resolution image

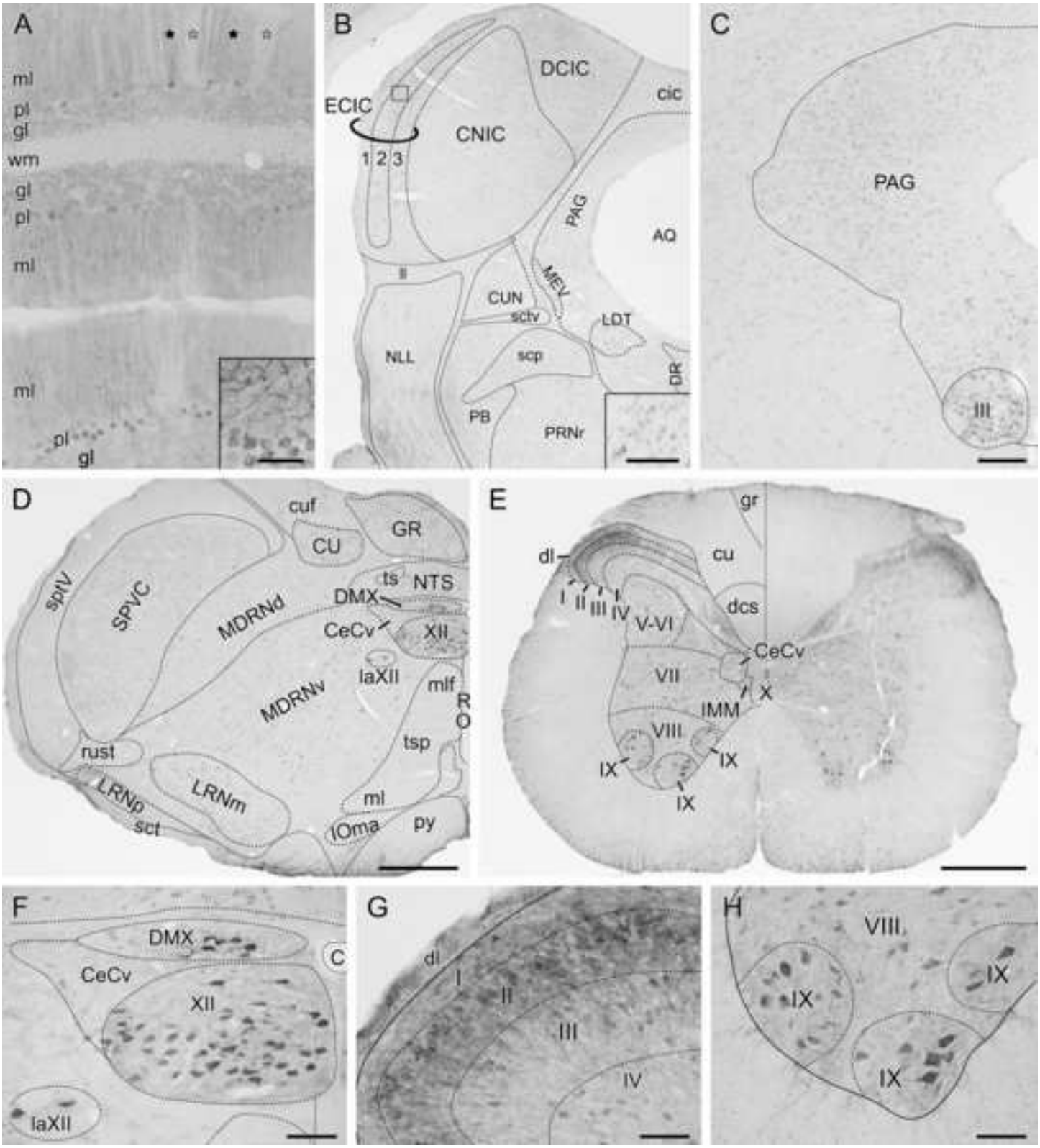

Figure 13

Click here to download high resolution image

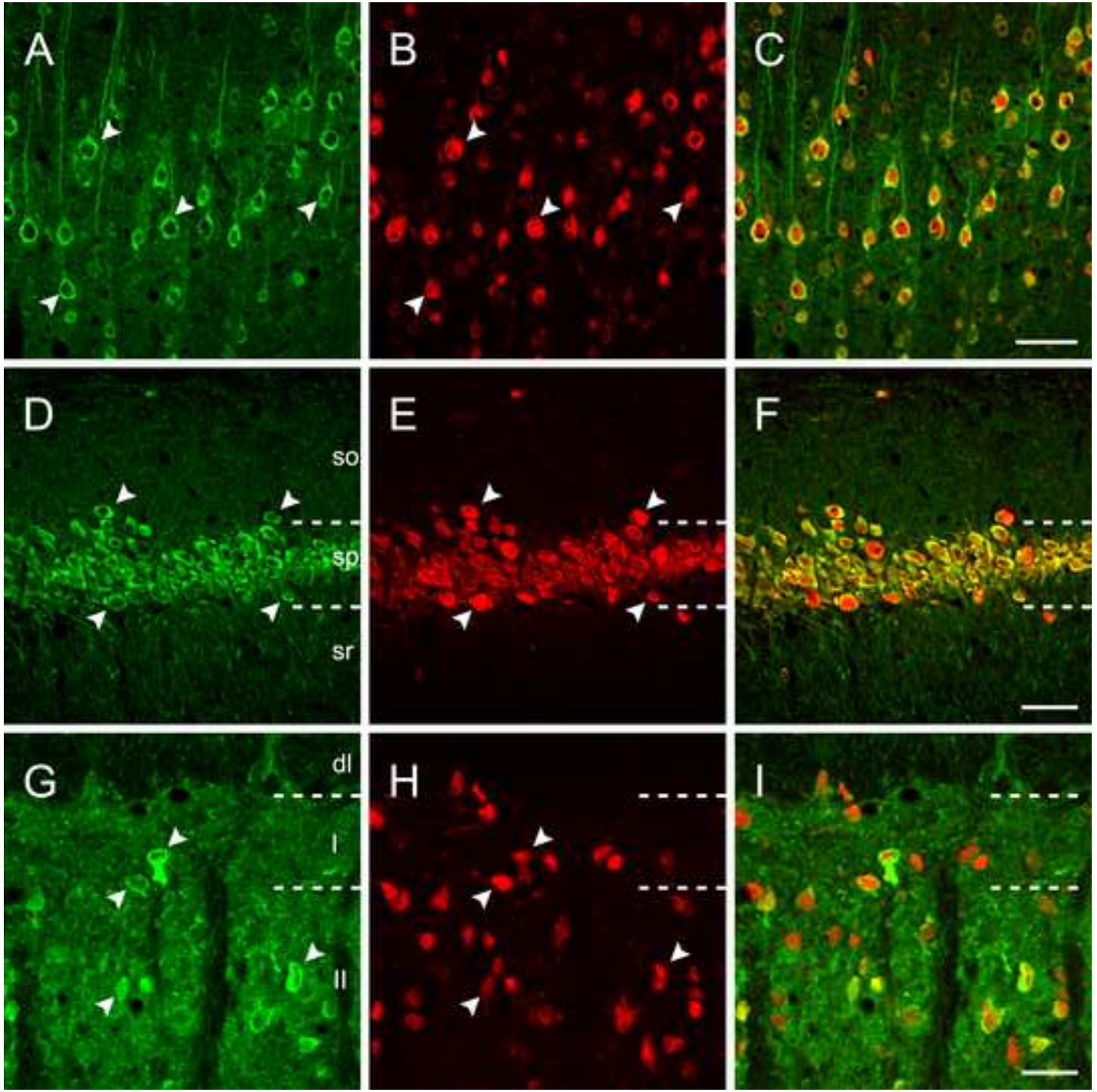

Figure 14

Click here to download high resolution image

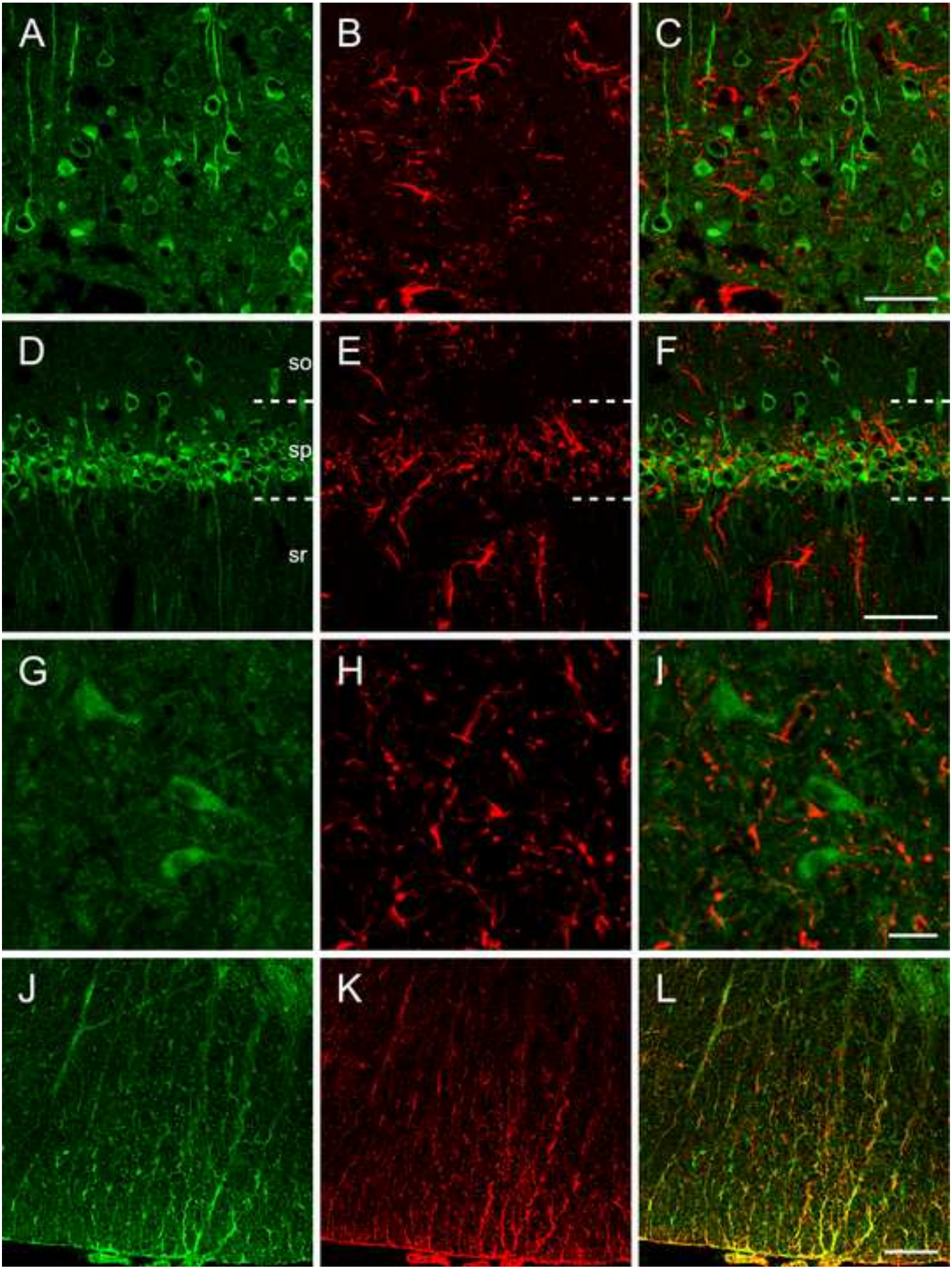

Figure 15

Click here to download high resolution image

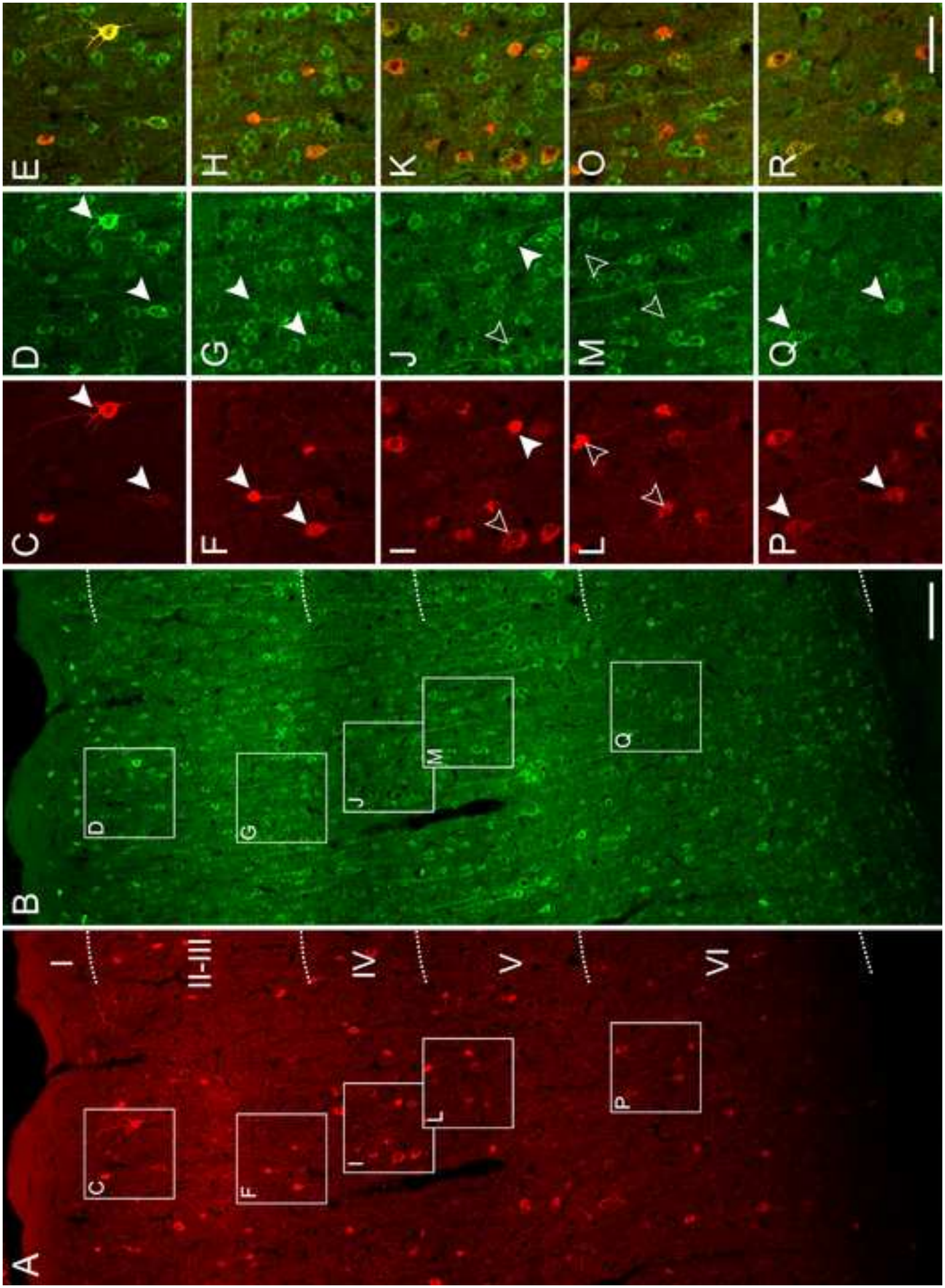

Figure 16

Click here to download high resolution image

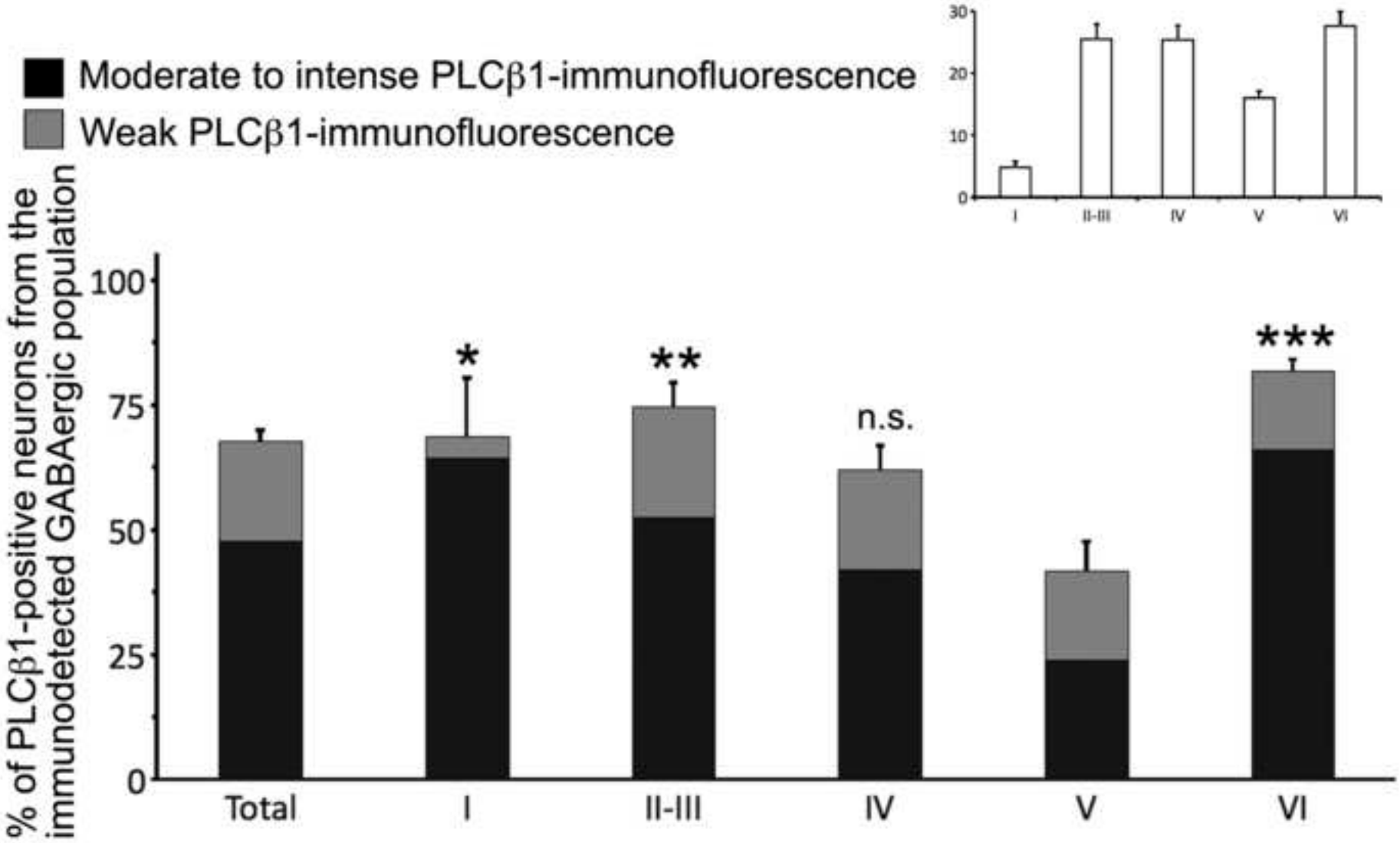

Figure 17

Click here to download high resolution image

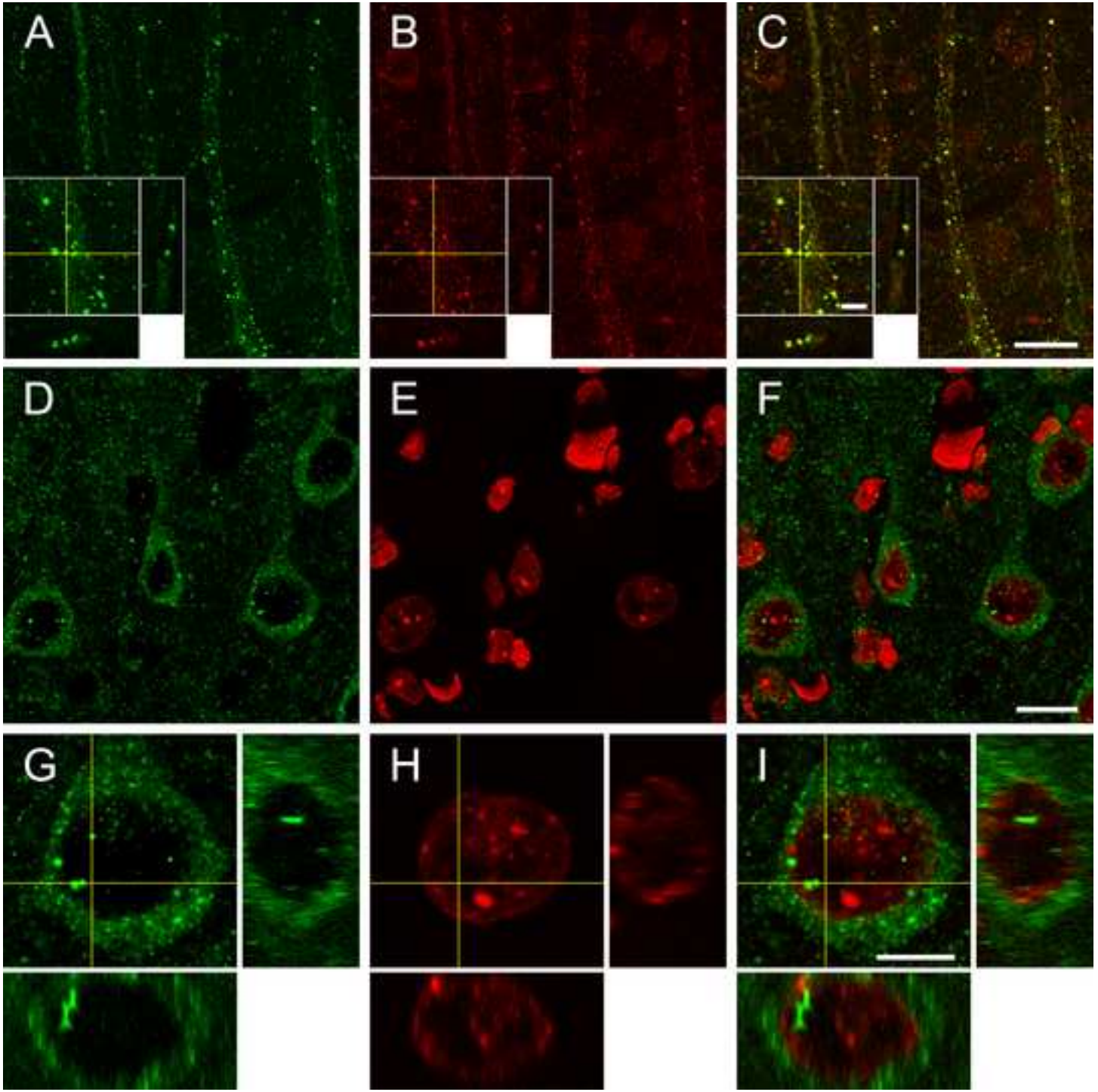

Figure 18

Click here to download high resolution image

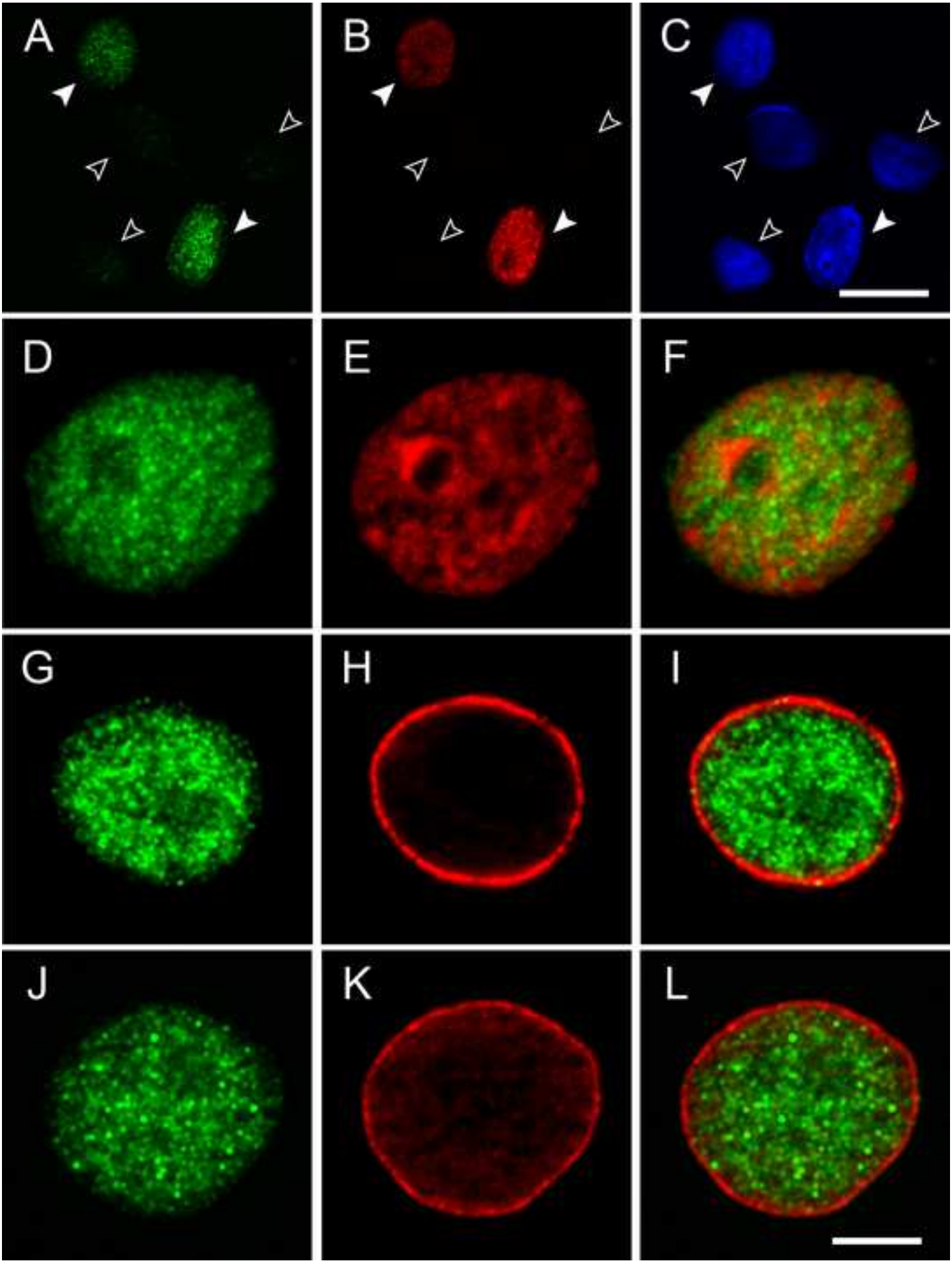

Figure 19

Click here to download high resolution image

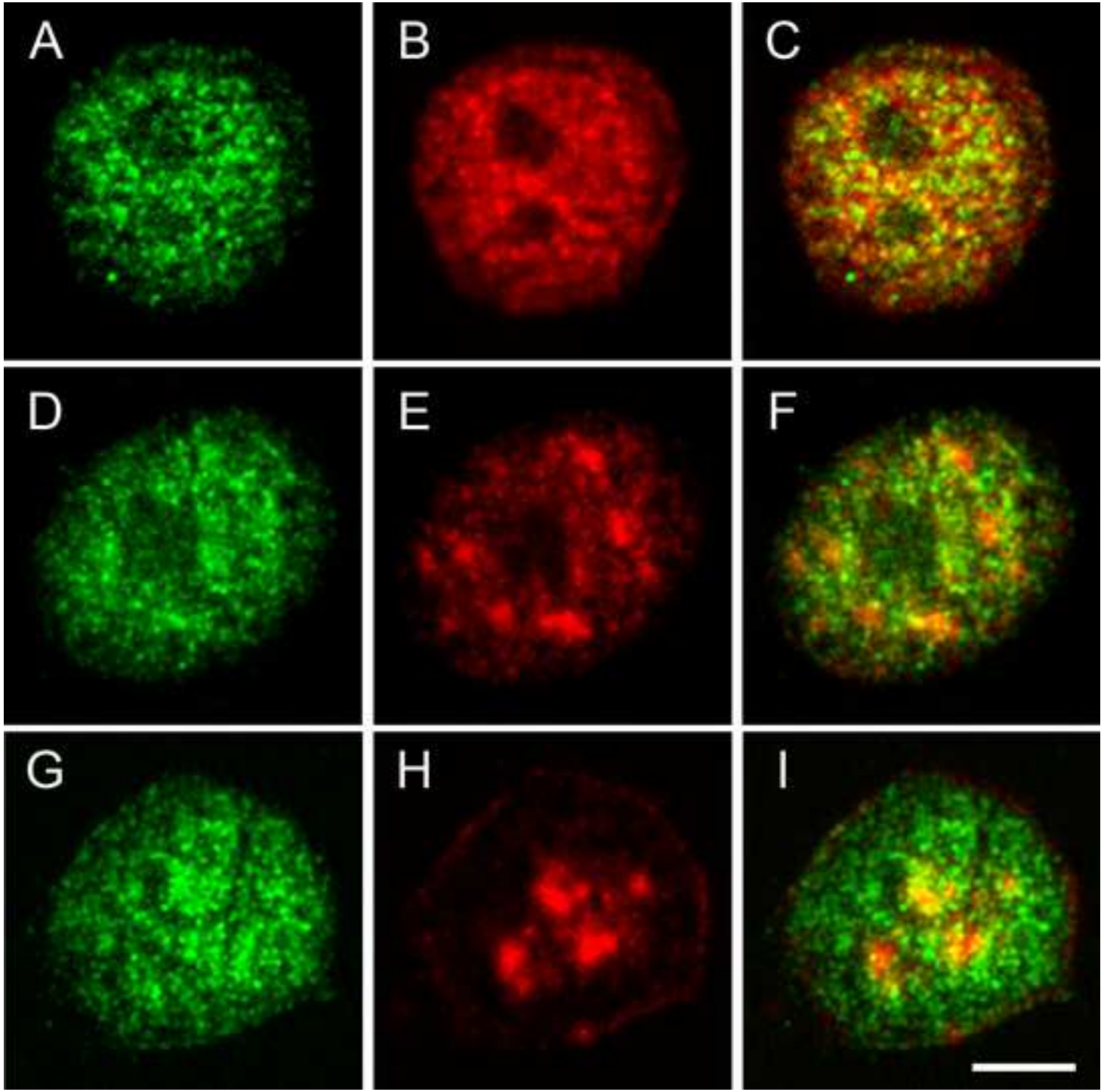

Figure 20

Click here to download high resolution image

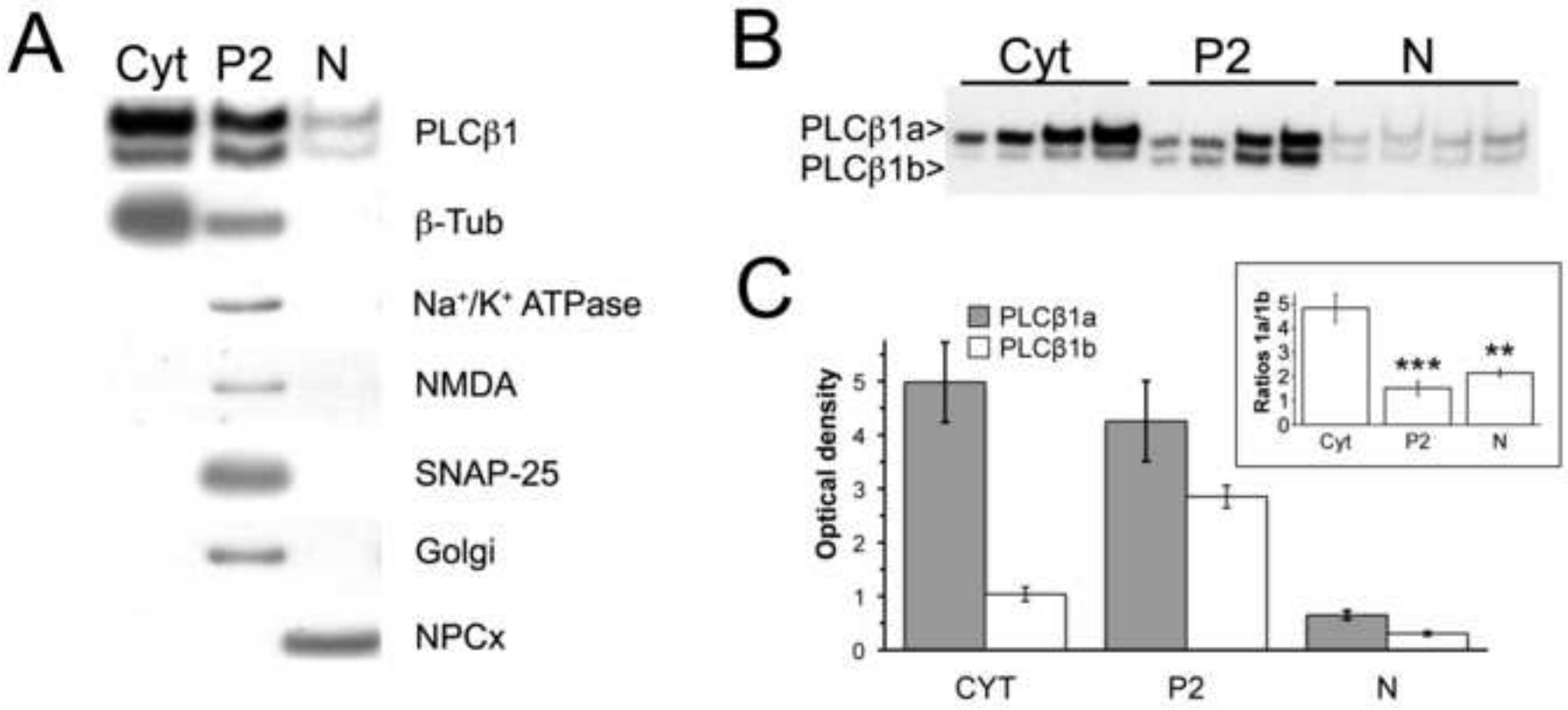

Supplementary Figure 1

Click here to download high resolution image

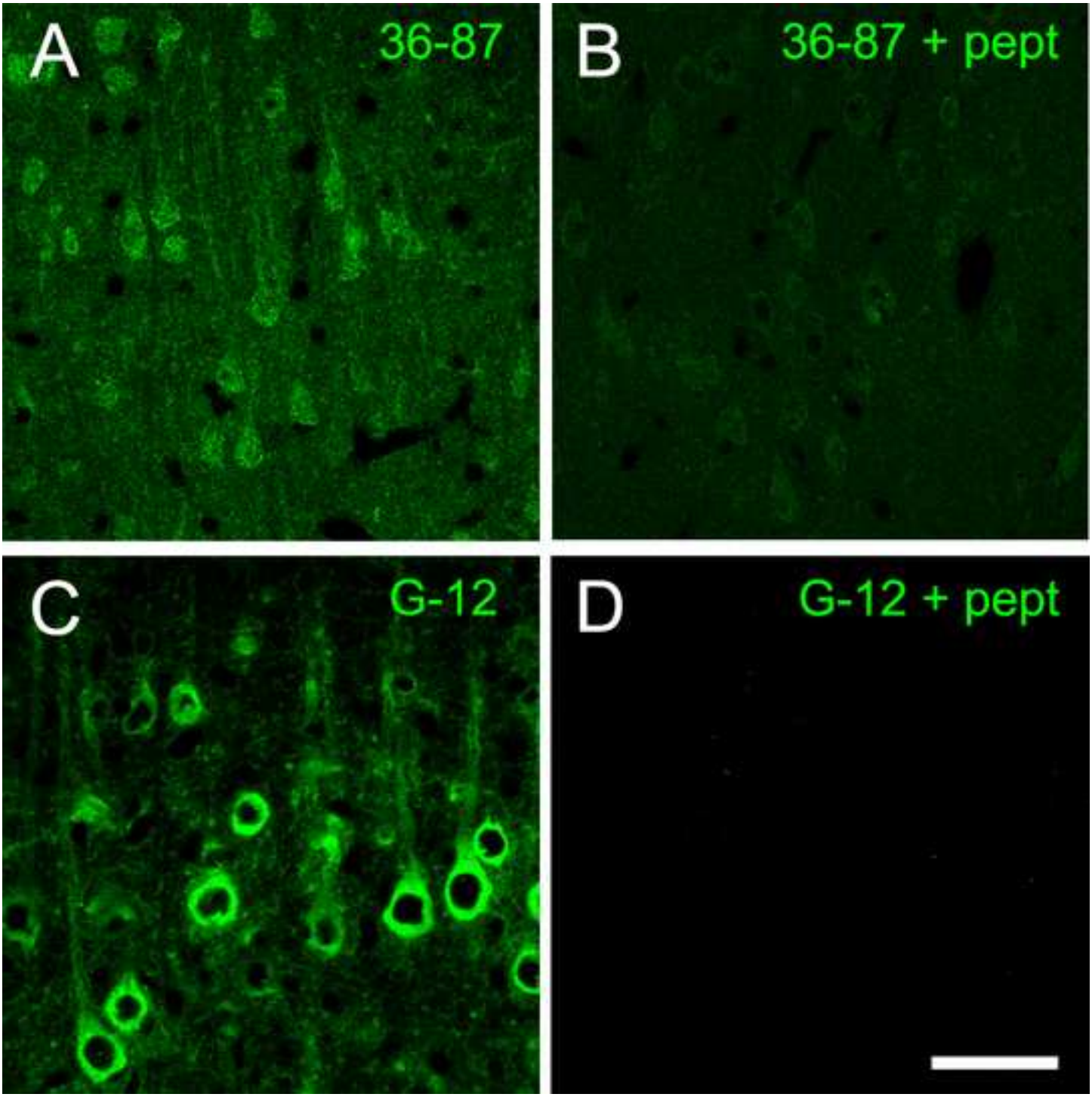

Supplementary Figure 2

Click here to download high resolution image

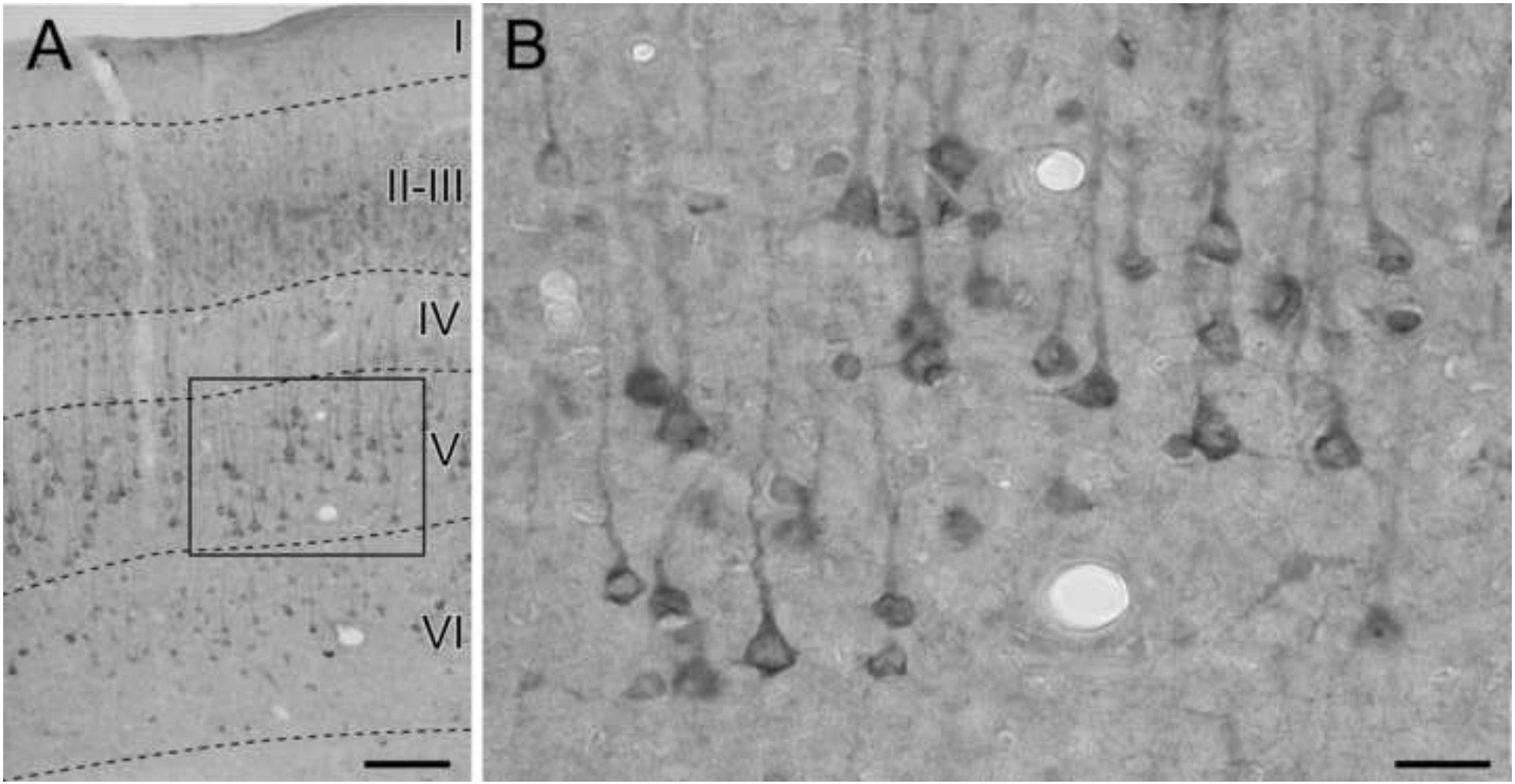

Captions for supplementary figures

Supporting Fig. S1. Peptide preabsorption assays. **A-D.** Preabsorption of PLCβ1$_{36\text{-}87}$ at a 5:1 ratio of peptide to antibody protein reduced greatly but not completely immunolabelling (A-B), whereas the same procedure at a 3:1 ratio completely abolished G-12 immunolabelling (C-D). Scale bars = 50 µm.

Supporting Fig. S2. Immunohistochemical staining provided by the anti-PLCβ1 mouse monoclonal antibody N-ter. **A.** Low power micrograph showing a distribution of immunolabelling. **B.** Higher magnification micrograph of the framed area in A. The immunostaining pattern resembled that found with R-233, D-8 and G-12 antibodies; however the immunofluorescence signal provided by this antibody was faint, making it useless for co-localization studies. Scale bars = 200 µm in A; 50 µm in B.

***Highlights (for review)**

We describe PLCβ1 protein distribution and subcellular localization in rat brain
We highlight neocortex, septum, hippocampus, and caudate putamen
PLCβ1 is not only expressed in pyramidal, but also in cortical GABAergic neurons
Evidences for the location of PLCβ1 in nuclear speckles
Some insights into the potential physiological and behavioural roles of PLCβ1

Graphical Abstract (for review)

Click here to download high resolution image